

RHELP (Regenerative High Efficiency Low Pressure) Air Purification System

Project No.: BB07PRO013

Prime Contract Number: HDTRA-07-C-0064

Subcontract Number: UF-EIES-0710012-CHA

Submitted to

Defense Treat Reduction Agency (DTRA)

**Chang-Yu Wu¹, Brian Damit¹, Qi Zhang¹, Myung-Heui Woo¹,
Wolfgang Sigmund², Hyoungjun Park²,
Jan Marijnissen³
Chang Yul Cha⁴, Alayna Jimenez⁴**

¹University of Florida, Department of Environmental Engineering Sciences

²University of Florida, Department of Materials Science Engineering

³Delft University of Technology, Department of Chemical Technology

⁴Cha Corporation

June 18, 2009

Report Documentation Page				Form Approved OMB No. 0704-0188	
Public reporting burden for the collection of information is estimated to average 1 hour per response, including the time for reviewing instructions, searching existing data sources, gathering and maintaining the data needed, and completing and reviewing the collection of information. Send comments regarding this burden estimate or any other aspect of this collection of information, including suggestions for reducing this burden, to Washington Headquarters Services, Directorate for Information Operations and Reports, 1215 Jefferson Davis Highway, Suite 1204, Arlington VA 22202-4302. Respondents should be aware that notwithstanding any other provision of law, no person shall be subject to a penalty for failing to comply with a collection of information if it does not display a currently valid OMB control number.					
1. REPORT DATE 18 JUN 2009		2. REPORT TYPE		3. DATES COVERED	
4. TITLE AND SUBTITLE RHELP (Regenerative High Efficiency Low Pressure) Air Purification System				5a. CONTRACT NUMBER HDTRA-07-C-0064	
				5b. GRANT NUMBER	
				5c. PROGRAM ELEMENT NUMBER	
6. AUTHOR(S) Chang-Yu Wu; Brian Damit; Qi Zhang; Myung Heui Woo; Wolfgang Sigmund				5d. PROJECT NUMBER BB07PRO013	
				5e. TASK NUMBER	
				5f. WORK UNIT NUMBER	
7. PERFORMING ORGANIZATION NAME(S) AND ADDRESS(ES) University of Florida, Division of Sponsored Research, 219 Grinter Hall, Gainesville, FL, 32611-5500				8. PERFORMING ORGANIZATION REPORT NUMBER	
9. SPONSORING/MONITORING AGENCY NAME(S) AND ADDRESS(ES)				10. SPONSOR/MONITOR'S ACRONYM(S)	
				11. SPONSOR/MONITOR'S REPORT NUMBER(S)	
12. DISTRIBUTION/AVAILABILITY STATEMENT Approved for public release; distribution unlimited.					
13. SUPPLEMENTARY NOTES The original document contains color images.					
14. ABSTRACT This project aims to develop a RHELP (Regenerative-High Efficiency-Low Pressure) air purification system using a novel ceramic nanofiber on silicon carbide in a microwave oxidizer that can effectively decontaminate air containing aerosolized chemical and biological (CB) agents. Nanofibermats of several materials were designed and fabricated using electrospinning process. Physical filtration testing showed performance (filter quality) exceeding military HEPA requirement. Multiple layers were found to have better filter quality than single layer of the same thickness. Biological agent testing showed effectiveness of microwave irradiation to deactivate a wide range of biological agents. System performance can be further enhanced by lowering face velocity during periodic microwave irradiation to minimize heat loss. Chemical agent testing showed excellent regeneration but destruction of the agent needs further improvement.					
15. SUBJECT TERMS					
16. SECURITY CLASSIFICATION OF:			17. LIMITATION OF ABSTRACT	18. NUMBER OF PAGES 103	19a. NAME OF RESPONSIBLE PERSON
a. REPORT unclassified	b. ABSTRACT unclassified	c. THIS PAGE unclassified			

EXECUTIVE SUMMARY

During attacks with chemical or biological warfare agents, personnel need a supply of clean air, whether in temporary or permanent shelters. Current methods rely on the use of high-temperature catalytic oxidation which requires hours of startup time and can generate toxic by-products such as NO_x and SO₂. This limits the usefulness of the system. A filtration system that can be regenerated in place is ideal. Microwave irradiation can be used for decontamination and regeneration with very little warm up time while generating almost none of the problematic by-products. The objective of this project is to develop a RHELP (Regenerative-High Efficiency-Low Pressure) air purification system using a novel ceramic nanofiber on silicon carbide in a microwave oxidizer that can effectively decontaminate air containing aerosolized chemical and biological (CB) agents.

In materials research and filter fabrication, the goal was to manufacture microwave absorbing nanofiber filter membranes for regenerative air filters. Nanofibermats of several materials were designed and fabricated: I) Polyacrylonitril (PAN) nanofibers on activated carbon fiber (ACF) mat; II) titania nanofibers; III) silicon carbide nanofibers; IV) titania carbon nanotube reinforced nanocomposite nanofibers; and V) titania silica nanocomposite nanofibers. Experimental protocols for electrospinning of all these fibers were developed and succeeded in achieving nanofibers. Sandwich structure of microfiber=nanofiber-microfiber enhanced the mechanical stability of the fiber mats. These nanofibers were also tested for morphology/microstructure, thermal degradation and mechanical stability. Furthermore, the test filters of varying size up to 20 inch×20 inch were delivered to the research partners for air filtration tests.

PAN nanofiber filters underwent rigorous physical filtration testing for collection efficiency, pressure drop, most penetrating particle size, and microwave sensitivity, among other characteristics. Experiments determined the optimal conditions for electrospinning deposition time and found that multilayered PAN filters had an increased quality factor. More importantly, the synthesized filters were found to exceed military standards for HEPA filter with lower pressure drop. This provided encouraging promise for biological agent testing.

Three microorganisms, *Escherichia coli*, MS2 Bacteriophage and *Bacillus subtilis* endospores were tested, as benign surrogates to more dangerous microbes. As the test organisms resemble a wide range of bioaerosols, they provided an appropriate estimation of the filtration and inactivation of possible bioterrorism agents. Static on-filter tests were first conducted to determine the plausibility of microwave inactivation of the microbes. All biological agents were able to be completely destroyed by microwave irradiation within 2 minutes, with *E. coli* being the most sensitive and *B. subtilis* endospores being the least sensitive.

A dynamic system was then developed for in-flight filtration which coupled PAN nanofiber filtration and microwave irradiation for the removal of bioaerosols. Experiments found that with an application power of 250 W for 2 minutes (per every ten minutes), the system was able to remove 99.9% of viable *E. coli* aerosols from the air stream. If the power was increased to 500 W, greater than 99.99% inactivation of viable *E. coli* was obtained. At 500 W of continuous microwave application, the system was able to remove over 95% of viable MS2 virus and *B. subtilis* endospores. MS2 and *B. subtilis* have shown less removal than *E. coli* at similar settings due to *E. coli*'s larger size and greater heat sensitivity. It was also found that system performance could be further enhanced by lowering face velocity during periodic microwave irradiation to minimize heat loss.

In addition to biological testing, experiments were carried out to investigate a method to first collect chemical warfare agent aerosols then destroy the collected aerosol with microwaves. A disk holder and microwave regeneration system was designed and built for testing fabricated nanofiber filter samples. A chemical warfare agent simulant, dimethyl methyl phosphonate (DMMP) was used on both lab-scale and bench-scale testing. Filters were used on porous silicon carbide disks with the lab-scale setup with the following compositions: polyacrylonitrile, cross-linked polyacrylonitrile, poly vinyl pyrrolidone, and titanium dioxide. In addition, a commercially available filter, Lydair HEPA grade 4450HS glass microfiber filter, was tested. The poly vinyl pyrrolidone filters dissolved in the chemical agent, rendering it useless as a filter. The polyacrylonitrile filters gave inconsistent results ranging from approximately 20-100% aerosol collection efficiency. In addition, they showed signs of degradation after regeneration under nitrogen. The other three filter compositions gave aerosol collection efficiencies over 90% without signs of degradation, even after regenerating under air. The cross-linked polyacrylonitrile and titanium dioxide filters, however, were brittle and easily damaged during handling, making them less than ideal. The regeneration process gave mixed results. While the filter and silicon carbide disk was completely regenerated and returned to their initial state in all tests, the destruction of the chemical agent was incomplete. Initial regeneration tests were under nitrogen due to concerns of the degradation of the filters under oxidizing conditions; however, later tests under air could achieve destruction efficiency over 90%, though inconsistently.

Bench-scale testing was initially done on two silicon carbide tubes from Vesuvius Ceramics with different porosities: 500 μm and 250 μm pore sizes. Aerosol collection efficiency was low, no greater than 65% with these tubes. Less porous tubes with smaller pore sizes, 26 μm and 42 μm , were obtained from Refractron Technologies and the reactor modified for the

different size tubes. The tubes had different diameters so that the larger tube could be used alone or the second tube could be added inside the first with a gap between the two. When both tubes were used, the Lydair HEPA grade 4450HS glass microfiber filter was wrapped around the outside of the inner tube with varying numbers of layers. The presence of the filter gave improved aerosol collection efficiencies with results greater than 85%, but increasing the number of layers did not consistently increase the collection efficiency. The destruction efficiency on the bench-scale reactor gave inconsistent results varying from about 40% to almost 100%.

In addition to aerosol collection followed by filter regeneration, tests were done on the bench-scale to directly oxidize the chemical agent aerosol with microwaves in the reactor. Initial tests on the first reactor gave promising results between about 75% and 95% destruction efficiency at various flow rates. The second reactor with the smaller pore size tubes was expected to increase the destruction efficiency with the greater surface area. The destruction efficiency, however, ranged from about 50% to almost 100 % with no clear relationship to the test variables.

Results of the testing had much lower aerosol collection efficiencies and destruction efficiencies than would be required for removing and neutralizing chemical warfare agents from air. Based on these results, a two stage system would be more desirable, with the second stage removing any aerosol not collected in the first. Microwave destruction would be done periodically as aerosol was collected and before aerosol was built up enough to overwhelm the system.

Because the project was not renewed for further funding consideration, a comprehensive study of the RHELP system which integrated nanofiber filtration, bioaerosol and chemical

aerosol removal, is not available. Nevertheless, in each individual research area, significant progress was made during the two year project:

- A PAN nanofiber filter which exceeded HEPA filter requirements with decreased pressure drop was successfully developed and tested.
- The development of a microwave absorbing nanofiber filter (pure TiO_2) and hybrid ceramic fibers of TiO_2 - SiO_2 has yielded encouraging results.
- Bioaerosol removal with microwave radiation was found to be effective with greater than 99% removal and inactivation for all microbial species at high power and application time.
- Chemical aerosol removal proved to be more challenging as mixed results were observed during aerosol collection and destruction. However, a two stage system has the potential to resolve this issue.

The above research has provided great insight into the capability of the to-be-completed RHELP system. Pending filter improvements, the progress has demonstrated that RHELP would serve as an effective air purification system for biological agents, with more research required to assess the effectiveness of its chemical aerosol removal.

PREFACE

This report was prepared by the Aerosol and Particulate Research Laboratory and Advanced Materials Processing Laboratory of the University of Florida and Cha Corp., under Contract Number **HDTRA-07-C-0064** for the Defense Threat Reduction Agency, 8725 John J. Kingman Road, MSC 6201, Fort Belvoir, VA 22060-6201.

This is a final report being submitted to DTRA. It describes work that was performed from March 19, 2007 to March 18, 2009. The DTRA Program monitor was Mr. William Buechter. We gratefully acknowledge the assistance of Major Analytical Instrumentation Center, Particle Engineering Research Center, Drs. Dale Lundgren and Samuel Farrah at the University of Florida, Dr. Tuett Sweeting at Vesuvius Ceramics, and Mr. Bill Cambo at Lydall Inc., without whom this study would not have been accomplished.

Table of Contents

List of Figures	x
List of Tables	xiv
Executive Summary	ii
1. Introduction	1
2. Experimental	6
2.1 Materials Research.....	6
2.2 Physical Filtration	11
2.3 Bioaerosol Testing	14
2.4 Chemical Aerosol Testing.....	19
3. Results and Discussion	30
3.1 Materials Research.....	30
3.2 Physical Filtration	43
3.3 Bioaerosol Testing	48
3.4 Chemical Aerosol Testing.....	57
4. Conclusions	81
4.1 Materials Research.....	81

4.2 Physical Filtration	82
4.3 Bioaerosol Testing	82
4.4 Chemical Aerosol Testing.....	83
5. Abbreviations and Symbols	85
6. References.....	87

List of Figures

Figure 1: Conceptual diagram of an electrospinning set-up.....	7
Figure 2: Aqueous sol preparation procedure with 3-glycidoxypyltrimethylsilane (GPTMS), nitric acid and TB.....	9
Figure 3: Proposed hydrolysis for GPTMS in aqueous HNO_3	10
Figure 4: Proposed chemical reactions between (GPTMS+ HNO_3) and TB.....	10
Figure 5: The schematic overview of the physical testing system.	12
Figure 6: The aerosol generation system.....	13
Figure 7: The aerosol dilution dryer.....	13
Figure 8: The Electrical Aerosol Analyzer (EAA).....	14
Figure 9: Front-view of the Scanning Mobility Particle Sizer (SMPS)	14
Figure 10: Schematic of experimental system used in static testing.....	16
Figure 11: Microwave quartz reactor in microwave oven.....	17
Figure 12: The schematic diagram of the microwave online testing system	18
Figure 13: Experiment Schematic for the saturation testing	20
Figure 14: Picture of Disk Holder	20
Figure 15: Schematic for Lab-Scale Regeneration Testing.....	21
Figure 16: Picture of Microwave Disk Regeneration System.....	22
Figure 17: Schematic for Bench-Scale Testing.....	25
Figure 18: Picture of First Bench-Scale Microwave System	25
Figure 19: Picture of Second Bench-Scale Microwave System.....	26

Figure 20: SEM image of (a) TiO ₂ nanofibers, (b) Millipore HEPA and (c)military HEPA. Scale bars are (a) 2 μm, (b) (c) 5 μm.	30
Figure 21: TEM images (a, b, c, d, e) and diffraction patterns (f, g, h, i, j) of electrospun TiO ₂ fibers heat-treated at different temperature for 3 hours: (a, f) 500 °C, (b, g) 600 °C, (c, h) 700 °C, (d, i) 800 °C, (e, j) 900 °C.	31
Figure 22: XRD patterns of TiO ₂ that were heat-treated at various temperatures and times.	32
Figure 23: XRD patterns of TiO ₂ fibers of different mixing ratios of precursors, TB:AA from 1:0 to 1:16 with fixed molar ratio of EtOH at 20.	33
Figure 24: Grain sizes of samples with different molar ratios of TB:AA from 1:0 to 1:16.	34
Figure 25: d_f and C_v of samples with different PVP and F108 concentrations.	35
Figure 26: TiO ₂ -SiO ₂ composite nanofibermat.	35
Figure 27: XRD patterns of samples at different temperature for 8 hours. For comparison, anatase peak from conventional TiO ₂ precursor sol is added on top.	36
Figure 28: XRD patterns of samples with different heat treatment time at 1100 °C.	37
Figure 29: Thermogravimetric diagram for electrospun fibers from aqueous sol and PVP.	38
Figure 30: ¹³ C-NMR spectra of (from bottom to top) pure GPTMS, mixture of HNO ₃ and GPTMS at molar ratio of 1:1, 2:1, 4:1, 8:1, 16:1 and methanol. The orange wedges show the peaks from transition states.	39
Figure 31: ¹³ C-NMR spectra of HNO ₃ :GPTMS=2:1, TB, HNO ₃ :GPTMS:TB=2:1:1 and 1-butanol (from bottom to top). The orange wedges show the peaks of 1-butanol.	40
Figure 32: ¹³ C-NMR spectra of (from bottom to top) HNO ₃ :GPTMS=2:1 and HNO ₃ :GPTMS:TB=2:1:1. The blue wedge shows the peak of methanol.	41

Figure 33: SEM images of (a) military HEPA filter, (b) Millipore HEPA filter, (c) as-spun PAN fibers and (d) crosslinked PAN fibers. Scale bars are 5 μm for (a, b) and 2 μm for (c, d).	42
Figure 34: Average diameter and C_v for Millipore HEPA filter, Military HEPA filter, as spun PAN fiber and cross-linked (X-linked) electrospun PAN nanofiber. Y-axis for left diagram is for diameter in nm. Y-axis on right plot is for C_v	42
Figure 35: Particle size distribution of aerosol generated from nebulization of 5% wt NaCl solution.....	46
Figure 36: The penetration curve of the 30 mins electrospun PAN nanofiber filter	46
Figure 37: <i>E. coli</i> inactivation on the PAN 60 filter after dynamic in-flight microwave irradiation under different microwave power levels and application times	51
Figure 39: Viable MS2 penetration fractions from the microwave/filtration system as a function of microwave power level and application time with PAN 60 filters.....	52
Figure 40: Viable MS2 penetration fractions from the microwave/filtration system as a function of microwave power level and application time with X-linked PAN filters	53
Figure 41: <i>B. subtilis</i> survival fraction on the filter after dynamic in-flight microwave irradiation under different microwave power level and application times	54
Figure 42: SiC disk temperature dependence on flow rate through reactor	55
Figure 43: Pressure Drop as a Function of Face Velocity on Uncoated SiC Disks.....	57
Figure 44: Pressure Drop as a Function of Face Velocity on PAN Coated SiC Disks.....	58
Figure 45: Pressure Drop as a Function of Face Velocity on PVP Coated SiC Disks on Second Saturation Configuration.....	59
Figure 46: Saturation with DMMP of Uncoated SiC Disks for 20 Minutes.....	60

Figure 47: Saturation with DMMP of PAN Coated SiC Disks for 20 Minutes.....	61
Figure 48: Saturation with DMMP of TiO ₂ Mats on SiC Disk for 20 Minutes at 5.4-cm/s Face Velocity.....	63
Figure 49: Saturation with DMMP of Cross-Linked PAN Mats on SiC Disk for 20 Minutes at 5.4-cm/s Face Velocity	66
Figure 50: Saturation with DMMP of Lydair Filter on SiC Disk for 20 Minutes at 5.4-cm/s Face Velocity.....	68
Figure 51: Pressure Drop as a Function of Face Velocity on Bench-Scale Reactors	69
Figure 52: Saturation with DMMP of SiC Tube on First Reactor for 50 Minutes	70
Figure 53: Saturation with DMMP on Second Reactor for One Hour	72
Figure 54: Regeneration on Second Reactor for 30 Minutes.....	73
Figure 55: Aerosol Collection Efficiency as a Function of Saturation Time on Second Reactor with Both SiC Tubes and a Single Layer Lydair Filter	75
Figure 56: DMMP Aerosol Collected on Filter as a Function of DMMP Nebulized with Both SiC Tubes and a Single Layer Lydair Filter for Six Hour Saturation.....	76
Figure 57: Percent Destruction Efficiency as a Function of DMMP Collected on Filter during Saturation Using 2.55 kW and 3.4-m ³ /h for One Hour	77
Figure 58: Direct Oxidation on First Reactor at 2.55 kW Microwave Power for One Hour.....	78
Figure 59: Direct Oxidation on Second Reactor at 2.55 kW Microwave Power for 1 Hour.....	79

List of Tables

Table 1:Complex permittivity values of selected materials.....	6
Table 2: Analysis result on fiber diameter.....	30
Table 3: Grain size of TiO ₂ phases after different heat treatment.	32
Table 4: (Heat-treated fiber)/(as-spun fiber) diameters in percentage.....	35
Table 5: Comparison of anatase grain size from conventional sol and aqueous sol.....	37
Table 6: Physical testing results ^a of PAN nanofiber filters	43
Table 7: Physical properties of different types of filters.....	45
Table 8: Physical testing results of PAN 5, 10, 15, 5*3 and 15*2.....	47
Table 9: Physical test results of PAN 5 and PAN 5*3 in triplicate	47
Table 10: Survival fraction of microorganisms– Static on-filter inactivation	49
Table 12: Reduced flow results for <i>B. subtilis</i> spores, triplicate data.....	57
Table 13: Regeneration of Uncoated SiC Disks for 20 Minutes with Warm-up	60
Table 14: Regeneration of PAN Coated SiC Disks for 20 Minutes	61
Table 15: Saturation with DMMP of TiO ₂ Mats on SiC Disk	63
Table 16: Regeneration of TiO ₂ Mats on SiC Disks	64
Table 17: Regeneration of Cross-Linked PAN Mats on SiC Disks for 20 Minutes	66
Table 18: Regeneration of Lydair Filter SiC Disks for 20 Minutes	68
Table 19: Regeneration on 500 µm Pore SiC Tube with 5 Minute Warm-up	71

1. INTRODUCTION

In the event of a terrorist attack or in military operations where chemical and biological (CB) warfare agents may be encountered, the protection of military personnel is of paramount importance. Ventilation systems can be easily contaminated through the introduction of CB warfare agents. Consequently, they are extremely vulnerable to incidental and malicious attacks by terrorists and saboteurs. When chemical warfare agents (CWAs) are released into air, they vaporize quickly but some part of the CWA stays in aerosol form until heat required for vaporization is transferred from the atmosphere. Biological aerosols, which are micrometer and nanometer sized in diameter, may remain suspended and viable for hours or even days under optimal conditions. When CBs are sprayed into the open environment to contaminate air in the combat zone, the military personnel in the heavily contaminated environment are initially dependent on the personnel protection devices. These personnel protection devices are made of a filter and an adsorbent and hence have a limited useful lifetime. If the CBs are sprayed into the environment for an extended period of time, the military personnel would go into temporary shelters. The air entering the shelter needs to be clean to protect the personnel inside for an extended period of time.

Currently, contaminated air stream with CWAs is treated with high-temperature catalytic oxidation (CATOX). This method has been used effectively in oxidizing volatile organic compounds (VOCs)^{1,2} in air and therefore can be used as a method for removing and destroying liquid and gaseous CWAs in air³. Also, catalysts have been developed that continue to function for hours during exposure to contaminants containing nitrogen, sulfur, and phosphorus. However, the current system is inadequate. The CATOX requires a significant amount of energy to heat the air to temperatures greater than 260-400 °C to oxidize the CWAs in air effectively⁴.

CATOX also produces harmful combustion by-products such as NO_x and SO₂. In addition, CATOX requires hours of startup time to reach a steady state operation to completely oxidize CWAs in air. This startup period causes some serious problems if only the CATOX is used as a collective protection method in stationary settings because air contaminated with CWAs flows through the system without being decontaminated. Treated air also needs to be cooled down to breathing temperature. Furthermore, there is a concern that the selected oxidation catalyst could be susceptible to phosphorus poisoning by plating of polymeric phosphorus oxide produced from the oxidation of CWAs containing organophosphorus compounds.

Adsorption-based filters can be installed in CATOX systems to provide reasonable protection for a practical amount of time⁵; however, they are expensive and need to be regenerated quickly to protect personnel in shelters for an extended period of time. Also, desorbed CWAs during regeneration of used filters should be destroyed to avoid potential contamination of air. Therefore an opportunity exists to develop an advanced low-temperature catalytic oxidation system that can completely destroy CWAs in air without requiring any startup period. In addition, a high efficiency filter that can completely capture the CWAs and be regenerated in place would eliminate issues of personnel handling CWA waste. Microwave energy may provide the solutions to these problems.

Microwave energy is a form of electromagnetic energy that penetrates deeply into many materials. It transforms energy directly into heat by exciting molecules into rapid oscillatory motion. With such unique attributes, microwaves offer several practical advantages, including reduced thermal gradients, selective heating, rapid energy deposition, and acceleration of certain chemical reactions. In many cases, microwave energy has been shown to be less expensive for driving reactions than any other energy source.

In addition to CWAs, terrorists or the enemy may use biological warfare agents. Therefore, it is desirable to destroy the biological agents in the air in addition to the CWAs. The effectiveness of microwaves used for sterilization has been well established by numerous studies over previous decades. Microwave energy is capable of destroying DNA and is distinguishable from that destroyed by external heating^{6,7}. Therefore, microwave energy could effectively destroy biological warfare agents in air during the microwave decontamination of air in heavily contaminated environments.

In designing a microwave assisted CB filtration system that is to operate for at least 100 hours, an efficient filter that is not only resistant to microwave heating but also has low pressure drop is required. High efficiency particulate air (HEPA) filters, which were developed as part of the Manhattan project to prevent the spread of airborne radioactive contaminants, are widely used from residential to pharmaceutical applications. However, due to their high pressure drop during filtration, HEPA filters cannot satisfy recent needs of low energy consumption filtration systems which are critical especially to use in places where resources are limited—e.g. shelter. Overall the pressure drop can be decreased by using thinner fibers for filtration based on Stoke's law as given in Equation 1.

$$F_D = \frac{3\pi\mu V d_f}{C_c} \quad (1)$$

Here F_D is the drag force that causes pressure drop, μ is air viscosity, V is air velocity, d_f is fiber diameter and C_c is the gas slip correction factor⁸. The gas slip correction factor is a function of the fiber diameter and mean free path of air, l ($= 66$ nm at standard temperature and pressure), as expressed in Equation 2^{9,10}.

$$C_c = 1 + \frac{l}{d_f} \left[2.34 + 1.05 \exp \left(-0.39 \frac{d_f}{l} \right) \right] \quad (2)$$

Furthermore, the larger surface area of the nanofiber filter is expected to yield a higher efficiency. Therefore, the goal of our work is to develop regenerable filtration media composed of nanofibers on the support structures of micron-size fibers. The nanofibermat would be regenerated based on microwave technology to extend the lifetime. Materials were selected based on their thermal properties as well as their ability to absorb and dispel as much energy from microwave as possible, i.e. the complex permittivity. With increased microwave absorption, it becomes more practical to devise a CB agent removal system.

The overall objective of this research therefore was to develop a RHELP (Regenerative-High Efficiency-Low Pressure) air purification system that can effectively decontaminate air containing aerosolized CB agents for collective protection. The RHELP system would integrate the high physical collection and low pressure drop of nanofiber filtration with microwave radiation. Greater filter quality, with the addition of microwave energy to catalytically oxidize chemical aerosols and destroy potentially harmful bioaerosols, would result in an effective air purification system. The proposed goals of the RHELP system were:

- To have a lower pressure drop than the current HEPA filter for aerosols ($< 50\%$ of HEPA) while achieving the same high removal efficiency ($> 99.97\%$),
- To destroy a wide range of CB agents in air at low temperature ($< 120\text{ }^{\circ}\text{C}$) to avoid NO_x formation ($< 10\text{ ppm}$),
- To remove sulfur oxides formed by the oxidation of CB agents containing sulfur ($> 99\%$),
- To operate for a long period of time ($> 100\text{ hours}$).

Because of the multidisciplinary nature of the project, the research was divided into four interrelated areas: materials synthesis and filter fabrication, physical filtration testing, biological

aerosol removal, and chemical aerosol removal. The project team combined the scientific expertise of an academic institution (University of Florida) and a microwave technology developing company (Cha Corporation). Dr. Chang-Yu Wu (UF) has expertise in aerosol sampling and testing. Drs. Wolfgang Sigmund and Jan Marijnissen (UF) are experts in the fabrication of nanofiber and nanocatalysts using electrospray process. Dr. Chang Yul Cha (Cha Corp.) is the leading expert in developing microwave process for environmental remediation, air purification and warfare agent decontamination. The team used an active feedback cycle approach which included monthly teleconferences to accomplish materials and system optimization.

2. EXPERIMENTAL

2.1 Materials Research

2.1.1 Material Selection

The most important criterion of material selection is the complex permittivity ϵ ,

$$\epsilon = \epsilon' + i\epsilon'' \quad (3)$$

where ϵ' represents the amount of energy which can be stored in a material while ϵ'' represents the amount of energy that a material can dissipate in the form of heat. Since we apply microwave technology to regenerate the filtration media, material with high ϵ' and ϵ'' is preferred. Table 1 shows values of ϵ' and ϵ'' of some selected materials¹¹. Although activated carbon has highest ϵ' and ϵ'' in the table, it cannot be adopted because it would be readily oxidized at elevated temperature by microwaving. Therefore, TiO₂ was chosen as the target material.

Table 1: Complex permittivity values of selected materials.

	TiO ₂	SiO ₂	Activated Carbon
ϵ'	7	3	10
ϵ''	0.4	0.2	3

2.1.2 Electrospinning for Filtration Media Synthesis

The filtration media were fabricated by depositing nanofibers randomly on the substrate via electrospinning. Electrospinning is the only known method to accomplish nanofibermats with long fibers. For electrospinning, precursor sol has to be prepared with polymers dissolved in order to induce entanglement at the molecular scale. This avoids the Raleigh breakup of the liquid in an electric field and allows it to achieve nanofiber fabrication. The prepared solution is fed in a syringe with a flat-tipped needle and infused by the syringe pump. When the needle tip

and the aluminum foil collector are charged at different polarities to develop the electric field, the solution is electrospun to form nanofibers in whipping motion during their tip-to-collector flight (Figure 1). As-spun fibers can be heat-treated if needed.

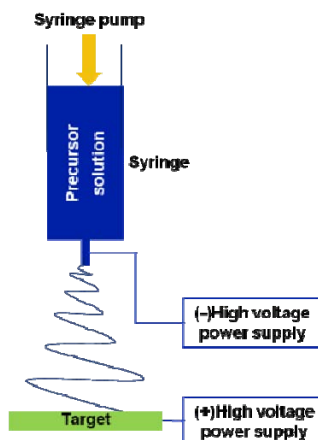


Figure 1: Conceptual diagram of an electrospinning set-up.

2.1.3 Electrospun TiO₂ Nanofibers and its Microstructure Analysis

TiO₂ nanofibermats were successfully electrospun on the activated carbon fiber (ACF) mats. Molar ratio of chemicals for TiO₂ nanofibermats was titanium (IV) n-butoxide (TB):acetic acid (AA):ethyl alcohol (EtOH)=1:4:20 with polyvinylpyrrolidone (PVP, M_w 1,300,000) 4% w/v in EtOH. Electrospinning condition was +5 (collector)/-10 (syringe tip) kV/15cm (tip-to-collector distance)@1ml/hr (infuse rate) for an intended deposition time. The fiber diameters were characterized by scanning electron microscope (SEM, JEOL JSM6400) and analyzed by ImageJ 1.38x, an image processing program.

Mechanical strength was predicted as the major weakness for the thin ceramic filtration media. Overall the microstructure impacts the mechanical properties. For example, the yield stress, i.e. the point where elastic deformation turns into plastic deformation, increases with smaller grains¹². The microstructure of electrospun TiO₂ fibers with varying conditions in

precursor preparation and heat treatment was studied. Parameters that were expected to impact the microstructure were molar ratio of chemicals in the sol, heat treatment temperature and time. Electrospun TiO₂ fibers from TB:AA:EtOH=1:4:20 precursor sol were heat-treated at different temperatures from 500 °C to 900 °C for 3 hours and observed by transmission electron microscope (TEM, JEOL TEM 200CX). Precursor sols of varying molar ratios from 1:0:20 to 1:16:20 of TB: AA: EtOH were electrospun, heat-treated at 500 °C for 3 hours and analyzed by XRD. Amount of EtOH was fixed. The samples were characterized by X-ray diffraction (XRD, Philips APD3720), SEM and TEM to observe the crystal structure, overall morphology and the grain morphology, respectively. Phase transformation between anatase and rutile of TiO₂ at different heat profile—time and temperature—was studied by XRD. For XRD sample preparation, the electrospun fibers that were delaminated from the wafers after heat treatment were ground and put on the double-sided tape to fix on the glass slide for XRD. Grain size for each sample was calculated by Scherrer's formula (Equation 4)

$$t = \frac{0.9\lambda}{B \cos \theta_B} \quad (4)$$

where t is the size of crystals, λ is the wavelength of the X-ray that was used, B is the full-width-at-half-maximum of the peak, θ_B is the average of lower and upper limits of the peak in radian.

2.1.4 Aqueous Sol System

Novel precursor system based on water was developed in our lab in a different project that is sponsored by industry. A patent on this aqueous sol-gel system is in progress. We decided to test this novel method to electrospin fibers for this work since the silica will close defects in the fiber and the aqueous system is not impacted by the changes in atmospheric conditions in Florida. Thermal treatment study by thermogravimetric analysis (TGA, Mettler Toledo

TGA/SDTA 851e) was done followed by XRD and SEM to characterize the crystal structure, overall morphology and the grain morphology, respectively. The chemistry of the aqueous sol system was extensively studied by nuclear magnetic resonance (NMR) spectroscopy (Mercury 300BB) to understand its mechanism and exceptional stability of TB with water. The aqueous approach is promising to alter the microstructure and allow for better mechanical strength. The overall procedure of sol preparation is described in Figure 2. Hypothesized chemical reactions between these three chemicals are shown in Figure 3 and Figure 4 for each step. Figure 3 displays how 3-glycidoxypyriltrimethylsilane (GPTMS) is fully hydrolyzed to form GPTHs through two transition states which are circled in orange and Figure 4 presents how the hydrolyzed GPTMS reacts with titanium tetra-n-butoxide (TB).

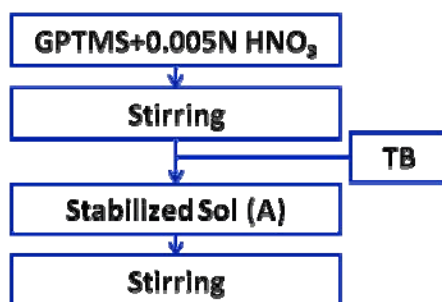


Figure 2: Aqueous sol preparation procedure with 3-glycidoxypyriltrimethylsilane (GPTMS), nitric acid and TB.

Fibers were successfully electrospun by adopting our general formulation of 0.005N HNO₃:GPTMS:TB=2:1:0.5. Effect of additive concentrations—PVP (M_w 630,000), surfactant BASF Pluronic[®] F108 Prill (F108)—and heat treatment profile on the crystalline phase and fiber thickness was studied. PVP was added to make the sol electrospinnable while F108, the non-ionic surfactant, was used to decrease the surface tension in order to achieve thinner fibers. Fiber diameters were measured from SEM images by ImageJ ver. 1.40g. The number of measurement

for each sample was 110 at least. The fibers' microstructures were examined for heat treatments at 500 °C, 700 °C, 900 °C and 1100 °C. PVP 0.25% w/v sol was electrospun for an hour to form a beta version of fibermat at +5 (collector)/-10 (syringe tip)kV/20cm@2ml/hr and heat-treated at 1100 °C for 3 hours. Thermal behaviors of electrospun fibers from aqueous sol as well as PVP for comparison were studied during the heat treatment by TGA. The chemical reaction of the aqueous sol-gel system was investigated via ^{13}C -NMR by the stepwise addition of chemicals as described in Figure 2.

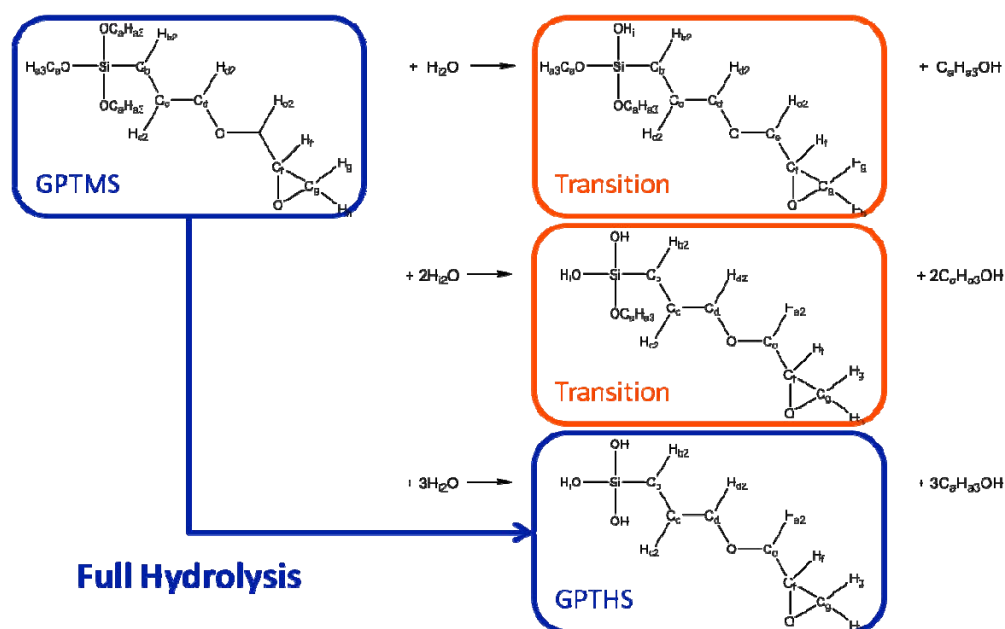


Figure 3: Proposed hydrolysis for GPTMS in aqueous HNO_3 .

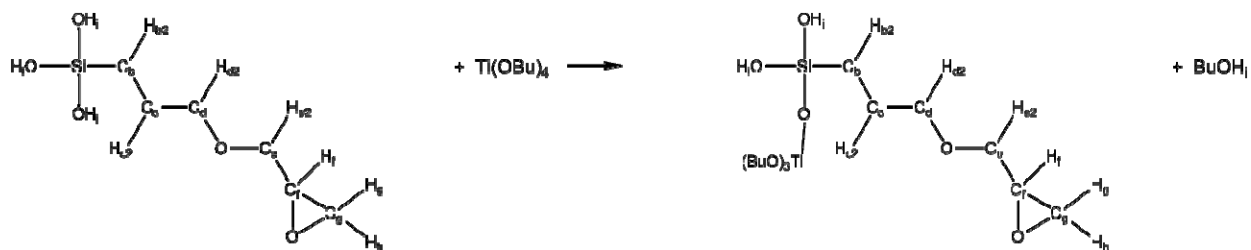


Figure 4: Proposed chemical reactions between (GPTMS+ HNO_3) and TB.

2.1.5 PAN Nanofiber Filter Fabrication

Polymer based nanofibers were synthesized in the beginning of the study to verify the working conditions of the electrospinning system and to compare with existing literature. Chemicals were polyacrylonitrile (PAN, Pfaltz & Bauer) of M_w 150,000 as the solute and *N, N*-dimethylformamide (DMF, 99.8%, Sigma-Aldrich) for solvent. PAN was dissolved in DMF immediately after vigorous stirring at 80°C to form 6 % w/v solution. The prepared solution was fed in the syringe with a 15-gauge needle (similar to Figure 1) and infused at 1mL/hour. When the needle tip and the aluminum foil collector were charged at -10 kV and 5 kV, respectively, solution was electrospun to form nanofibers in a whipping motion during their 20 cm flight. As-spun PAN fibers were heat-treated at 250 °C for 1 hour to induce crosslinking between PAN molecules in order to improve chemical resistance. In the solubility test, the crosslinked PAN withstood immersion in DMF at 80 °C.

Fibers were characterized using SEM. Images taken by SEM were analyzed to measure the fiber diameters by ImageJ ver.1.38x of National Institutes of Health. The number of measurement was over 150 for each sample. Two other kinds of HEPA filters were selected for comparison—Millipore HEPA (CAT. NO.: AP1504700, Millipore, MA, USA) and military HEPA (LydAir[®] High Alpha HEPA air filtration media-HEPA Lydair grade 4450H, product that is equipped by U.S. Army).

2.2 Physical Collection Efficiency

The experimental system for testing the PAN filter's physical removal efficiency consisted of 4 major sections: aerosol generation, aerosol drying, filtration and aerosol size distribution measurement. Figure 5 is the schematic overview of the entire system. Particle free

air from the cylinder passed through the Collision nebulizer to produce the test aerosol. An additional air flow from the cylinder was used as dilution air. These two flows met at the dilution dryer to remove the moisture content of the aerosol. A valve was used to direct the flow either to the filter or to the measurement device. The particle size distribution was then determined upstream and downstream of the filter and the filter's penetration could be calculated.

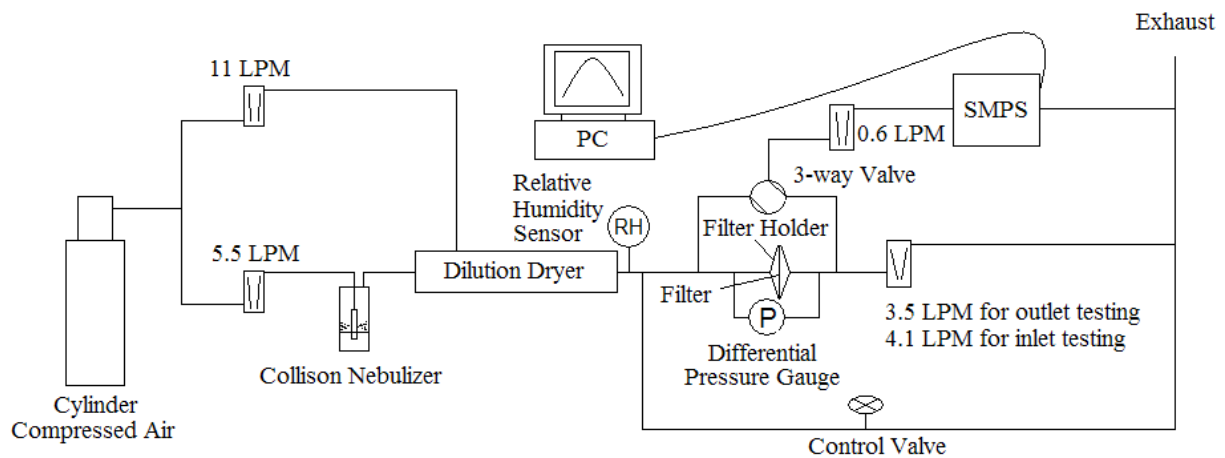


Figure 5: The schematic overview of the physical testing system.

Figure 6 shows the aerosol generation unit. Figure 7 displays the aerosol drying section. Figure 8 is the Electrical Aerosol Analyzer (EAA) used for aerosol size distribution measurement. The EAA was replaced by the newly purchased Scanning Mobility Particle Sizer (SMPS) after it was delivered by the manufacturer at the end of July 2007. Figure 9 shows the front view of the whole SMPS system.

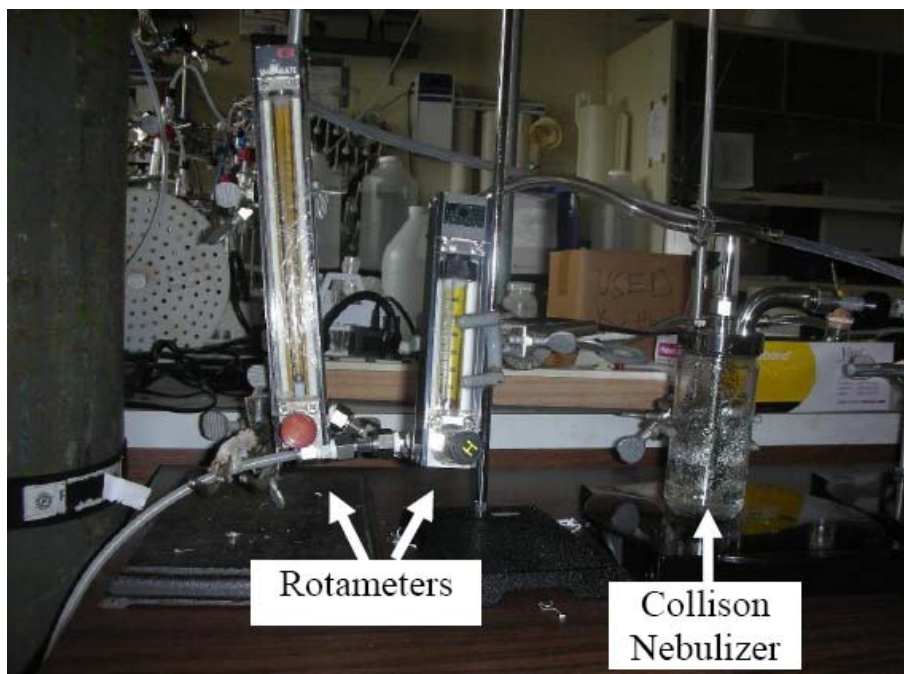


Figure 6: The aerosol generation system.

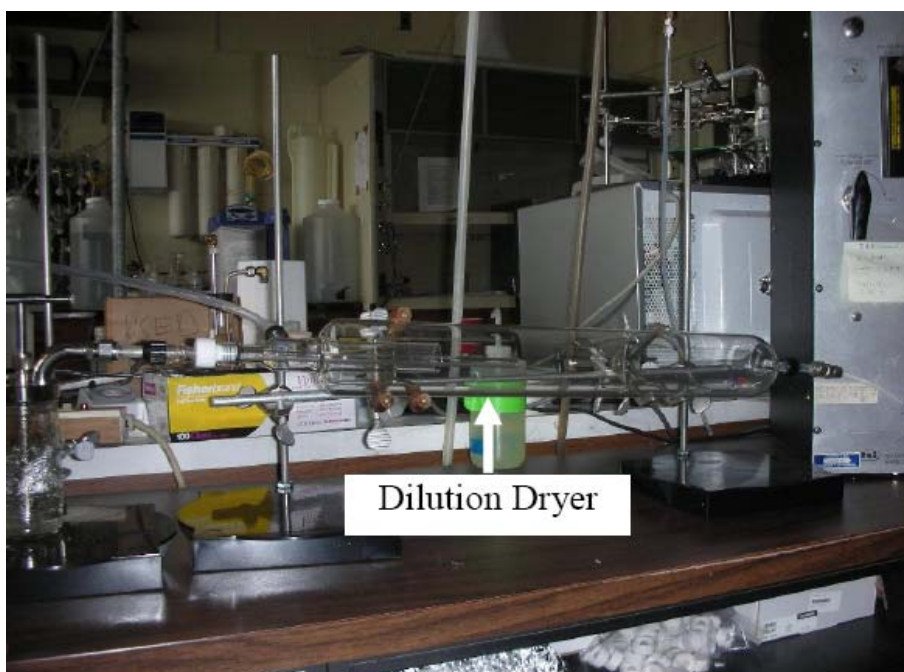


Figure 7: The aerosol dilution dryer.



Figure 8: The Electrical Aerosol Analyzer (EAA)



Figure 9: Front-view of the Scanning Mobility Particle Sizer (SMPS)

2.3 Bioaerosol Testing

2.3.1 Culturing and Assay of Test Microorganisms

Escherichia coli - A non-pathogenic strain of *E. coli* (ATCC number 15597) was used to represent vegetative cells. It was first inoculated on a Difco Nutrient Agar (Becton, Dickinson and Company, Lot No.: 8057703, MD) plate from stock. This plate was then incubated at 37 °C for 24 hours. Before each experiment, a single colony was inoculated on a Difco Nutrient Agar slant and incubated for 24 hours. The *E. coli* population on the slant was then transferred to Ringer's solution (Fisher, Cat. No.: S77939, NY) by vortex. In this way, *E. coli* suspension was prepared for bioaerosol generation. Every three (3) days, a new colony was inoculated into another Difco Nutrient Agar plate to renew the culture.

MS2 Bacteriophage - MS2 bacteriophage (*E. coli* bacteriophage, MS2; ATCC® 15597-B1™) was used to represent viruses in the testing. Freeze-dried MS2 was suspended in DI water to produce a concentration of approximately 10^8 to 10^9 PFU/mL as the virus stock suspension. MS2 was propagated in *E. coli*.

Bacillus subtilis endospores - *B. subtilis* (strain 168) endospores were tested because of their relative high heat resistivity compared to both *E. coli* and MS2 bacteriophage. African violet agar, which included 200 mL African violet soil extract, 800 mL DI water, 1 g Yeast Extract (Fisher Scientific) and 15 g Difco Nutrient Agar recommended by the American Type Culture Collection was used to induce sporulation. *B. subtilis* vegetative cells were inoculated in this agar and incubated at 37 °C for endospore development. After one week, a 2 mL DI water suspension of *B. subtilis* was created from the slant and heated in a water bath at 80 °C for 30 minutes to kill remaining vegetative cells. The suspension was subsequently cooled and centrifuged at 3,500 RPM for 10 minutes to remove cell debris. After applying the malachite

green spore-staining technique, microscopic analysis showed the absence of vegetative cells in the purified suspension.

After an experiment, liquid samples were taken. Each sample was serially diluted, plated with the appropriate growth medium and incubated at 37 °C for 24 hours. Standard microbiological protocol was followed. Afterward, the number of colony/plaque forming units (CFU/PFU) on the plates was counted. Only plates with between 30 and 300 units were recorded and used in efficiency calculations.

2.3.2 Static Inactivation of Test Microbes

The experimental set-up for collecting bioaerosols in the preliminary static on-filter testing is shown in Figure 10. The cylinder air provided clean, dry air with stable flow to the system. The air flow was first split into two ways. The first one led to a 6-jet Collison nebulizer (Model CN25, BGI Inc., MA) with 5.5 LPM flow rate to generate the testing bioaerosols. The second flow at 11 LPM carried air to the dilution dryer to evaporate water from the aerosol. After passing through the dilution dryer, the air flow was again split into two different paths. The first flow went through the filter holder with a 4.1 LPM flow rate on the filter surface while the excess air was directed to the second flow.

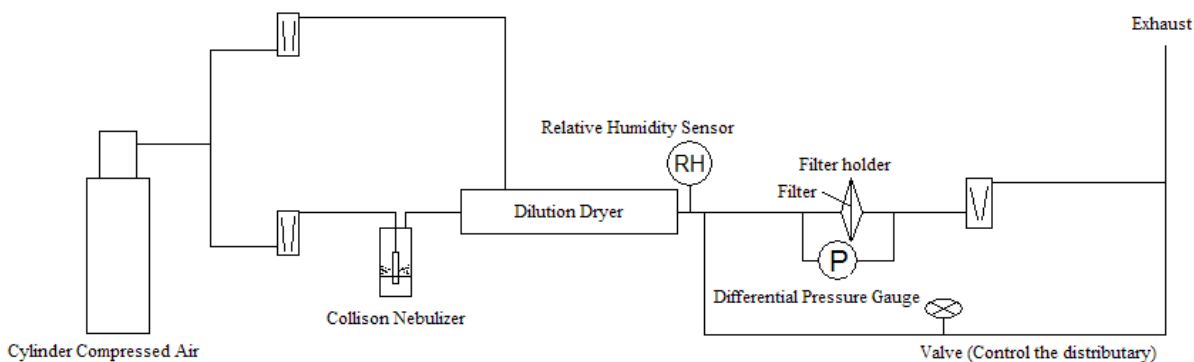


Figure 10: Schematic of experimental system used in static testing

The experiments ran for 30 minutes in order to collect enough microorganisms for adequate experimental resolution. After collection, the filter was taken out of the filter holder and cut into four equal quadrants for microwave testing. Each quadrant was placed at the center of the microwave and tested with a different microwave power and application time. Care was taken to demonstrate that every condition received the same amount of filter loading overall, considering triplicates.

2.3.3 Construction of the Microwave Online Testing System

Because common filter holders may be damaged with direct microwave exposure, a pure quartz filter holder that is transparent to microwaves was designed and placed inside the microwave oven. Figure 11 shows the microwave quartz reactor located inside the microwave oven.

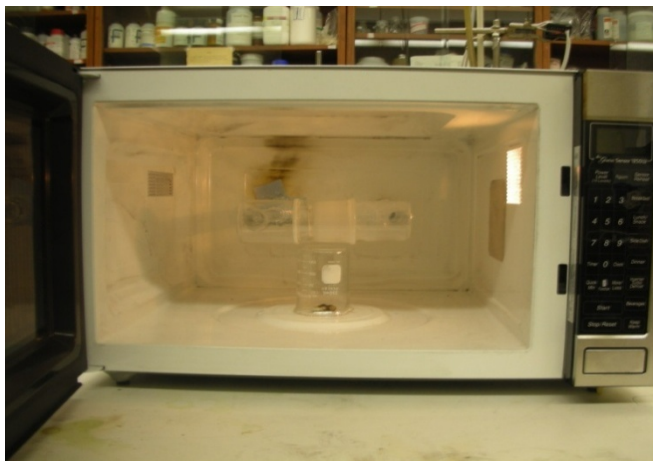


Figure 11: Microwave quartz reactor in microwave oven

Noncombustible silicon carbide (SiC) mats (plain weave ceramic grade Nicalon cloth, COI Ceramics, UT) were used in this oven to provide adequate mechanical support for the PAN nanofiber filter media. The experimental set-up for the in-flight tests is shown in Figure 12.

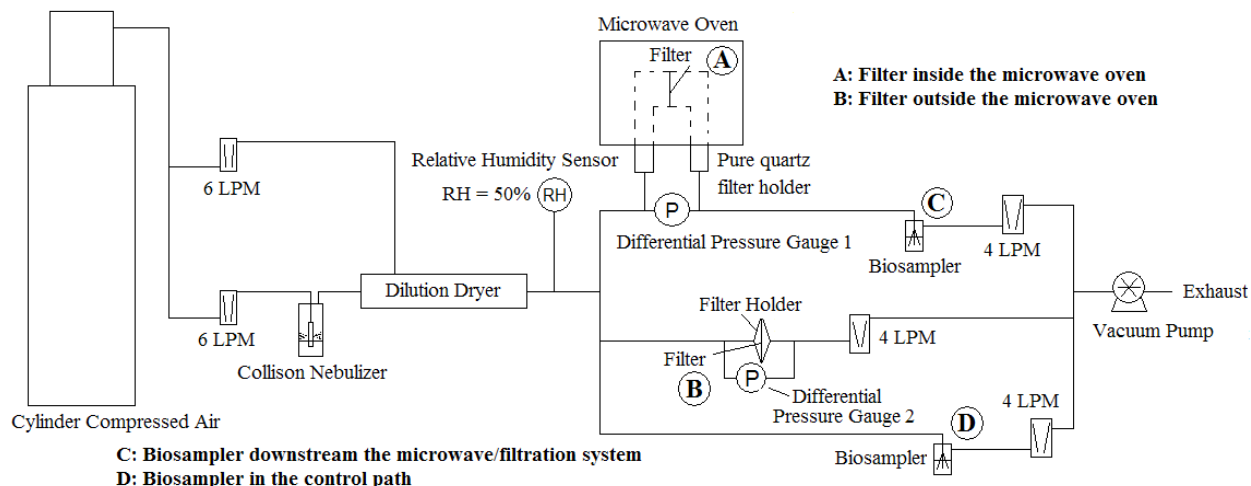


Figure 12: The schematic diagram of the microwave online testing system

The air flow rates supplied to the nebulizer and the dilution dryer were both set at 6 LPM to produce a suitable relative humidity (about 50%) for the biological testing. After the dilution dryer, the air flow was split equally into three paths of 4 LPM each. The first path was directed to the quartz filter holder inside the microwave oven. The pressure drop across the filter was monitored by a differential pressure gauge and the flow rate across the microwave/filtration system was adjusted according to the pressure drop. The corresponding face velocity across the quartz filter holder was 5.3 cm/s based on the effective filter diameter in the quartz filter holder (40 mm).

Downstream of the microwave/filtration system, the air stream was directed into a Biosampler (SKC, Eighty-Four, PA) to collect the penetrating aerosol. The second 4 LPM split stream was directed to a filter holder outside the microwave oven with an identical filter type as was present in the microwave oven. The third split stream was directed to a second Biosampler without any filter to determine the feed concentration. Low numbers of CFU were noticed in the preliminary *B. subtilis* spore data. Therefore, the flow rates of the system were increased by 25% for the spore tests.

The bioaerosol collection and inactivation was carried out for 30 minutes of three 10-minute-cycles for each experiment. Different microwave power levels and microwave application times were combined and used as microwave irradiation conditions. Experiments without filters or microwave irradiation were also conducted to ensure there was an even distribution of bioaerosols across the system. All three test microbes were tested. The results displayed a similar number of CFU/PFU for the control and experiment samples indicating no intrinsic bias.

2.4 Chemical Aerosol Testing

2.4.1 Lab-Scale Testing Apparatus

Figure 13 shows a schematic of the saturation apparatus. For the original design for the saturation apparatus, the disk holder (picture shown in Figure 14) was fabricated from aluminum bar stock. The disk sat on an expanded Teflon seal inside the one half of the holder. Another expanded Teflon seal was placed on the top of the disk. The second half of the holder was then threaded into the first half to act as a retainer. The opening across the disk was 60 mm, and the disks were 19 mm thick with a 70 mm diameter. The Collison nebulizer (BGI Inc.) was used to produce the testing aerosol. The pressure through the nebulizer was adjusted to change the rate of the nebulization. Additional air could also be added directly to the system if desired. The outlet air was bubbled through water to trap the chemical agent.

The disk holder for the saturation apparatus had to be reconstructed after testing had been started. During preliminary experiment, the two halves galled while unscrewing them. It was severe enough that the two halves could not be separated and necessitated cutting it open to remove the disk. The new configuration eliminated the potential for this problem by bolting

together the two halves with a Teflon gasket between them. The new configuration did have a smaller diameter opening at 45 mm and was slightly shorter in overall length. The rest of the system was unchanged.

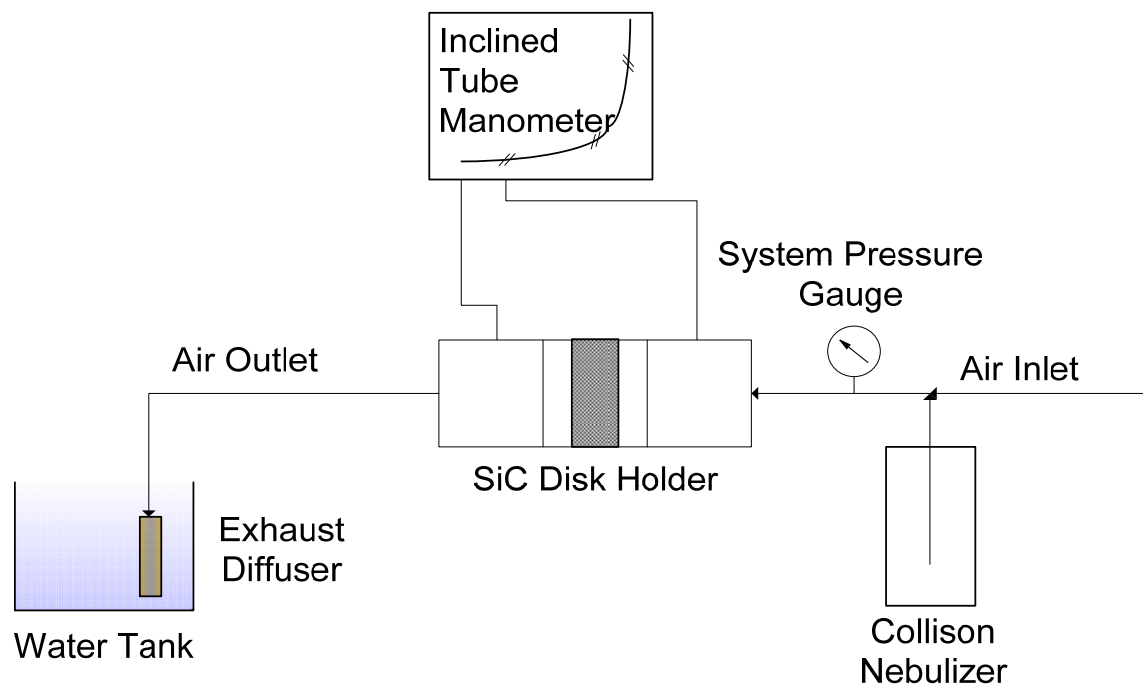


Figure 13: Experiment Schematic for the saturation testing



Figure 14: Picture of Disk Holder

After saturation, the disk was moved to a regeneration apparatus and placed inside an 80 mm quartz tube that passed through a cavity microwave applicator. Figure 15 shows the schematic for the disk regeneration system. A picture of the regeneration system is shown in

Figure 16. Process air flow could be varied up to 10.2- m³/h (6-scfh) and microwave power could be varied up to 3 kW. The outlet air from the microwave generator was bubbled through water to trap the chemical agent or its degradants.

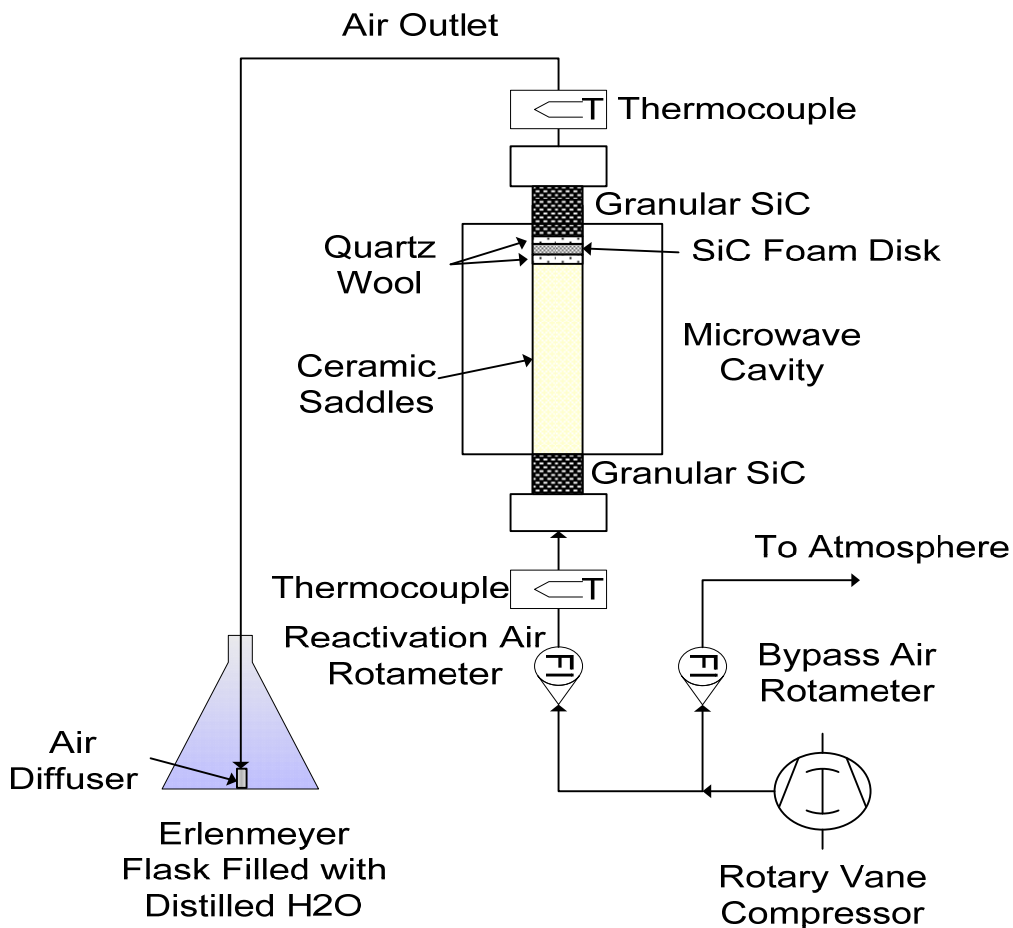


Figure 15: Schematic for Lab-Scale Regeneration Testing

Pressure drop data were taken at various air flow rates on the saturation apparatus without the nebulizer. To conduct these tests, the process air flow rate was varied. The system was allowed to stabilize at each flow rate, and then the differential pressure from the inclined manometer was recorded.



Figure 16: Picture of Microwave Disk Regeneration System

2.4.2 Saturation/regeneration procedure for lab scale testing

On both configurations for saturation testing, the pressure through the nebulizer was varied to give the desired face velocity. Changing the pressure also changed the rate of nebulization. For testing fiber mats, each mat was trimmed to fit, then placed on a SiC disk that had first been smoothed with sandpaper in order to avoid damage to the disk. The outlet air from the disk holder was bubbled through water (about 4.5-L water; actual amount determined by mass) to trap chemical agent that was not captured by the filter, and the water was analyzed to determine the amount of the agent. Saturation tests were performed at various nebulizer pressures using dimethyl methylphosphonate (DMMP) for 20 minutes. Disk mass was determined before and after saturation for weight gain by capturing aerosol. For determination of DMMP in the water, a phosphonate water test that is specific for phosphonates only was used.

It converts phosphonate to orthophosphate and measures it as that, with appropriate blank samples to subtract background. The aerosol collection efficiency was calculated based on the amount of DMMP collected on the disk and in the water. At this time there is no known method to measure the amount of DMMP presented to the disk; hence, this is the most accurate determination available at the moment. It was possible that some DMMP that was bubbled through the water was not collected. However, since it was water soluble, the amount that was not captured in water should be negligible. It was also unknown how much that passes through the disk was lost to the system before reaching the water. Overall the system was relatively long and allowed for loss of the aerosol on the walls. DMMP was occasionally noticeable in the system as a film, but there were no noticeable pools of DMMP.

Regeneration tests were performed at various microwave powers for 20 minutes with or without an initial microwave warm-up of five minutes. Either air or nitrogen could be used at various flow rates. Disk mass was determined before and after regeneration to determine weight loss, which was then compared to the weight gain during saturation to determine the percent efficiency of the regeneration process. The outlet gas was passed through about 1.8-L water (actual amount determined by mass) to collect any DMMP or degradants that did not completely oxidize. The DMMP was determined as in the saturation testing. The inorganic phosphate was tested as acid hydrolyzable phosphates, which included meta-, pyro- and other polyphosphates, as well as orthophosphate. This test is an accepted USEPA method for water analysis and converts the analyte to orthophosphate and measures it as that, with appropriate blank samples to subtract background. The reported phosphorus recovered in water was the determined phosphonate plus the determined inorganic phosphate collected in the water during microwave regeneration, converted to DMMP equivalent by mass. This was compared to the total amount

of DMMP lost from the disk to determine the actual destruction capability of the regeneration process. What was not recovered was presumed to be destroyed.

2.4.3 Bench-scale testing apparatus

The first reactor for bench-scale testing was designed and built to use porous SiC tubes supplied by Vesuvius Ceramics. Figure 17 is the process flow diagram for the bench-scale system, and Figure 18 is a picture of this system. The contaminated air flowed into one end of the tube, with the other end being closed. The air passed through the porous tube and into the cavity. The tubes were 115 mm OD, 75 mm ID, and 200 mm long with two different pore sizes: 500 and 250 μm . The tube was sealed in the cavity with a set of compression end caps. The bottom cap was solid and fixed. The top cap consisted of a collar that was fixed to the top of the cavity, and a cap that was inserted into the collar and bolted down, compressing the tube and sealing the ends with graphite gaskets. The chemical inlet was in this cap. During construction, some difficulty was encountered sealing all of the seams in the cavity. High temperature silicone was applied to the seams to seal the system. Once the cavity was sufficiently sealed, it was mounted in a rack and connected to an existing 3 kW Cober microwave generator. This unit was used to perform both saturation and regeneration experiments. For saturation experiments, the air compressor provided air to the nebulizer to give the desired flow and nebulization rates. Additional process air was added to dilute the aerosol and bring the overall flow rate up to the desired level. For reactivation testing, only process air was injected, and microwaves were applied to the cavity. In addition, direct oxidation experiments were run where the microwaves were applied to the cavity while the aerosol was being introduced.

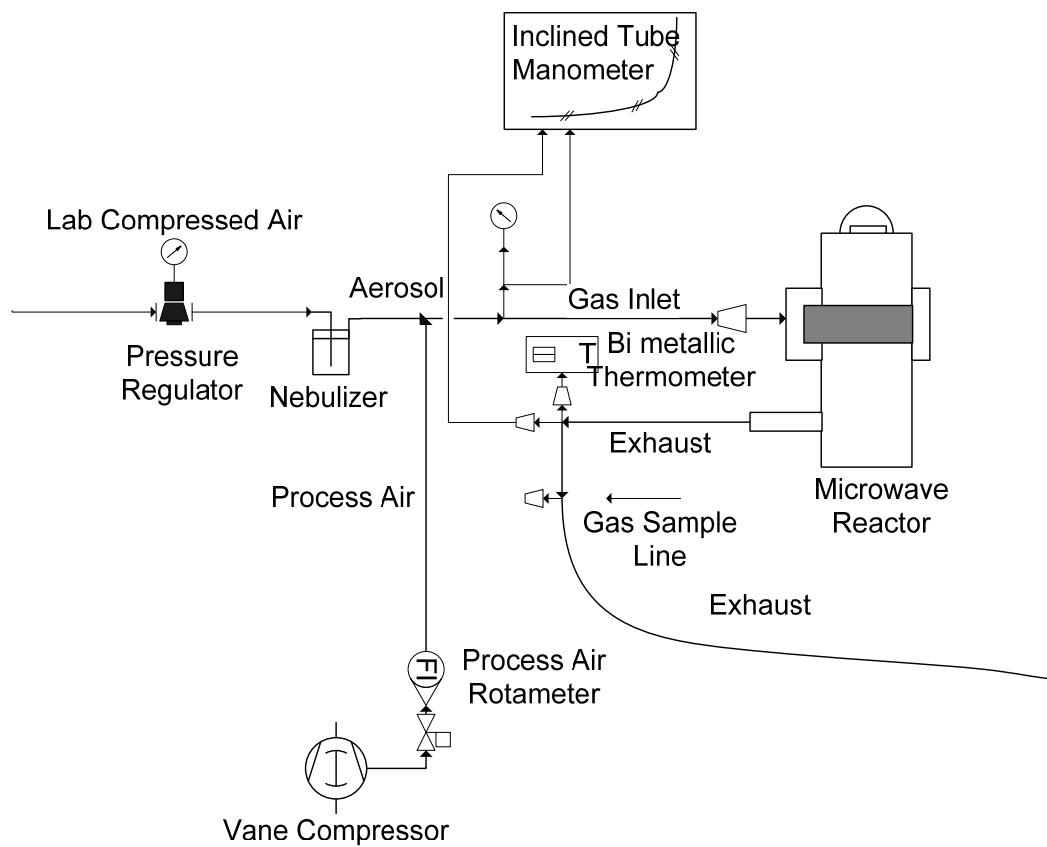


Figure 17: Schematic for Bench-Scale Testing

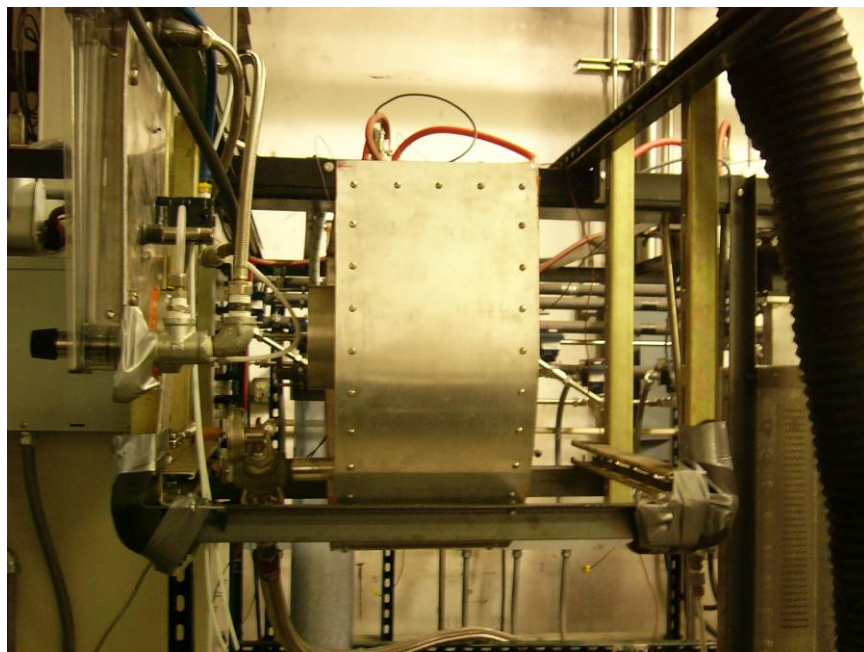


Figure 18: Picture of First Bench-Scale Microwave System

The second microwave cavity was designed and built for a newly obtained SiC tube from Refractron Tech. Figure 19 shows the picture of the second bench-scale microwave system. This tube had a 26 μm pore size and was 610 mm long with a 64 mm OD and 44 mm ID. The smaller pore size should allow better collection of the aerosol. The top cap consisted of a collar that was fixed to the top of the cavity with an adjustable cap that was inserted into the collar and bolted down. There was also a fixed end cap at the bottom of the reactor with a gasket in the middle to prevent cavity leakage. The tube was put into compression by tightening bolts through the adjustable end cap into the collar. There was a vapor outlet on the bottom plate. The caps were designed to hold a SiC tube with an eighth inch gasket between the cap and the tube. The bolt through design allowed for different lengths of bolts so the bolt heads would remain flush to the top of the adjustable end cap. The reactor was designed such that a second, inner SiC tube could also be added. This second SiC tube had a 42 μm pore size and was 610 mm long with a 36 mm outer diameter and a 25 mm inner diameter. This left a small gap between the two tubes.



Figure 19: Picture of Second Bench-Scale Microwave System

Pressure drop data was obtained on both reactors. On each, the process air flow rate was varied and the system was allowed to stabilize for five minutes at each flow rate. The differential pressure from the inclined manometer was then recorded.

2.4.4 Saturation/regeneration procedure for bench-scale testing

Saturation and regeneration tests were performed on the first reactor with each of the two SiC tubes sized for it. The second reactor was used in several different configurations for saturation and regeneration testing. The reactor was tested with the single, larger diameter SiC tube by itself and with both tubes with filters wrapped around the outside of the inner tube. For tests with the filters, several filter configurations were used: a single layer, a double layer, a double layer with five narrow strips at regular intervals. The filter used was a Lydair HEPA grade 4450HS filter. The filter was lightly glued down to initially hold it in place, then wrapped with quartz thread to hold it in place once the glue was burned off in the microwave. For the double layer with strips, the strips should restrict flow at those points and spread out the DMMP through the tube more evenly. The top, inner edge of each tube was blocked with metallic tape to a half inch below the top edge of the microwave cavity to prevent bypass, and the bottom of the tube was completely plugged for about 3 cm with a high-temperature, air-setting refractory ceramic cement. In addition, the single and double layer configurations were tested without the ceramic plug.

Regardless of the microwave cavity used, all saturation testing was set so that both the nebulizer pressure and the additional air flow rate could be varied. For the second reactor, the outlet air was bubbled through about 11-L water (actual amount determined by mass) to collect any DMMP that was not collected on the SiC tube. The water was then tested for phosphonate content. Experimental time was also varied between different tests.

Aerosol collection efficiency for the first reactor was calculated as the DMMP collected on the SiC tube divided by the weight loss of DMMP in nebulizer. It did not take into account the amount of DMMP lost to the system that never reached the SiC tube. Consequently, the collection efficiencies calculated were much lower than the actual efficiencies. For the second reactor, collection efficiency was calculated based on the mass loss of DMMP in the nebulizer and the amount of DMMP collected in the water. This did not take into account any DMMP lost to the system before and after passing through the SiC tube. The mass of the SiC tubes for this reactor was too high to meaningfully measure the small weight gain and loss of the DMMP.

For regeneration, testing was performed at various microwave powers for various times at different air flow rates. The outlet air from the SiC tube was bubbled through a known mass of water to collect any DMMP, degradants, or oxidized phosphorus that was released upon regeneration. The water was tested for both phosphonate and inorganic phosphate.

For the first bench-scale reactor, the percent regeneration efficiency was based on the weight loss of the tube compared to the weight gain during saturation. For the second bench-scale reactor, the phosphorus recovered in water was the sum of both the determined phosphonate and the determined inorganic phosphate collected in the water during microwave regeneration, converted to DMMP equivalent by mass. The phosphorus recovered as percent of aerosol collected in SiC tube was the total phosphorus recovered during regeneration divided by the DMMP collected in the tube during saturation. It was assumed that the DMMP not collected was destroyed. Hence, the destruction efficiency is based on the amount of DMMP collected during saturation and the amount recovered in the water during regeneration. Since work with the first reactor showed regeneration of the SiC tube under all regeneration conditions, it was assumed on the second reactor to completely regenerate as well.

2.4.5 Direct Oxidation Procedure

Tests were done to examine the possibility of directly oxidizing DMMP aerosols in air using the bench-scale system rather than first capturing the aerosols in the SiC tube and then oxidizing captured aerosols afterwards. Tests were done on the first reactor with each of the two SiC tubes sized for it. The second reactor was used in several different configurations: with the single, larger tube, with both tubes, with both tubes packed with fine grit SiC granules, and with both tubes with a layer of a Lydair HEPA grade 4450HS filter on the outside of the inner tube. The top of the tubes was blocked by sealing the inner surface of each tube to a half inch below the top edge of the microwave cavity with a metallic tape. For tests with the Lydair filter and for some of the tests with the SiC granules between tubes, the bottom of the inner tube was sealed with the ceramic coating as described in the Saturation/Regeneration procedure.

Regardless of the microwave cavity used, all direct oxidation testing was set so that the nebulizer pressure, the additional air flow rate, and the microwave power could be varied. Tests were run for one hour. The outlet was analyzed in one of two ways: direct measurement by a Total Hydrocarbon (THC) Analyzer or by bubbling the outlet air through 11-L water (actual amount determined by mass) and analyzing for organic and inorganic carbon or phosphorus content. A minimum 20 min preheat period with process air was used to warm up the chamber.

When the THC Analyzer was used, THC readings were recorded at five minutes intervals. When testing for carbon, the carbon was tested on a Total Organic Carbon (TOC) analyzer which was capable of testing total carbon (TC) and inorganic carbon (IC) and was reported as carbon. For TC, the entire sample was combusted and the CO₂ generated was measured. For IC, the sample was reacted with acid to convert carbonates to CO₂ and the CO₂

measured in the gas released. The organic carbon was determined as the difference between TC and IC.

3. RESULTS AND DISCUSSION

3.1 Materials Research

3.1.1 Electrospinning TiO₂ Nanofibers

Table 2 and Figure 20 are the results of characterization on the fiber diameter. The number of measurement for diameter of TiO₂ nanofiber was over 150 for each sample. d_f of nanofibers was 149 nm and coefficient of variation (C_v =standard deviation/mean) was 0.24. d_f of TiO₂ nanofibers were about 25% with narrower fiber diameter distribution compared to that of HEPA filter fibers.

Table 2: Analysis result on fiber diameter.

	TiO ₂	Millipore HEPA	Military HEPA
d_f (nm)	149	619	527
C_v	0.24	0.77	0.75

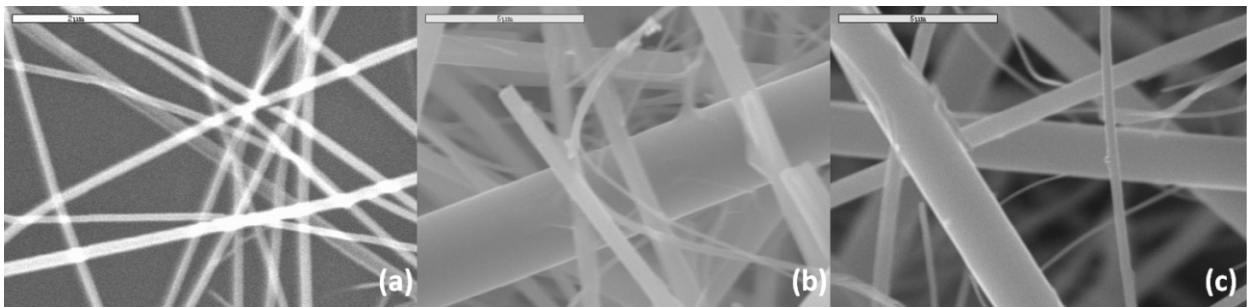


Figure 20: SEM image of (a) TiO₂ nanofibers, (b) Millipore HEPA and (c)military HEPA.

Scale bars are (a) 2 μm, (b) (c) 5 μm.

When the Stoke's law in Equations 1 and 2 is applied with the average diameter of HEPA filter fibers and TiO₂ fibers—573 nm and 149 nm, respectively— F_D of TiO₂ fibers is expected to

be reduced to 8.27% of HEPA, which implies a dramatic decrease of pressure drop as well. Furthermore, narrower fiber diameter distribution than fibers of HEPA filters leads to superior quality control for the filtration media.

3.1.2 Microstructure of TiO_2

TEM images (Figure 21) show that the grain size of 700 °C-, 800 °C- and 900 °C-heat-treated samples are larger than those of 500 °C- and 600 °C-heat-treated samples.

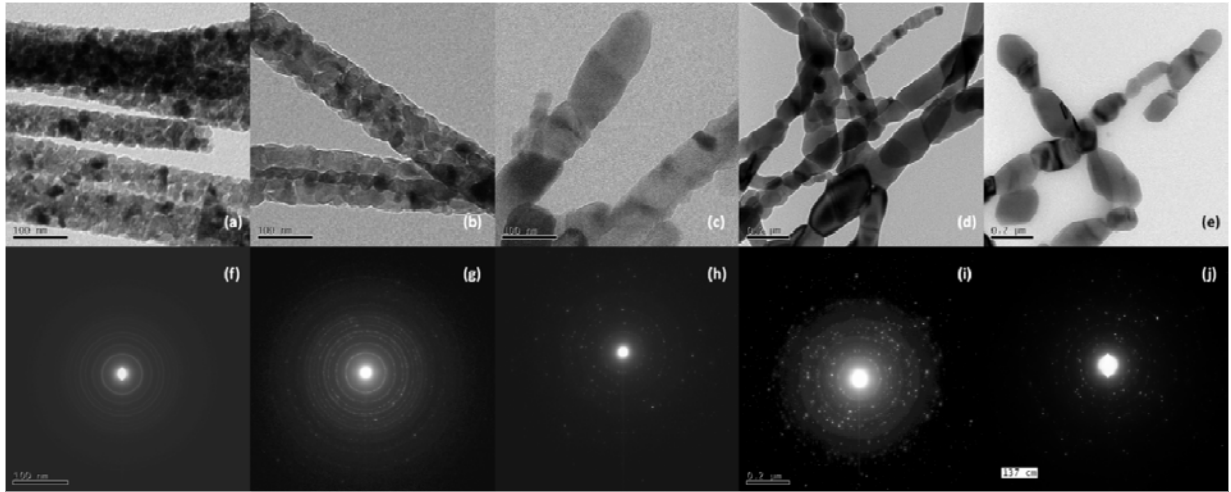


Figure 21: TEM images (a, b, c, d, e) and diffraction patterns (f, g, h, i, j) of electrospun TiO_2 fibers heat-treated at different temperature for 3 hours: (a, f) 500 °C, (b, g) 600 °C, (c, h) 700 °C, (d, i) 800 °C, (e, j) 900 °C.

Electron diffraction patterns of TEM indicate orientation of crystalline structure in the grain. If the sample is a single crystal, it shows corresponding spots without rings. If the sample is polycrystalline, each single crystal—grain—induces corresponding spots at different rotating angles which eventually form rings. If the sample is amorphous, diffraction pattern looks similar to that from polycrystalline material, but the rings are broader¹⁴. For the result of heat-treated samples at different temperatures, diffraction patterns show distinctive spots for samples heat-

treated at higher temperatures (Figure 21 (h, i, j)) which is because of the larger and fewer grains in a frame. The morphology of samples and the diffraction patterns agree to the result from the literature¹⁵.

In regard to the grain size shown in Table 3 analyzed based on the XRD result in Figure 22 after different heat treatment times and temperatures, it tended to increase at higher temperature for longer time. As rutile phase develops in the sample of 500°C-5 hours and 600°C-5 hours, anatase phase got less dominant. Peaks for rutile could not be detected by the analysis program—Origin[®] ver.8.0—for samples of 500°C-3 hours and 600°C-3hours.

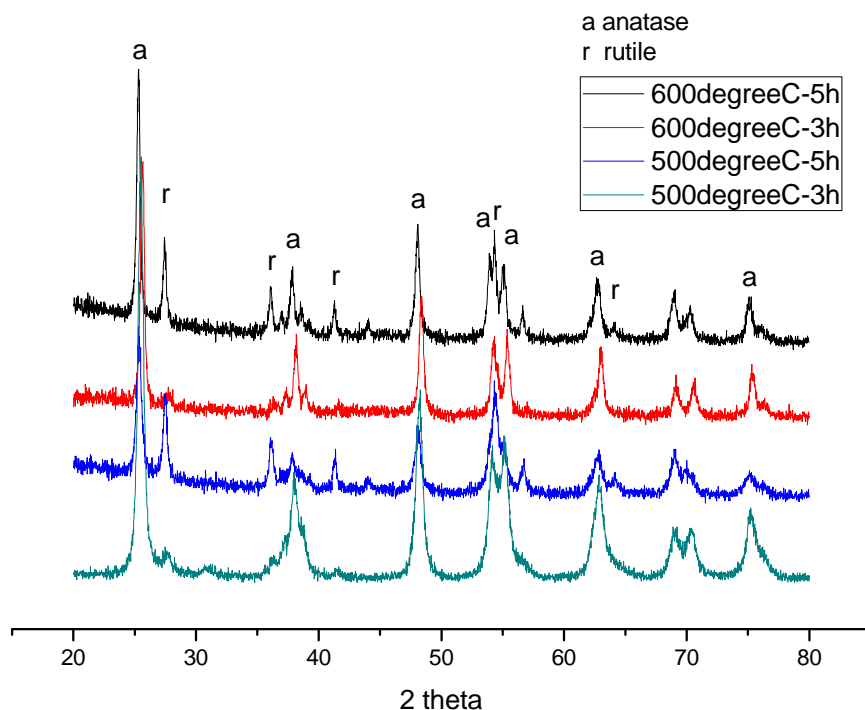


Figure 22: XRD patterns of TiO₂ that were heat-treated at various temperatures and times.

Table 3: Grain size of different TiO₂ phases after different heat treatment.

	500°C-3 hours	500°C-5 hours	600°C-3 hours	600°C-5 hours
anatase	16	27	22	24

rutile	-	25	-	32
--------	---	----	---	----

Figure 23 is the XRD patterns of electrospun TiO_2 fibers from precursor sols of different mixing ratios—TB:AA=1:0~1:16. Sharp peaks at 33° and 70° from some samples were from the silicon wafers used as the substrate. Grain size for each sample was calculated by Scherrer's equation and shown in Figure 24. In order to achieve the smallest grains for higher yield strength, the heat treatment temperature should be lowered and the time should be shortened. Among the experimental conditions that we've tested, 500°C for 3 hours was the best condition to get the most mechanically stable fibermats. With varying molar ratio of TB:AA, the grain size did not change significantly at higher AA content than TB:AA=1:4.

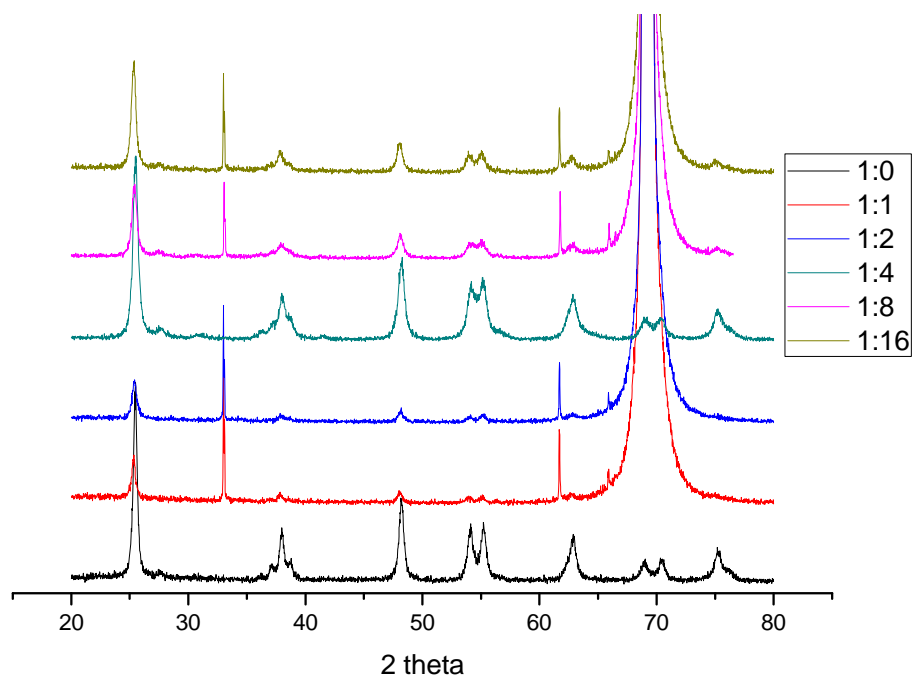


Figure 23: XRD patterns of TiO_2 fibers of different mixing ratios of precursors, TB:AA from 1:0 to 1:16 with fixed molar ratio of EtOH at 20.

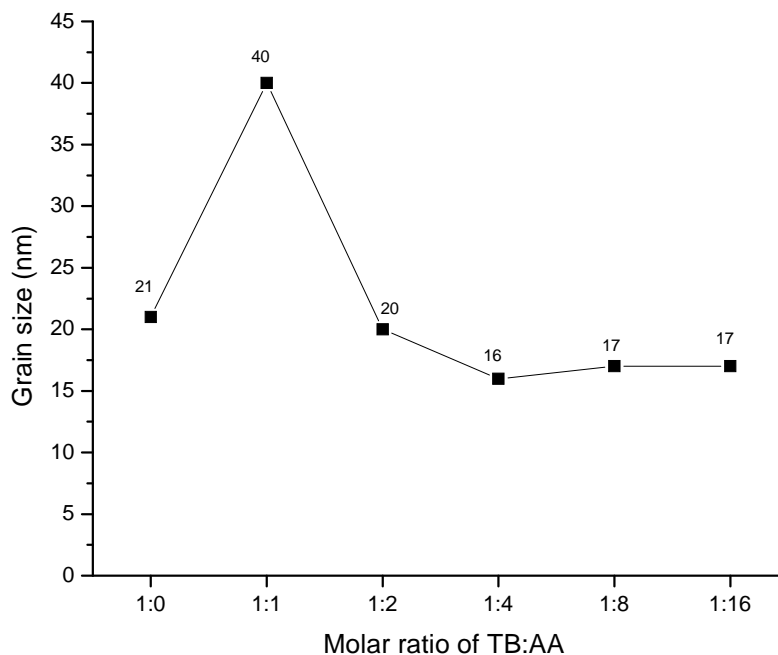


Figure 24: Grain sizes of samples with different molar ratios of TB:AA from 1:0 to 1:16.

3.1.3 Aqueous Sol

Overall, d_f decreased at similar shrinkage rate and C_v of fiber diameters increased through the heat treatment (Figure 25, Table 4). Samples are named as concentrations of [(PVP)-(F108)] in the unit of %w/v sol. Only the fiber diameters of 1100°C-3h samples were compared because they are thinner than the other two samples and composed of the desired crystalline phase—anatase. The advancement of the pure aqueous sol-gel chemistry of highly reactive species allowed a breakthrough in mechanical properties for nanofibermats. Mechanically stable nanofibermats were synthesized as shown in Figure 26.

In regard to the fiber diameters of electrospun fibers, C_v of [0.25-0.25] for 1100°C-3h in Figure 25 is abnormally high but still much lower than C_v of commercial HEPA filter fibers, 0.75 (Table 2). When [0.5-0] and [0.25-0] were compared, d_f decreased from 1877 to 960 and C_v increased from 0.16 to 0.22. When F108 was added, d_f decreased with similar C_v s except [0.25-0.25] of erratically high value. Therefore, as long as the fibrous morphology is retained, PVP

concentration should be decreased for thinner fibers. Effect of F108 concentration is not obvious but it is evident that the existence of F108 helps to reduce d_f .

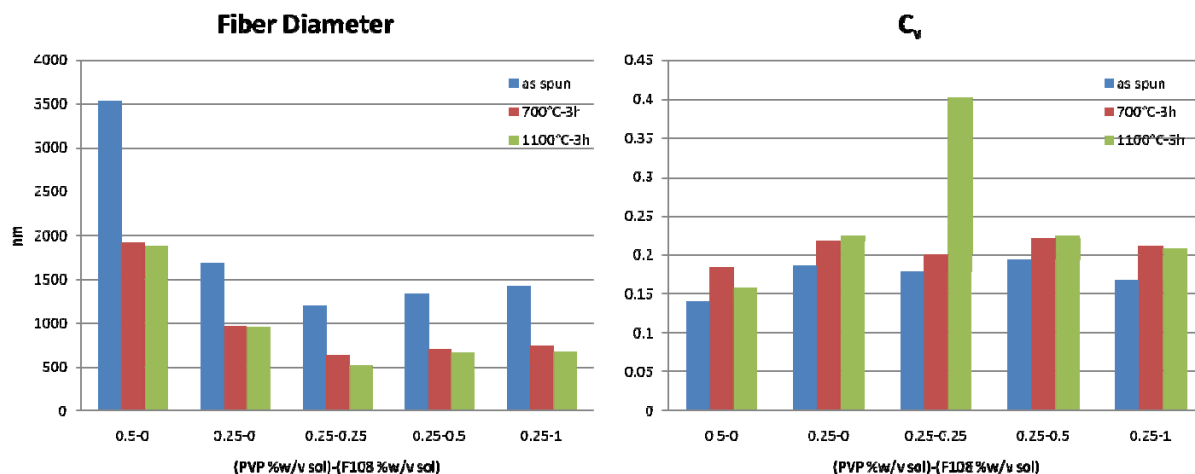


Figure 25: d_f and C_v of samples with different PVP and F108 concentrations.

Table 4: (Heat-treated fiber)/(as-spun fiber) diameters in percentage.

%	0.5-0	0.25-0	0.25-0.25	0.25-0.5	0.25-1
700°C-3h	54	58	53	53	52
1100°C-3h	53	57	44	50	48

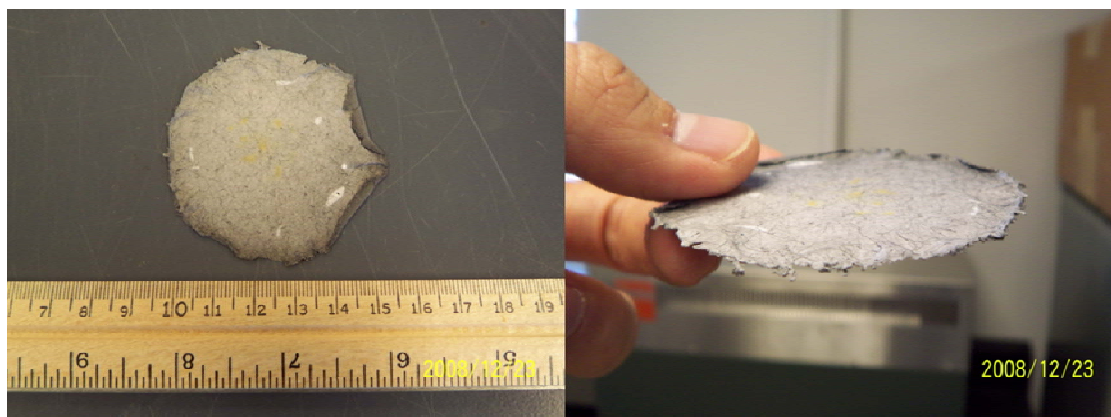


Figure 26: $\text{TiO}_2\text{-SiO}_2$ composite nanofibermat.

With ever higher temperatures the rutile phase develops, and anatase finally is fully transformed into rutile with larger grain size. The new aqueous process achieved a very different result. Heat-treatment was for 8 hours. Characterization by XRD shows development of anatase phase at over 900 °C while the TiO₂ from conventional EtOH-AA-TB sol crystallized as anatase at 500 °C within 3 hours (Figure 27). The broad peak around $2\theta = 22^\circ$ is assigned to amorphous SiO₂¹³ that originated from chemical aids of the aqueous sol-gel process. The sample was also heat-treated at 1100 °C for 3 hours (1100°C-3h) for comparison with 1100°C-8h in order to see effect of heat treatment time (Figure 28). Table 5 shows the grain sizes of anatase in each sample calculated by Equation 4.

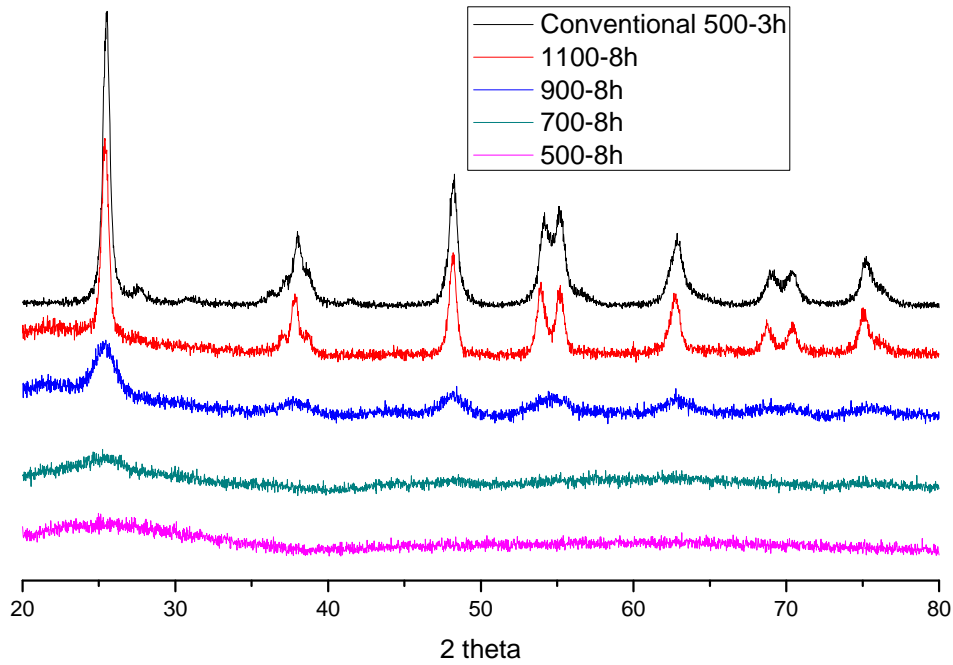


Figure 27: XRD patterns of samples at different temperature for 8 hours. For comparison, anatase peak from conventional TiO₂ precursor sol is added on top.

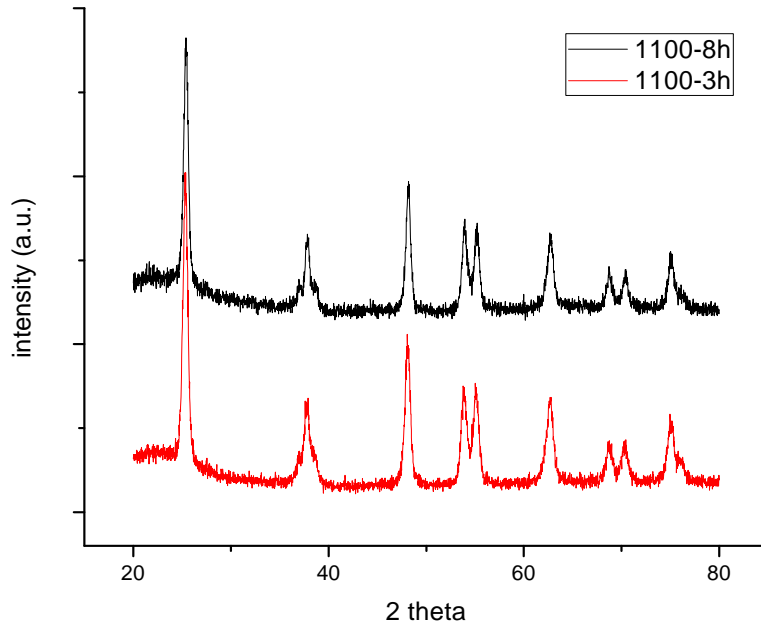


Figure 28: XRD patterns of samples with different heat treatment time at 1100 °C.

For reference, PVP and F108 degrade at under 400 °C and 250 °C, respectively. With different heat treatment times, the anatase grain size of 1100°C-3h sample was 14nm which is 2 nm smaller than that of 1100°C-8h sample (Table 5). The XRD patterns along with the calculated grain sizes (Table 5) indicate a change in transformation and grain growth rate. Therefore, it was concluded that a Ti-O-Si bond forms that hinders the crystallization of anatase. In addition to the shorter processing time, since the material with smaller grain size tends to have higher yield strength according to Hall-Patch equation, heat profile of 1100°C-3h is preferred.

Table 5: Comparison of anatase grain size from conventional sol and aqueous sol.

Grain size (nm)	Heat Treatment Temperature (°C)			
	500	700	900	1100
Conventional sol for 3 hours	16	28	R	r
Aqueous sol for 3 hours	N/A	α	N/A	14
Aqueous sol for 8 hours	α	α	6	16

α : amorphous, r : rutile

Figure 29 is the TG graph of electrospun fiber (aqueous sol+PVP), PVP, and aqueous sol system without PVP (aqueous sol). The temperature ranged from 25 °C to 1600 °C for [aqueous sol+PVP] and [aqueous sol] while from 25 °C to 1000 °C for [PVP].

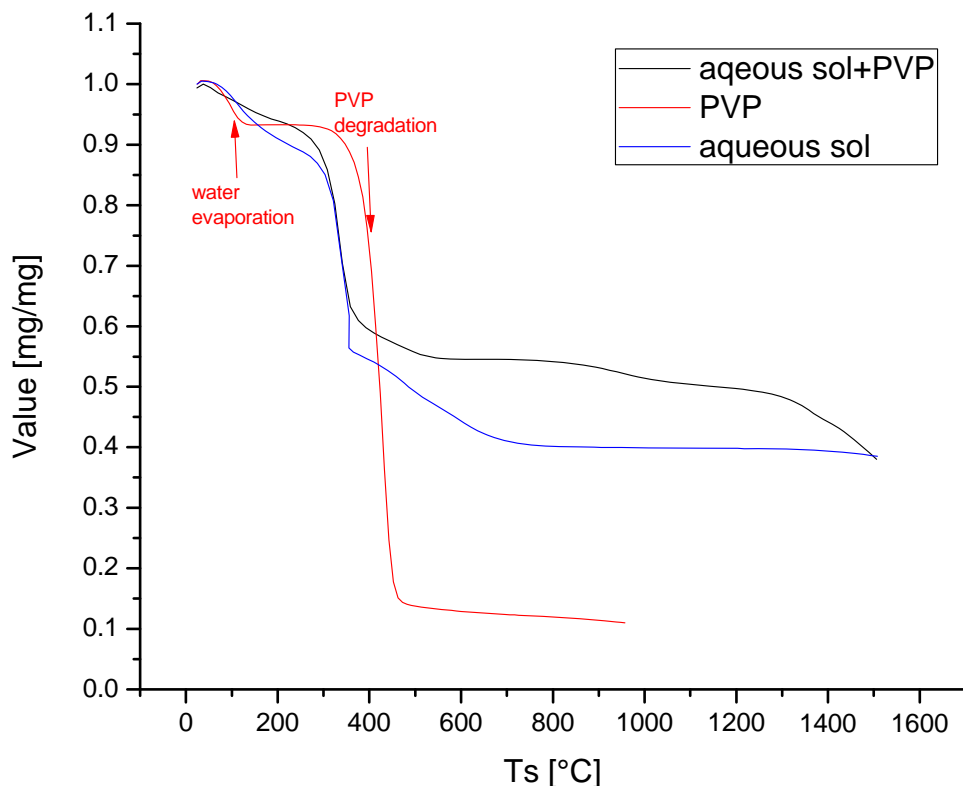


Figure 29: Thermogravimetric diagram for electrospun fibers from aqueous sol and PVP.

The weight loss of [PVP] sample at around 100 °C was due to evaporation of water that was absorbed by the polymer, and the weight loss at around 400 °C was by the PVP degradation. For the data from [aqueous sol], there was a weight loss at around 300 °C and continuous weight loss followed until around 700 °C. For [aqueous sol+PVP] sample, PVP degradation was not clearly observed due to its relatively low weight ratio—10%—in the whole sample while the weight loss at 300 °C was obviously shown. The weight loss at over 1400 °C was not observed in the [aqueous sol].

Mixture of GPTMS and HNO_3 was investigated by ^{13}C -NMR. The orange wedges in Figure 30 show the carbons in the transition state. As more HNO_3 was added, GPTMS got more hydrolyzed.

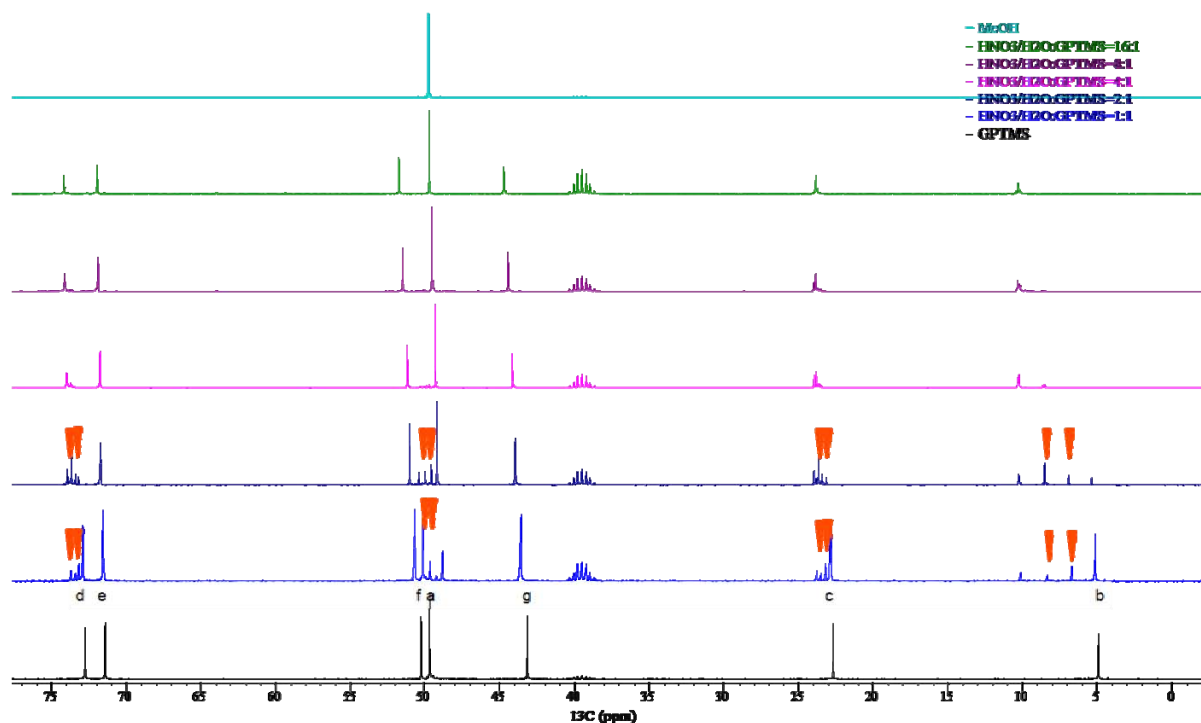


Figure 30: ^{13}C -NMR spectra of (from bottom to top) pure GPTMS, mixture of HNO_3 and GPTMS at molar ratio of 1:1, 2:1, 4:1, 8:1, 16:1 and methanol. The orange wedges show the peaks from transition states.

Chemical reaction with the addition of TB to the $[\text{HNO}_3:\text{GPTMS}=2:1]$ sol was studied by ^{13}C -NMR as well. Molar ratio of the final sol was $\text{HNO}_3:\text{GPTMS}:\text{TB}=2:1:1$, and it was selected because this mixture was typically used in electrospinning with PVP. In Figure 31, the sol of the third spectrum from the bottom is from the mixture of two below it. Orange wedges in Figure 31 indicate the formation of 1-butanol which is the byproduct in Figure 4. The enlarged spectrum of

[HNO₃:GPTMS:TB=2:1:1] sol in Figure 32 confirmed the existence of carbons from GPTMS and methanol indicated by a blue wedge.

In the NMR study of HNO₃-GPTMS sol, at the molar ratio of HNO₃:GPTMS=4:1 or higher, peaks from transition states were not observed which meant full hydrolysis. The peak of carbon *a* (described in Figure 3) shifted downfield to form a peak for methanol which is the byproduct of the reaction in Figure 3. Therefore, the proposed reactions in Figure 3 are confirmed.

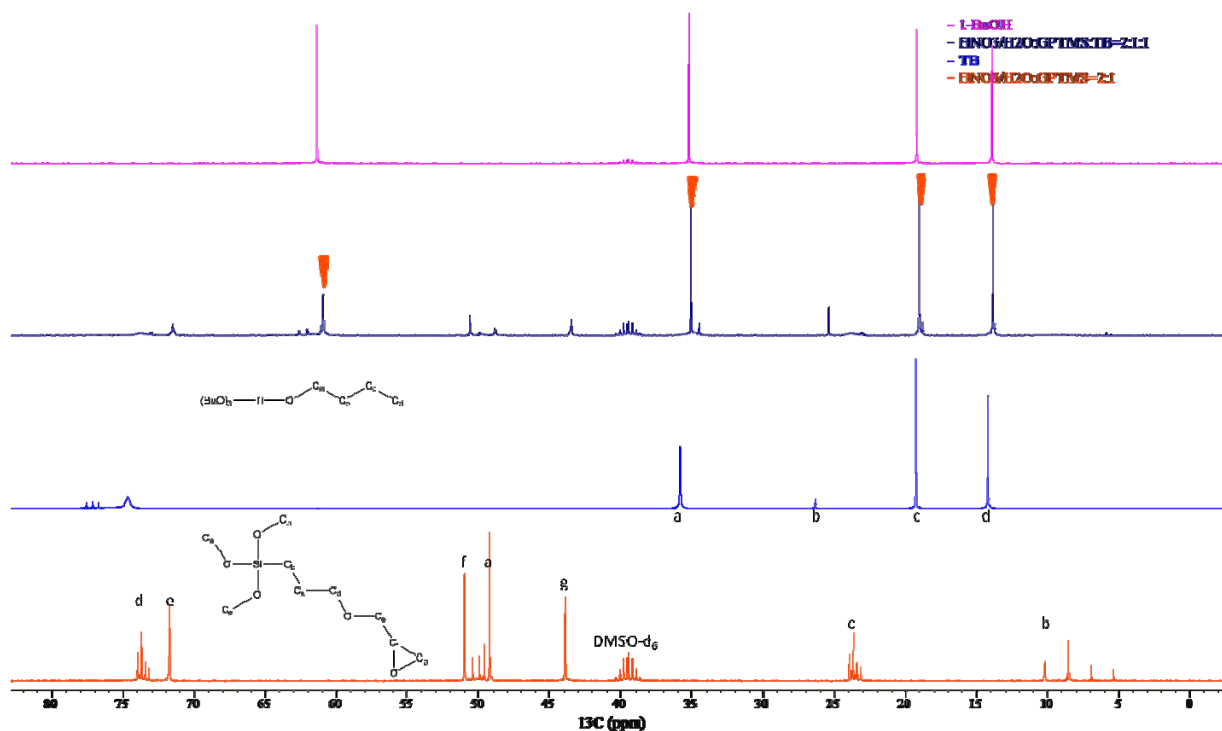


Figure 31: ¹³C-NMR spectra of HNO₃:GPTMS=2:1, TB, HNO₃:GPTMS:TB=2:1:1 and 1-butanol (from bottom to top). The orange wedges show the peaks of 1-butanol.

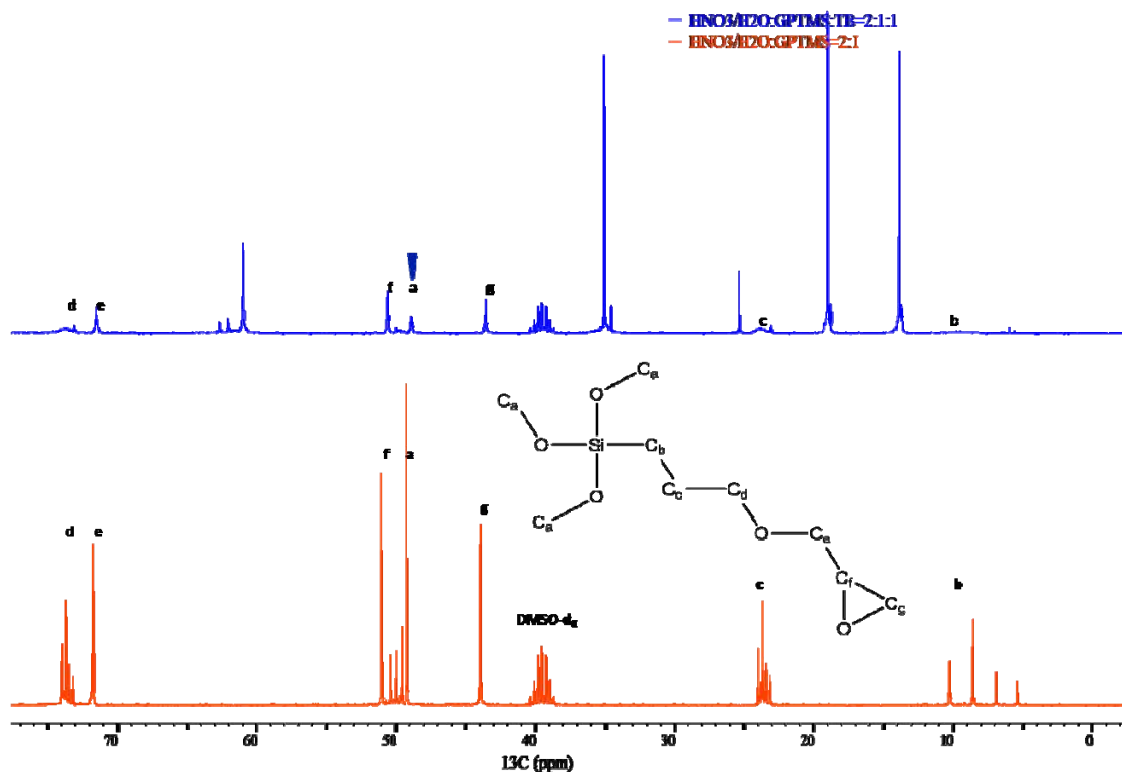


Figure 32: ^{13}C -NMR spectra of (from bottom to top) $\text{HNO}_3\text{:GPTMS}=2\text{:}1$ and $\text{HNO}_3\text{:GPTMS:TB}=2\text{:}1\text{:}1$. The blue wedge shows the peak of methanol.

3.1.4 PAN Nanofiber Filter Fabrication Results

Figure 33 shows SEM images of current HEPA filters (a, b with scale bars of $5\ \mu\text{m}$) and electrospun PAN fibers (c, d with scale bars of $2\ \mu\text{m}$). Figure 34 contains the results for fiber diameter picture analysis. Fiber diameters were 619 nm, 527 nm, 212 nm and 195 nm while C_v 's were 0.77, 0.75, 0.21 and 0.17 for Millipore HEPA, military HEPA, as-spun PAN and crosslinked PAN, respectively. As shown, PAN fibers were about 35% in fiber diameter and 25% C_v compared to fibers that compose HEPA filters. When the Stoke's equation is applied with average diameter of HEPA filter fibers and PAN fibers—573 nm and 203.5 nm, respectively— F_D of PAN fibers is expected to be reduced to 24.3% of HEPA, which implies a dramatic decrease of pressure drop.

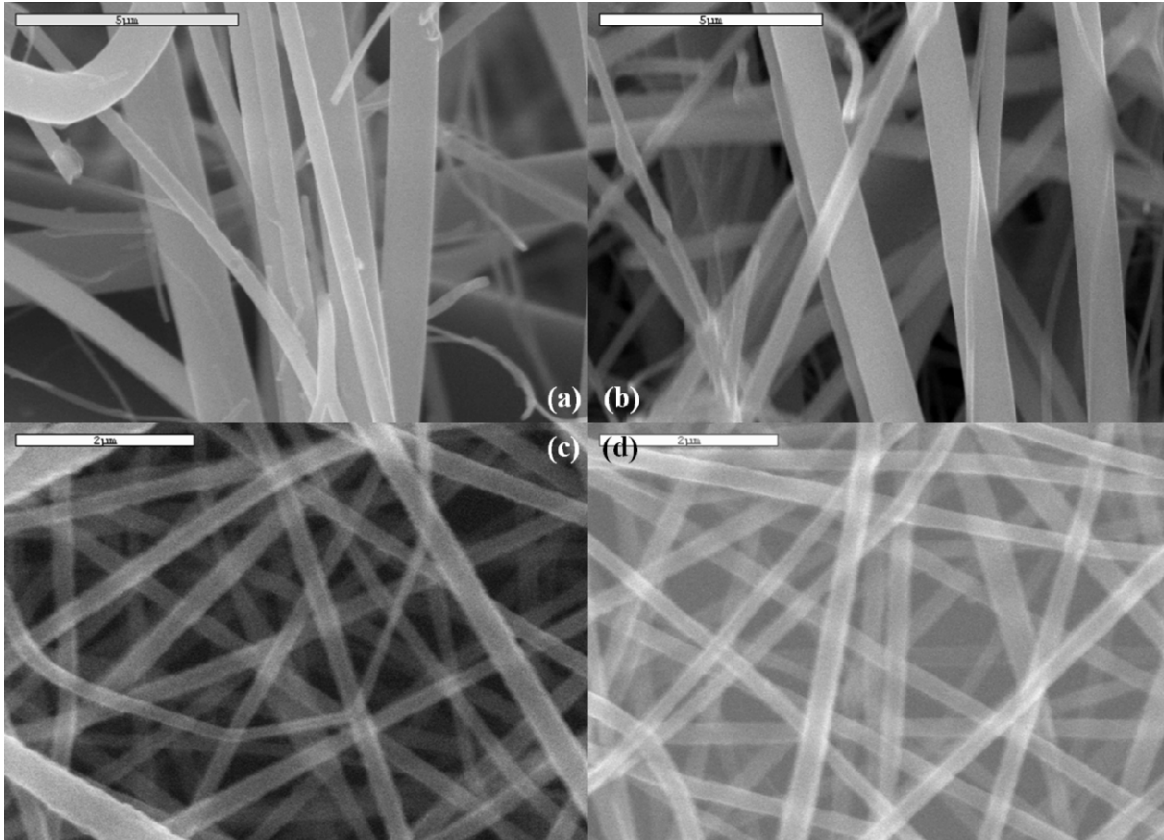


Figure 33: SEM images of (a) military HEPA filter, (b) Millipore HEPA filter, (c) as-spun PAN fibers and (d) crosslinked PAN fibers. Scale bars are 5 μm for (a, b) and 2 μm for (c, d).

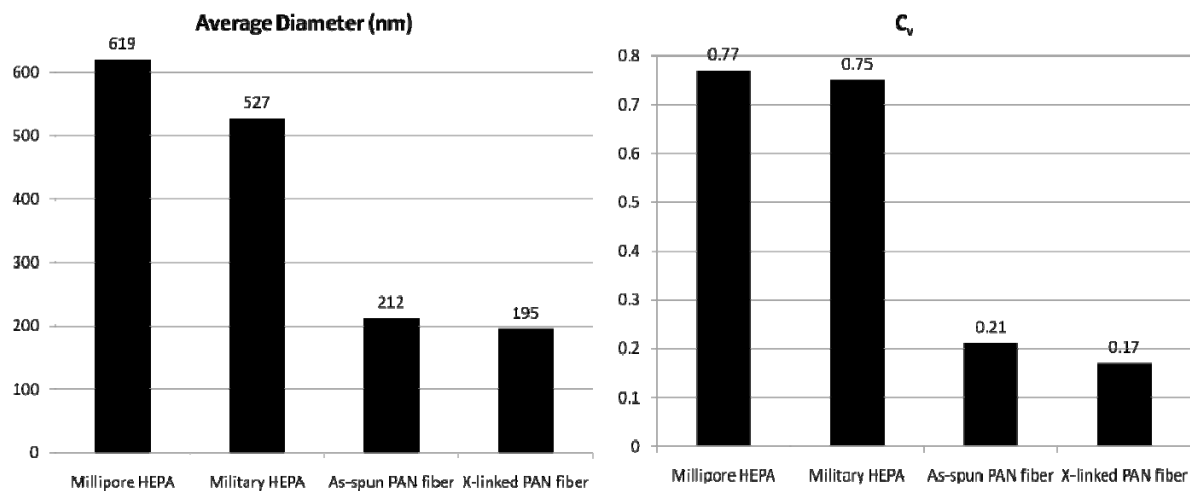


Figure 34: Average diameter and C_v for Millipore HEPA filter, Military HEPA filter, as spun PAN fiber and cross-linked (X-linked) electrospun PAN nanofiber. Y-axis for left diagram is for diameter in nm. Y-axis on right plot is for C_v .

3.2 Physical Collection Efficiency Experiments

3.2.1 Physical Tests of PAN Nanofiber Filters

Three batches of PAN nanofiber deposited on the activated carbon fiber (ACF) mats were tested using the system shown in Figure 5. Four PAN nanofiber mats deposited for 15, 20, 25, 30 mins of Batch A, four PAN nanofiber mats deposited for 60, 90, 120, 150 mins of Batch B, and three mats deposited for 30, 60, 90 mins of Batch C were tested. Batch A was tested with NaCl particles while Batch B and C were tested with 300 nm polystyrene latex (PSL) particles. Results are listed below in Table 6.

Table 6: Physical testing results^a of PAN nanofiber filters

Filter	Penetration Fraction ^b (P , dimensionless)	Pressure Drop ^c (Δp , Pa)	Quality Factor (q_F , Pa ⁻¹)
PAN A ^d 15 ^e	6.02×10^{-3}	172	0.0297
PAN A 20	7.12×10^{-3}	215	0.0230
PAN A 25	1.03×10^{-3}	272	0.0253
PAN A 30	4.35×10^{-3}	340	0.0160
PAN B 60	5.50×10^{-2}	86	0.0337
PAN B 90	2.48×10^{-3}	207	0.0290
PAN B 120	1.36×10^{-5}	493	0.0227
PAN B 150	9.74×10^{-6}	725	0.0159
PAN C 30	2.42×10^{-2}	179	0.0201
PAN C 60	5.81×10^{-4}	473	0.0158
PAN C 90	2.93×10^{-4}	646	0.0128

a, the results are of PAN nanofiber only, ACF and structure effects were eliminated;

b, penetration fraction for 300 nm particles;

c, Batch A filters were tested under 7.14 cm/s, their pressure drop data were then converted to 5.3 cm/s condition, Batch B filters were tested directly under 5.3 cm/s;

d, batch symbol;

e, electrospinning deposition time.

Due to the different conditions of the electrospinning process for the three batches, the two batches should not be compared. However, comparing the data within each batch shows that the longer deposition time resulted in less penetration, but at a cost of higher pressure drop and worse quality factor. This suggests that the long term deposition may have disturbed the inner structure of the PAN nanofiber, resulting in diminished quality factor. Therefore, the strategy to get a qualified PAN filter was to overlap two or more layers of the PAN nanofiber, instead of simply increasing the deposition time.

3.2.2 Comparison between PAN nanofiber filters and conventional HEPA filters

For comparison, the military HEPA standard (MIL-F-51079D), the filtration performances of a Millipore HEPA filter (Cat. No.: AP1504700, Millipore, MA), a LydAir High Alpha HEPA (Grade 4450H), the highest quality PAN nanofiber filter among the seven listed in Table 6, and an ACF double-layer-mats are listed in Determination of PAN nanofiber filter's true most penetrative particle size

The PAN nanofiber filters used in this study had a fiber diameter smaller than conventional HEPA filters; so, their most penetrative particle size was expected to be smaller than the conventional HEPA filters. In order to determine the most penetrative particle size, physical collection tests conducted by aerosolizing polydisperse NaCl particles were analyzed to obtain a penetration curve for particles ranging from 10 to 400 nm. The typical NaCl particle size distribution of 5% wt was obtained by SMPS (Figure 35). Important statistical values are: Median: 79 nm; Geo Mean: 80 nm; Mode: 75 nm; GSD: 1.91; Total number conc.: 106 #/cc.

Table 7. As shown, the LydAir and PAN A 60 had their quality factor higher than the military standard for HEPA filters. This means that they can achieve both the minimum penetration and maximum pressure drop limit by themselves (LydAir) or multi-layer (PAN).

3.2.3 Determination of PAN nanofiber filter's true most penetrative particle size

The PAN nanofiber filters used in this study had a fiber diameter smaller than conventional HEPA filters; so, their most penetrative particle size was expected to be smaller than the conventional HEPA filters. In order to determine the most penetrative particle size, physical collection tests conducted by aerosolizing polydisperse NaCl particles were analyzed to obtain a penetration curve for particles ranging from 10 to 400 nm. The typical NaCl particle size distribution of 5% wt was obtained by SMPS (Figure 35). Important statistical values are:

Median: 79 nm; Geo Mean: 80 nm; Mode: 75 nm; GSD: 1.91; Total number conc.: 10^6 #/cc.

Table 7: Physical properties of different types of filters

Filter	Penetration Fraction ^a (P , dimensionless)	Pressure Drop ^b (Δp , Pa)	Quality Factor (q_F , Pa ⁻¹)
M-STD ^c	3.00×10^{-4}	400	0.0203
Millipore ^d	1.03×10^{-4}	783	0.0117
LydAir ^e	1.80×10^{-4}	284	0.0304
PAN A 60 ^f	5.50×10^{-2}	86	0.0337
ACF 2 ^g	8.66×10^{-1}	21	0.0069

a, penetration fraction for 300 nm particles;

b, pressure drop under 5.3 cm/s air face velocity;

c, military HEPA standard (MIL-F-51079D);

d, data revised by eliminating the system structure effects;

e, data provided by the manufacturer's specs sheet;

f, PAN nanofiber filter with the best quality factor among the seven listed in Table B2;
g, double-layer ACF mats, background.

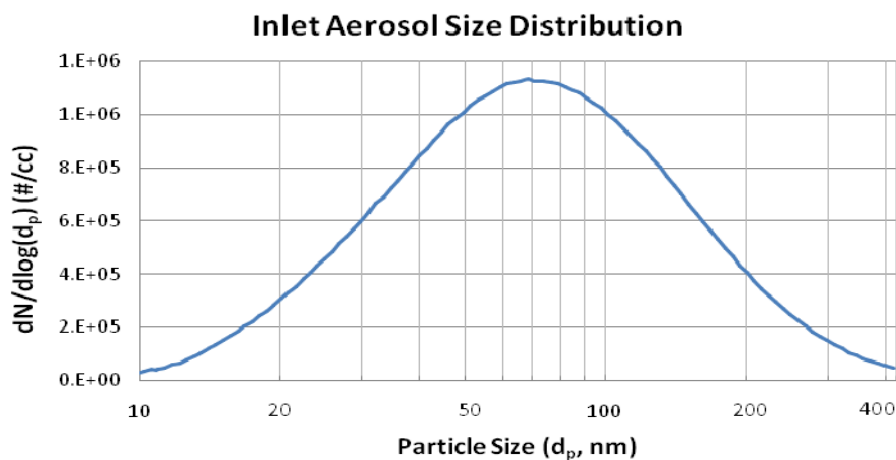


Figure 35: Particle size distribution of aerosol generated from nebulization of 5% wt NaCl solution

Figure 36 shows the 30 mins electrospun PAN nanofiber filter's penetration curve. The most penetrative particle size of that filter was less than 100 nm, which agreed with expectations.

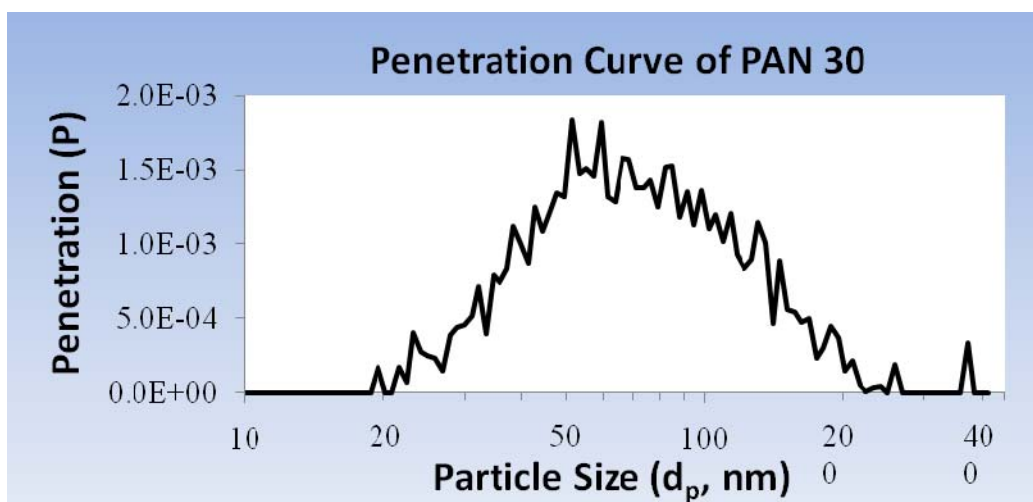


Figure 36: The penetration curve of the 30 mins electrospun PAN nanofiber filter

3.2.4 Characterization of Multi-Layer PAN Sandwich Filter

Multi-layer PAN nanofiber filters were evaluated for the physical collection efficiency to compare with the single-layer PAN nanofiber filters as proposed in section 3.2.1. Several tests for physical collection efficiency of PAN nanofiber filters (single layer or multi layers) were conducted in order to evaluate the efficiency of electrospinning deposition time. Results are shown below in Table 8.

Table 8: Physical testing results of PAN 5, 10, 15, 5*3 and 15*2

Filter	Penetration fraction	Pressure drop (Pa)	Quality factor (/Pa)
PAN 5	0.345	18	0.0591
PAN 10	0.191	61	0.0271
PAN 15	0.102	98	0.0233
PAN 5*3	0.0727	54	0.0488
PAN 15*2	0.0207	152	0.0255

The PAN x*y stands for y layers of PAN x filters. Ideally, the PAN 15 should have the same quality factor as the PAN 5*3. However, the results showed that the quality factor of PAN 5*3 was much higher than PAN 15. The phenomenon that longer-term deposited PAN fiber filters have lower quality factor was also observed in this batch of filters.

In order to demonstrate the reproducibility of the result that multi-layer filters have better quality than single-layer filters, triplicate tests for PAN 5 and PAN 5*3 (three layer of PAN 5) were carried out. The results are listed below in Table 9. Three tests within each triplicate experiment were not very different from each other. However, this time the PAN 5*3 had a better quality factor than PAN 5.

Table 9: Physical test results of PAN 5 and PAN 5*3 in triplicate

Filter	Penetration fraction	Pressure drop (Pa)	Quality factor	Filter	Penetration fraction	Pressure drop (Pa)	Quality factor
---------------	-----------------------------	---------------------------	-----------------------	---------------	-----------------------------	---------------------------	-----------------------

			(Pa ⁻¹)				(Pa ⁻¹)
PAN 5-1	0.611	17	0.0290	PAN 5*3-1	0.0749	38	0.0682
PAN 5-2	0.465	19	0.0403	PAN 5*3-2	0.0867	42	0.0582
PAN 5-3	0.493	17	0.0416	PAN 5*3-3	0.0768	42	0.0611
Avg	0.523	18	0.0370	Avg	0.0795	41	0.0625

The results shown above gave us the confidence that the multi-layer PAN filters would be a good candidate of the filtration media in this project. The project goal (< 50% HEPA pressure drop w/ > 99.97% collection efficiency) could be adjusted by multi-layers of thin PAN fiber filters. In bioaerosol testing, however, only one filter at a time was tested to determine the plausibility of using a single layered filter. This was also done to make efficient use of each filter in obtaining data.

3.3 Bioaerosol Testing

3.3.1 Static Inactivation of Test Microbes

Static inactivation tests were conducted using the system described in Figure 10 to determine the plausibility of on-filter inactivation. Table 10 summarizes the results at 500 W indicative of the general inactivation trend. Survival fraction was calculated according to Equation 5 below.

$$S = \frac{CFU_{Experiment}}{CFU_{Control}} \quad (5)$$

where S is the survival fraction, CFU is the number of colony forming units (or plaque forming units for MS2 virus) from the control or experiment samples. As shown in Table 10, in 90 seconds survival fraction dropped below the detection limit. These results suggested that

microwave irradiation can effectively inactivate microbes on the filtration media. Irradiation of *E. coli* proved especially effective with greater than 99% inactivation after 60 s.

Table 10: Survival fraction of microorganisms under 500 W microwave irradiation – Static on-filter inactivation

		Microwave irradiation time			
		30 s	45 s	60 s	90 s
<i>E. coli</i>	Mean	2.38%	–	0.46%	0.17%
	SD	3.20%	–	0.64%	0.22%
MS2	Mean	33.25%	–	4.14%	0.81%
	SD	6.34%	–	0.81%	0.34%
<i>B. subtilis</i>	Mean	74.0%	6.00%	1.26%	0.20%
spores	SD	7.42%	2.04%	0.87%	0.15%

Microwave power was held at 500 W for *E. coli* and MS2 experiments and 750 W for *B. subtilis* experiments

As shown in Table 10, microwave irradiation inactivates MS2 with a similar trend as *E. coli*, however the survival fraction of MS2 was higher than that *E. coli* because of its supposed greater heat resistance. The survival fraction of MS2 decreased as microwave power and applied time were increased.

B. subtilis spore tests show a similar trend in inactivation as the other microorganisms, but were noticeably more challenging to kill. After irradiation for 30 s., 74.0% of viable *B. subtilis* still remained on the filter. Less powerful microwave power applications, proved even less effective. For 250 W (not shown), for example, 60 s of application time was required to achieve any inactivation at all. Application times of less than one minute at 250 W resulted in zero removal of the spores on the filter. Overall, microwave application was found to be more

effective during static testing than in-flight testing to be discussed next, though the efficiency is species dependent.

3.3.2 In-flight Inactivation of Test Microbes

In-flight inactivation experiments were conducted with the system described by Figure 12. Inactivation on the filter and removal (R) from the air stream were calculated according to Equation 6 below

$$R = 1 - S \quad (6)$$

where S is the survival (Equation (5)). Log removal, defined in Equation (7), was also reported as it gave a more accurate description of the degree of sterilization. It is insightful when survival values (S) approach zero or removal (R) values approach one. As the three test microorganisms have different structure, size and heat sensitivity, varying results were observed.

$$\text{Log Removal} = -\log(S) \quad (7)$$

3.3.2.1 *E. coli*

The dynamic in-flight on-filter (PAN 60) inactivation of *E. coli* as a function of microwave application time at three microwave power levels is displayed in Figure 37. When 500 W microwave power was used, at least 3.7 logs of the viable *E. coli* were inactivated (regardless of whether the microwave was applied to the system continuously (10 min per 10-minute-cycle), or periodically (5 or 2.5 min per 10-minute-cycle). This suggests that 2.5 min per cycle is sufficient to inactivate the *E. coli*. At a lower power level, less inactivation was achieved. A statistical analysis (ANOVA two-way) identified that the microwave power was the major factor that affects the *E. coli* inactivation. The p -value was 0.003. On the other hand, the microwave application time did not exhibit a significant influence. Overall, compared to the

other test microbes, *E. coli*, with its relatively large size and greater heat sensitivity, was removed the most effectively.

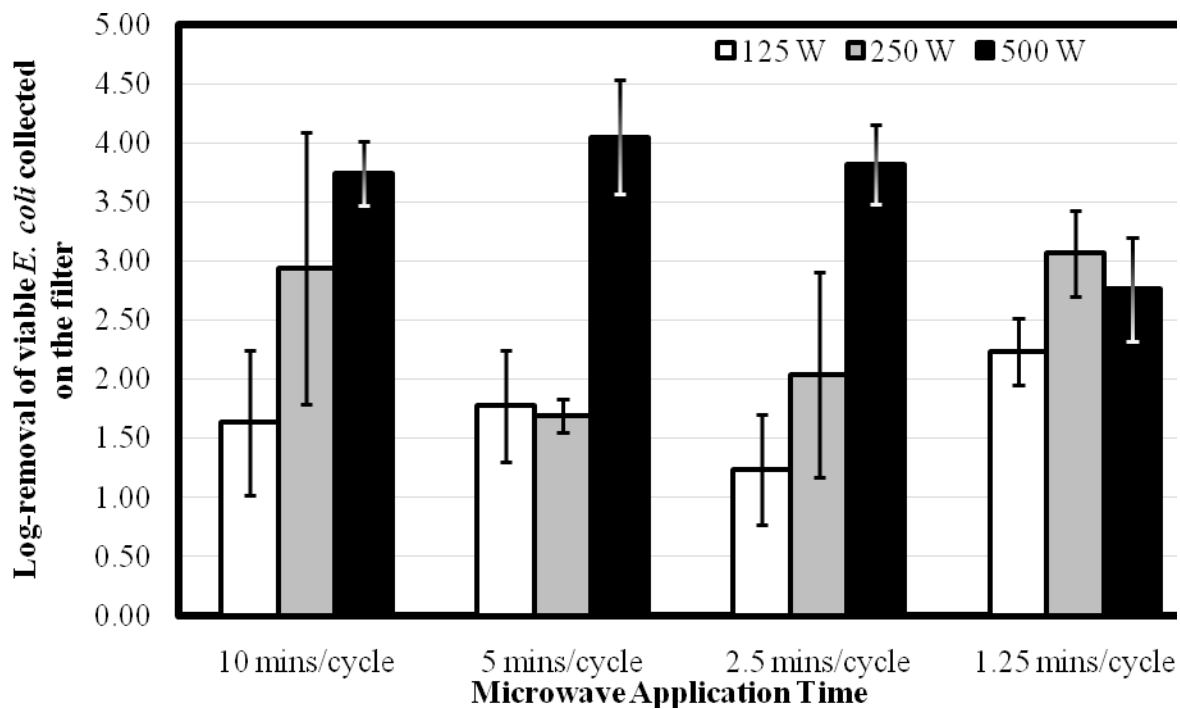


Figure 37: *E. coli* inactivation on the PAN 60 filter after dynamic in-flight microwave irradiation under different microwave power levels and application times

3.3.2.2 MS2 Virus

Duplicate experiments were carried out for MS2 with two types of filters: PAN and X-linked PAN. The calculated removal of MS2 from the air stream under different microwave powers and time intervals when PAN was used are shown in Figure 38. The inactivation effect of microwave against MS2 is dependent on both microwave power and time. Longer microwave irradiation time and high power cause increased virus inactivation. However, this inactivation effect for virus is less than that of *E. coli*. About 2.45 log removal was observed with continuous microwave treatment at maximum power (500 W). It was noticed that the mechanical property of PAN filter was altered after continuous test because of high temperature. This issue necessitates the use of X-linked PAN filters. The MS2 log removal with X-linked PAN filters are displayed

in Figure 39. For both PAN filter and X-linked PAN filter, microwave power was found to be a more significant factor than application time (p -value < 0.05).

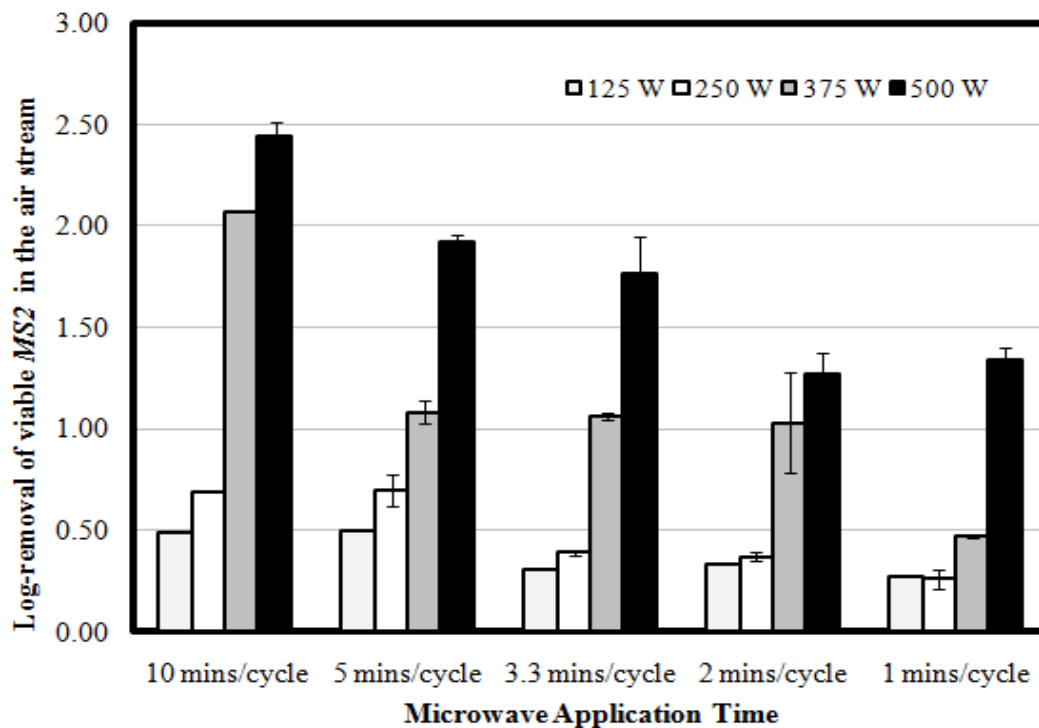


Figure 38: Viable MS2 penetration fractions from the microwave/filtration system as a function of microwave power level and application time with PAN 60 filters

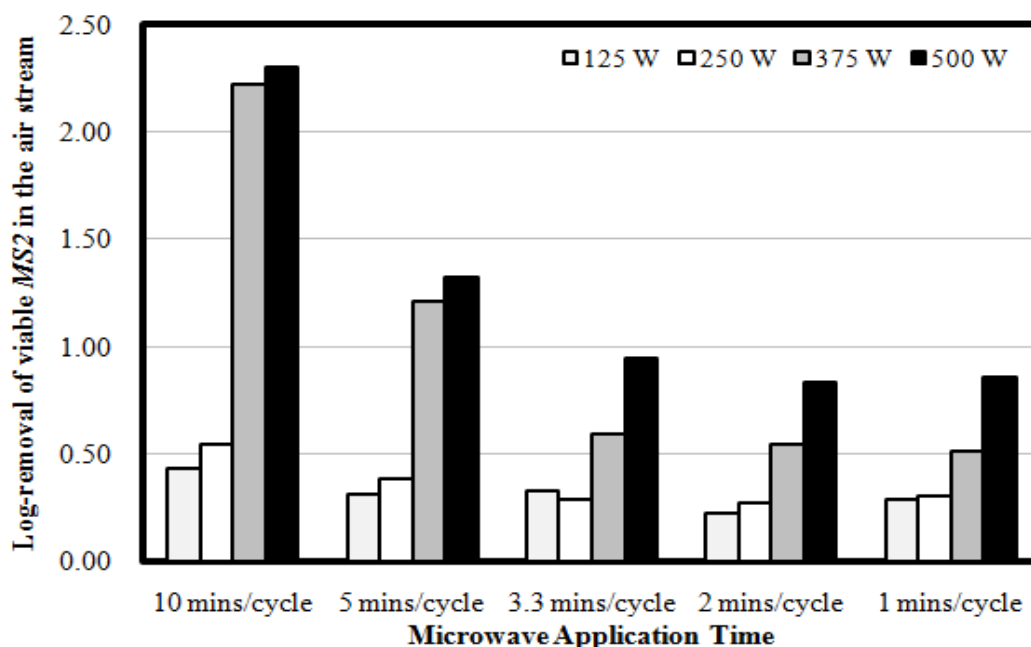


Figure 39: Viable MS2 penetration fractions from the microwave/filtration system as a function of microwave power level and application time with X-linked PAN filters

3.3.2.3 *B. subtilis* endospores

In-flight microwave filtration of *B. subtilis* aerosols was tested with the heat resistant X-linked PAN filters. Initially, experiments were conducted using the SiC fibermat support in the quartz reactor, identical to the *E. coli* testing. Preliminary experiments with this set-up proved ineffective in endospores inactivation on the filter. At 500 W and the longest application time (continuous 30 minutes), microwave inactivation of the spore bacteria was at most 90.55% (log removal of 1.02). This is significantly lower than the proposed inactivation.

To resolve this issue, a silicon carbide (SiC) disc support coupled with a different reactor, was used in place of the SiC fibermat support. With the X-linked PAN filter in direct contact with the microwave opaque SiC disk, more energy was delivered uniformly to the filter surface

at lower microwave power. This modification caused the microwave transparent PAN filters to heat up more quickly resulting in greater microorganism inactivation.

With this modification, tests were run in a similar fashion to previous experiments. The tests were run at a higher setting (750 W) to account for the high heat resistivity of endospores and to ensure complete inactivation. The results of the SiC disc support tests (Figure 40) indicate better microwave inactivation than when using the SiC fibermat support. At 500 W of continuous 30 min irradiation, 99.85% (1.82 increase in log removal) of the spores was observed.

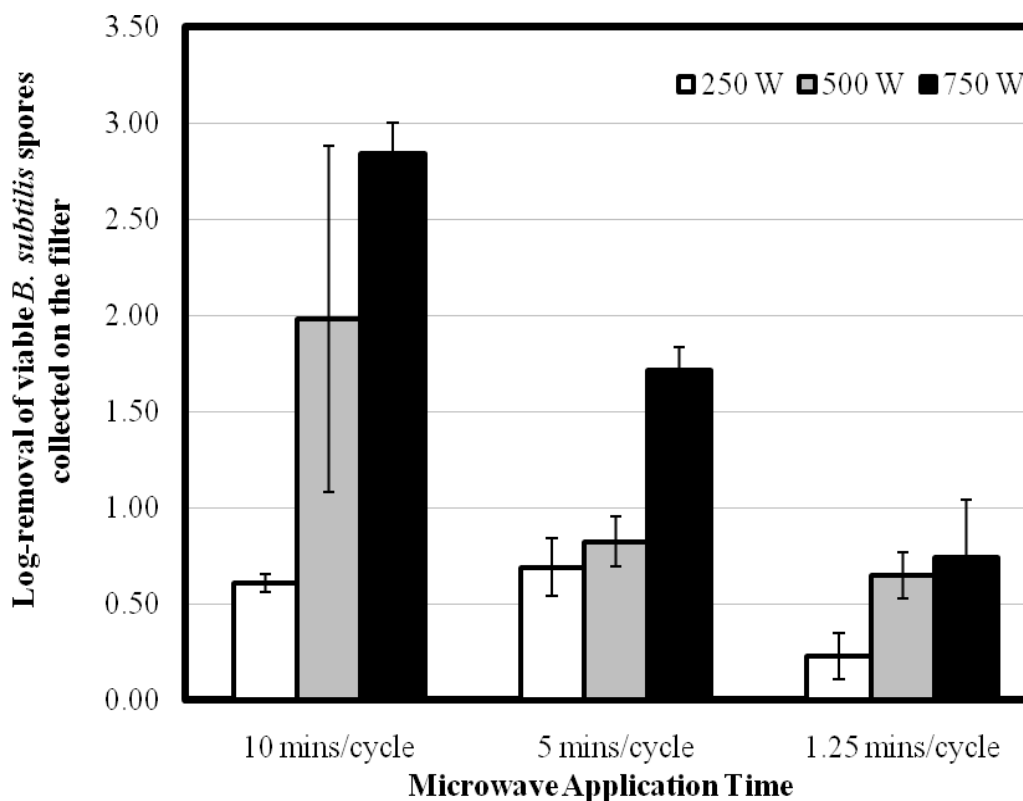


Figure 40: *B. subtilis* survival fraction on the filter after dynamic in-flight microwave irradiation under different microwave power level and application times

Although the inactivation of the spore aerosols was improved, the complete inactivation noticed in the bacteria and virus testing was not practically achieved with the described set-up and experimental conditions. Almost complete inactivation was observed only at high powers

(500 W and 750 W). While bacteria and virus testing has shown almost complete inactivation at a relatively low microwave power (250 W), spore inactivation proved more challenging. This difficulty can be attributed to the spore's heat resistivity and low water content.

3.3.3 SiC disk heat loss tests

As microbe inactivation was found to be more effective during static tests than in-flight tests, it was hypothesized that heat loss from the SiC disk to the flow was a significant factor. The SiC disks are the source of heat for the filters and subsequently are essential for microorganism inactivation. Minimalizing the heat loss will therefore improve microbe removal.

Tests were run simulating static conditions and flow conditions to investigate SiC disk temperature. For each test except the control, the SiC disks were irradiated at 500 W for a continuous 10 min period. The flow rates were then varied from 0 to 12 LPM to determine the effect of velocity on SiC disk temperature. The results of these tests are shown in Figure 41.

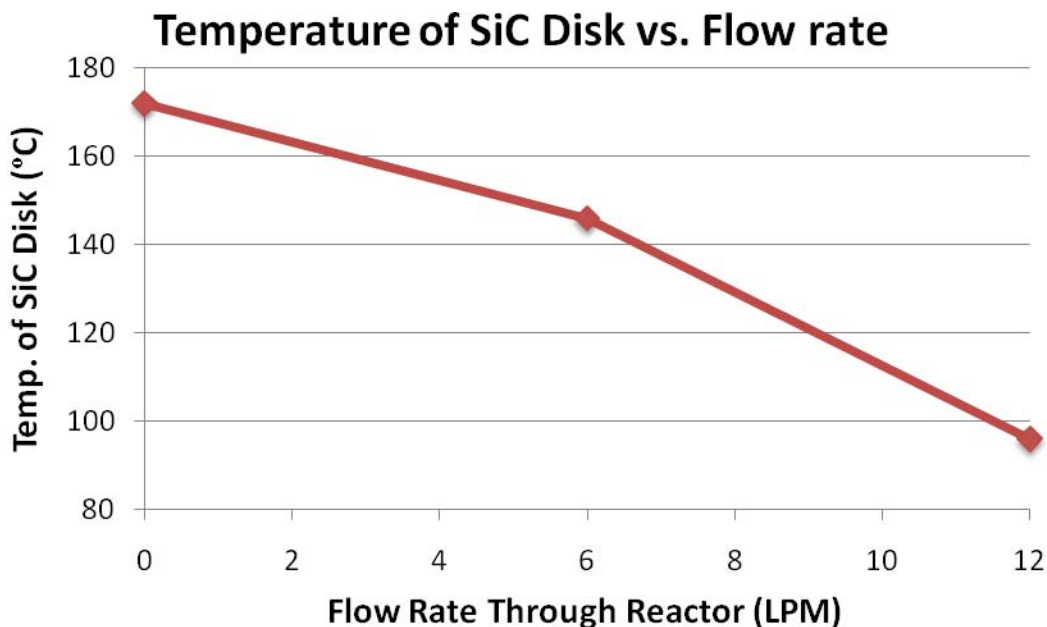


Figure 41: SiC disk temperature dependence on flow rate through reactor

Although there is a significant decrease in temperature with increased flow rate, it does not necessarily imply that the temperature decrease is significant enough to have a reduced biocidal effect on the endospores. Also, at a decreased power level (i.e. 250 W, 125 W), the reduction in energy will not be as much due to the decreased temperature gradient.

It was concluded that the flow velocity should be varied and decreased to correspond when the microwave is on. As shown in previous in-flight experiments, a short burst of heat inactivates more microorganisms than a long, low power application. For example, during *E. coli* testing, irradiation at 500 W for 1.25 min/cycle resulted in 2.76 log removal compared to continuous 30 minute irradiation at 125 W which resulted in 1.63 log removal. Therefore during periodic irradiation trials, whenever the microwave is turned on, the flow should be decreased. During this time, the filter would quickly become hotter and may be able to reach the temperature needed for inactivation. This would simulate the static test conditions.

3.3.4 Reduced flow rate experiments

As argued in 3.3.3, by decreasing the flow rate during microwave irradiation, the SiC disk would be able to achieve a higher temperature and subsequently kill more microorganisms. In previous experiments, the microwave was turned on periodically without changing the flow rate or face velocity. In these experiments, however, while the microwave was on, the flow rate was decreased by 50% corresponding to a decrease in face velocity of 6.59 cm/s. The results of these experiments for the 750 W, 1.25 minutes condition are shown Table 11. For this condition, by decreasing the face velocity 50%, inactivation on the filter increased by 19.1%. This corresponds to a 0.636 increase in log removal. The reduced flow results provide evidence that heat conduction to the flow affects microbial inactivation on the filter. They may also provide

evidence that thermal effects are the dominant factor, rather than radiation effects, in microbe inactivation.

Table 11: Reduced flow results for *B. subtilis* spores, triplicate data

Power (W)	Irradiation Time (min/10 min)	Decrease in filter face velocity (%)	Inactivation on the filter (%)	Inactivation on the filter with no flow reduction (%)
750	1.25	50	94.25	75.15

3.4 Chemical Aerosol Testing

3.4.1 Lab-Scale Pressure Drop Testing

The pressure drop across the disk was determined on each saturation apparatus for the uncoated SiC disks as a baseline and is shown in Figure 42. Due to the change in surface area exposed on the disk, the face velocity at identical flow rates was not the same, but the data are given in face velocity since that is the more critical factor.

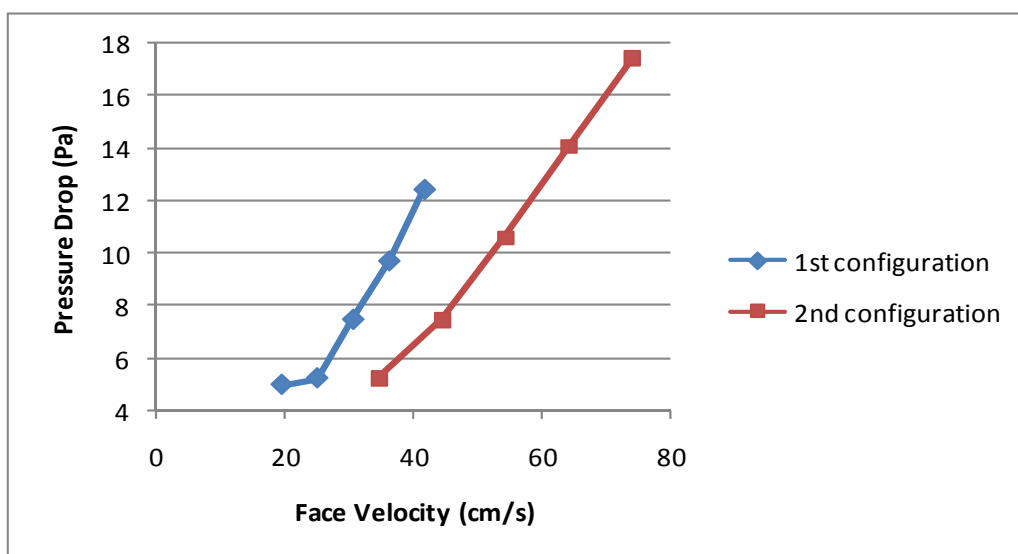


Figure 42: Pressure Drop as a Function of Face Velocity on Uncoated SiC Disks

Two different sets of disks with a PAN coating were received at different times and tested. There were two disks at each of the following deposition times for each set: 10 min, 20 min, 30 min, and 40 min. The saturation apparatus was changed between the two different sets. The pressure drop results are presented in Figure 43. Compared to the baseline, the pressure drop increased due to the PAN fiber mat.

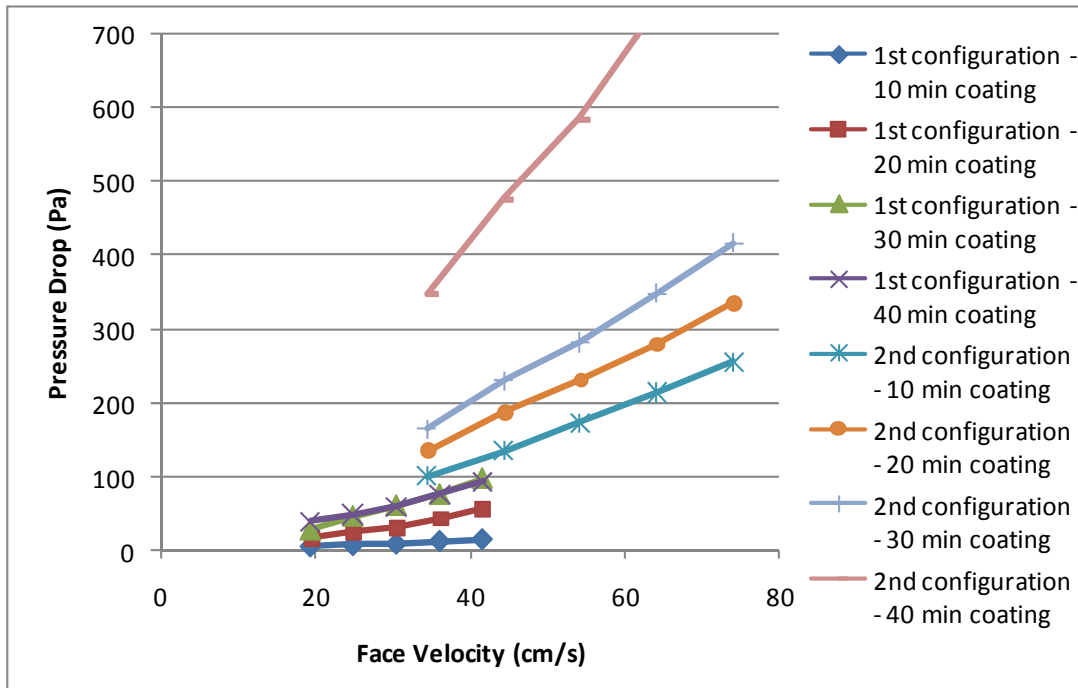


Figure 43: Pressure Drop as a Function of Face Velocity on PAN Coated SiC Disks

Additionally, one set of disks with a poly vinyl pyrrolidone (PVP) coating was received and tested. There were two disks at each of the following deposition times: 10 min, 20 min, 30 min, and 40 min. Figure 44 shows the pressure drop data on the second saturation configuration. For all of the 10, 20, and 30 minute disks, the pressure drop was lower than HEPA filters for the face velocities tested.

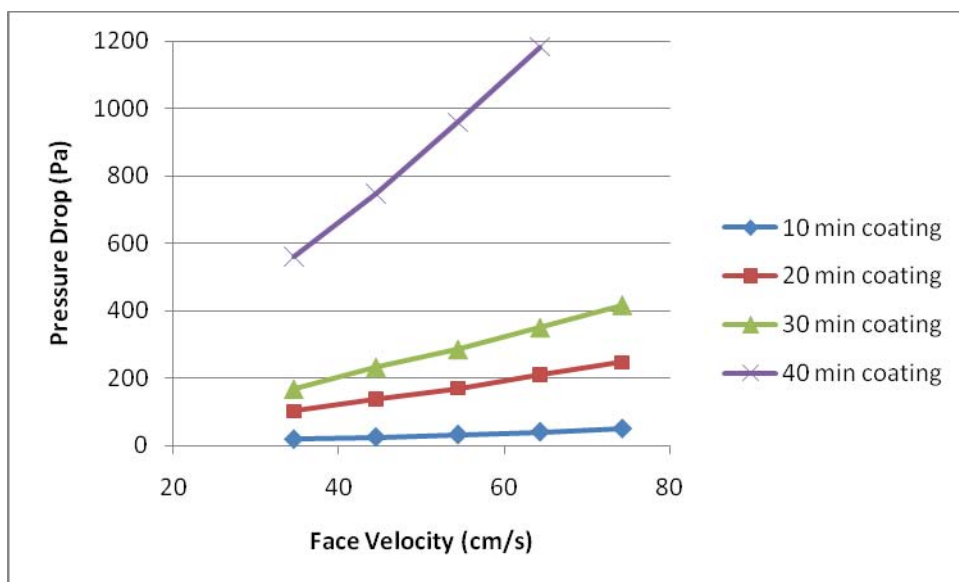


Figure 44: Pressure Drop as a Function of Face Velocity on PVP Coated SiC Disks on Second Saturation Configuration

3.4.2 Lab-Scale Saturation/Regeneration

3.4.2.1 Uncoated SiC Disks

Initial testing was performed on uncoated SiC disks to give a baseline. Since the saturation apparatus changed during the course of testing, the disks were tested on both configurations. Regeneration was done under air. Figure 45 shows the saturation results on both configurations at the face velocities tested. Table 12 shows a summary of the regeneration results at the different microwave powers and air flows tested. The amount of inorganic phosphate recovered in the water was negligible. The disks readily returned to their initial condition, although the destruction efficiency of the DMMP was lower than desired.

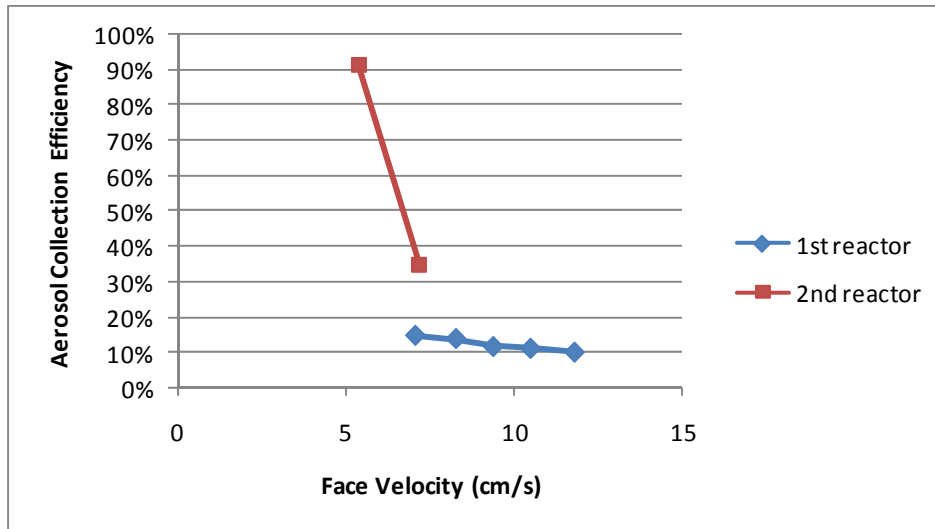


Figure 45: Saturation with DMMP of Uncoated SiC Disks for 20 Minutes

Table 12: Regeneration of Uncoated SiC Disks for 20 Minutes with Five Minute Warm-up

Microwave Power (W)	Air Flow Rate (m ³ /h)	Regeneration Efficiency	Destruction Efficiency
300	1.7	102.2%	40.4%
300	2.5	100.9%	43.6%
600	1.7	103.9%	37.4%
600	2.5	103.2%	26.6%

3.4.2.2 PAN Coated SiC Disks

Regarding the PAN coated SiC disks, one was tested on the first lab-scale saturation apparatus and the other was tested on the second apparatus. For the regeneration, nitrogen was used instead of air to prevent oxidation of the polymer coating. Some of the disks were tested more than once. Figure 46 shows the saturation results. The second set of PAN coated SiC disks had much greater DMMP aerosol collection efficiencies than the first set of coated SiC disks.

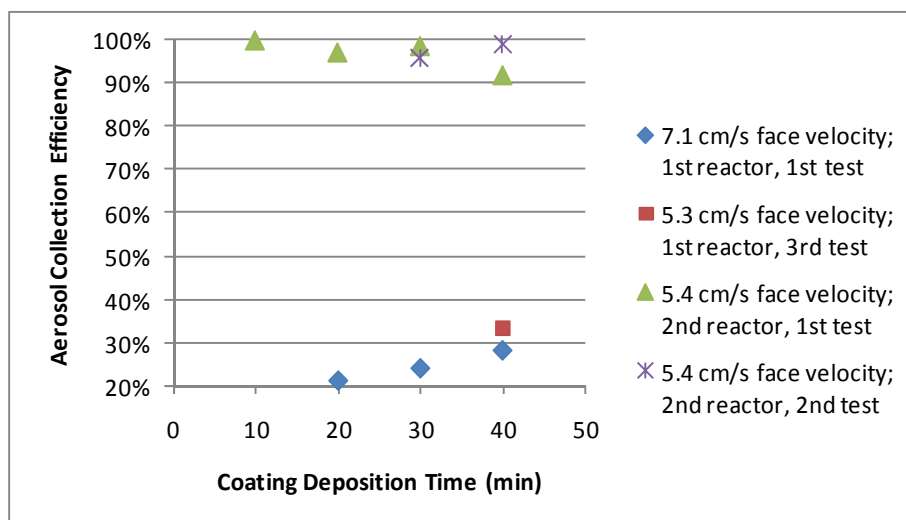


Figure 46: Saturation with DMMP of PAN Coated SiC Disks for 20 Minutes

The regeneration data are quite encouraging, indicating that the system heated rapidly and readily returned to close to the initial core mass during the first use. Although the aerosol destruction efficiency of the DMMP was not optimized, the amount of inorganic phosphate recovered in the water was negligible. However, after the second regeneration on the disks, the filters ended up visibly cracked or scorched indicating some of the PAN was degraded. Later, regeneration tests were done with only the mildest conditions to minimize the scorching and cracking since all the conditions used on the first set showed complete regeneration. Table 13 shows the average results for each condition tested.

Table 13: Regeneration of PAN Coated SiC Disks for 20 Minutes

Microwave Power (W)	Nitrogen Flow Rate (m ³ /h)	Regeneration Efficiency	Aerosol Destruction Efficiency
300	1.7	98.4%	90.5%
300	2.5	97.1%	56.7%
600	1.7	96.8%	87.1%
600	2.5	95.7%	39.4%
900	2.5	100.2%	53.1%

3.4.2.3 Poly Vinyl Pyrrolidone (PVP) Coated SiC Disk

The two 10-min PVP coated SiC disks were run for saturation/regeneration testing. However, after each regeneration test it was noticed that no coating remained. After the saturation test for the third disk, a 20-min disk, the disk was examined and it appeared to have already lost its coating. A small piece of PVP was taken from the edge of an untested disk and a drop of DMMP was added. It dissolved immediately. The piece was then tested with a drop of ethyl 2-chloroethyl sulfide, which is another chemical agent simulant, and the same results were obtained. Testing was aborted on the coated disks after that disk.

3.4.2.4 SiC Disks with TiO₂ Nanofiber Mats

For initial testing, a piece of TiO₂ fiber mat was received. As a preliminary test, it was weighed and sandwiched between two SiC disks, then put through the regeneration process at 300-W of microwave power and 1.7-m³/h (1.0-scfm) N₂, which are conditions shown to remove the DMMP on the PAN coated disks previously tested. Visibly, the TiO₂ fiber mat did not have the dry, cracked appearance that was noticeable with the PAN. The mass before and after was within the variability of the balance with the mass after slightly higher. This preliminary screening indicated that the TiO₂ should not have the degradation issues seen with PAN and had the promise for use as a coating.

Full SiC disk size TiO₂ fiber mats were then received. Two of the mats were sandwiches of microfiber-nanofiber-microfiber. The first mat, the heat-treated 3-layer one, was tested through two cycles of saturation and regeneration. The second mat, the 3-layer one without heat-treatment, was tested through six regeneration cycles. These results are shown in Figure 47. In addition, a control sample was tested that did not have the nanofiber layer; it was a 2-layer

microfiber sandwich. Table 14 shows the results of these tests with the control being the average of the two control mats. The control mats were so brittle that only one cycle per mat was able to be performed.

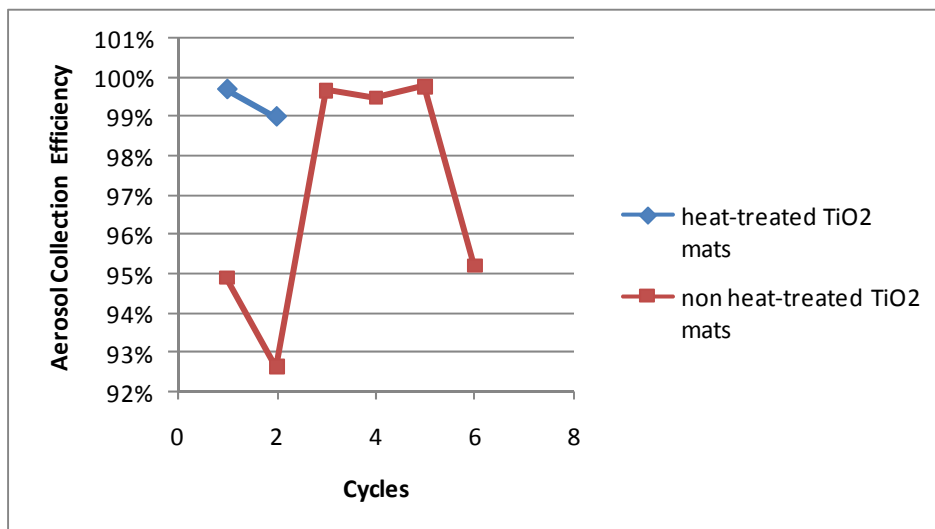


Figure 47: Saturation with DMMP of TiO₂ Mats on SiC Disk for 20 Minutes at 5.4-cm/s Face Velocity

Table 14: Saturation with DMMP of TiO₂ Mats on SiC Disk for 20 Minutes at 5.4-cm/s Face Velocity

Disk	Aerosol Collection Efficiency
3-layer, 10-20-10	99.9%
3-layer, 10-40-10	99.9%
3-layer, 10-80-10	100.0%
2-layer 10-10, control	94.3%

The summary of the regeneration results are presented in Table 15. There was an issue with the regeneration reactor during the first regeneration test that put too much nitrogen flow through and ended up causing damage to the mat, which explains the high weight loss average on that disk. None of the mats showed visible damage from the microwave regeneration, although there was some damage due to handling. Recovery of inorganic phosphate in water at the outlet continued to be negligible.

Table 15: Regeneration of TiO₂ Mats on SiC Disks for 20 Minutes at 300-W and 1.7-m³/h

Air Flow

Disk	Regeneration Efficiency	Destruction Efficiency
3-layer, heat treated	117.9%	99.8%
3-layer, not heat treated	99.8%	96.1%
3-layer, 10-20-10	100.3%	7.7%
3-layer, 10-40-10	100.6%	39.4%
3-layer, 10-80-10	100.6%	16.2%
2-layer 10-10, control	100.2%	1.1%

Aerosol collection and microwave regeneration test results to date indicate that the TiO₂ nanofiber mat can easily be regenerated by microwave energy and collected aerosols are decomposed by microwaves. The TiO₂ nanofiber mats were damaged by mechanical contact during transporting the SiC disk from the SiC disk holder to the microwave reactor for the destruction of aerosols collected by nanofiber mat. Testing was stopped when the damage became too great to continue.

3.4.2.5 SiC Disks with Cross-Linked PAN Fiber Mats

A single cross-linked PAN nanofiber mat that had been processed for about two and a half hours was received for initial testing. The mat was tested through multiple saturation/regeneration cycles, until the handling caused too much damage. The results show excellent aerosol collection efficiencies. The disk tore slightly on the edge during saturation test #5, which explains the lower aerosol collection efficiency result. For subsequent tests, the tear was placed so that it was under the gasket such that it would not affect the collection of the aerosol. During handling after the seventh test, it tore further so testing was terminated. Overall the results remain consistently high aerosol collection efficiency instead of steadily losing efficiency with each cycle of testing like previous fiber mats had done. Saturation tests were done with 5.4-cm/s face velocity for 20 minutes.

Since the initial cross-linked PAN fiber gave promising results, four additional cross-linked PAN fibers that had been processed for varying lengths of time were received and tested under the same conditions. The two, three, and four hour cross-linked PAN fibers were tested for four saturation/regeneration cycles each, while the one hour cross-linked PAN fiber was tested for three saturation/regeneration cycles since it tore during handling on the third test. Additional one and four hour fiber mats were then received and tested. All saturation data are shown in Figure 48. Overall the cross-linked PAN fibers show excellent aerosol collection efficiencies. The two hour mat tore slightly during handling for the last test, which probably explains the lower result there.

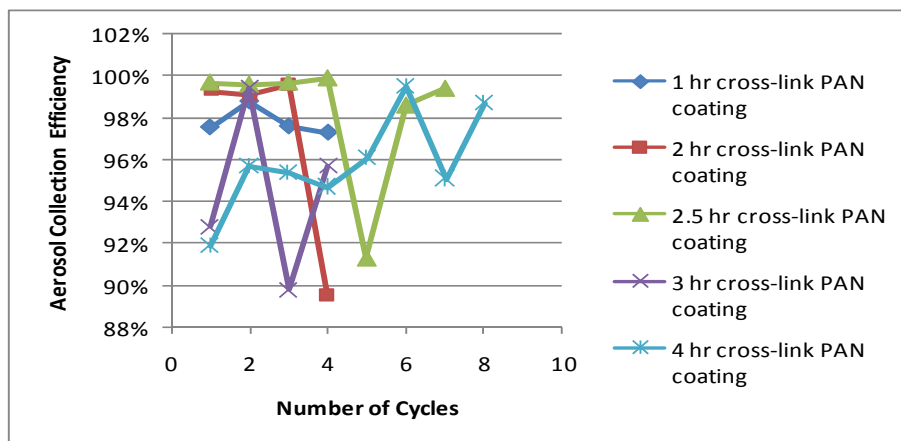


Figure 48: Saturation with DMMP of Cross-Linked PAN Mats on SiC Disk for 20 Minutes at 5.4-cm/s Face Velocity

The filters demonstrate a continued ability to collect aerosol efficiently after several cycles of regeneration with no loss in efficiency. This indicates the fiber was not being degraded with exposure to microwaves, even under oxidizing conditions. Regeneration tests were initially performed at 300-W microwave power and 1.7-m³/h (1.0-scfm) nitrogen flow rate. Later tests were done under air, since using compressed air on scale-up would be more desirable than using nitrogen. The results are shown in Table 16.

Table 16: Regeneration of Cross-Linked PAN Mats on SiC Disks for 20 Minutes

Microwave Power (W)	Flow Rate (m ³ /h)	Conditions	Regeneration Efficiency	Destruction Efficiency
300	1.7	N ₂ , 5 min Warm-up	100.5%	19.3%
600	1.7	Air, 5 min Warm-up	100.8%	47.1%
600	1.7	Air, No Warm-up	100.4%	19.4%
600	2.5	Air, No Warm-up	100.6%	0.5%
750	1.7	Air, No Warm-up	100.9%	27.3%

The regeneration cycles show complete removal of the DMMP based on weight loss and there was no visible damage to the filters after each cycle in the microwave. Initial tests were done with a warm up period for the microwave without any air flow. The warm-up period was eliminated in later tests to see if it was causing DMMP to evaporate without being destroyed. The results do not indicate the warm-up period was a problem since the destruction efficiency without it was still very low. Even with the addition of air, there remained an insignificant amount of inorganic phosphate recovered.

3.4.2.6 SiC Disks with Lydair HEPA Grade 4450HS Filter Mats

A commercially available filter, Lydair HEPA grade 4450HS glass microfiber filter, was also tested. A single filter was tested for six saturation/regeneration cycles. Regeneration was done under nitrogen. The sixth regeneration cycle had no data because the quartz tube in the reactor cracked shortly after starting the microwave. No further tests were done on this filter because the damaged quartz tore the filter. The regeneration cycles show complete removal of the DMMP and there was no visible damage to the filter after each cycle in the microwave. Data obtained on the lab-scale unit indicate that this commercially available microfiber filter is a viable alternative to the nanofiber filters being investigated.

A second series of saturation and regeneration tests were done on a Lydair HEPA grade 4450HS filter with regeneration testing that was done under air instead of nitrogen to examine the filter's abilities to withstand oxidation conditions needed to destroy the DMMP aerosols. Regeneration testing was done at 600-W microwave power and variable flow rates.

Figure 49 shows the average aerosol collection efficiencies of the two mats, while Table 17 shows a summary of the regeneration at the different conditions tested. All tests gave greater than 90% aerosol collection efficiency with most above 95%, showing retention of collection

efficiency with repeated cycles. The filter demonstrated a continued ability to collect aerosols efficiently after several cycles of microwave regeneration under air with no loss in efficiency by the fourth cycle. This indicates the fiber was not being degraded with exposure to microwaves under oxidizing conditions. The regeneration cycles showed complete removal of the DMMP based on weight loss and there was no visible damage to the filter after each cycle in the microwave. The destruction efficiencies, however, were still much lower than desired and the inorganic phosphate remained negligible, even with oxidation under air.

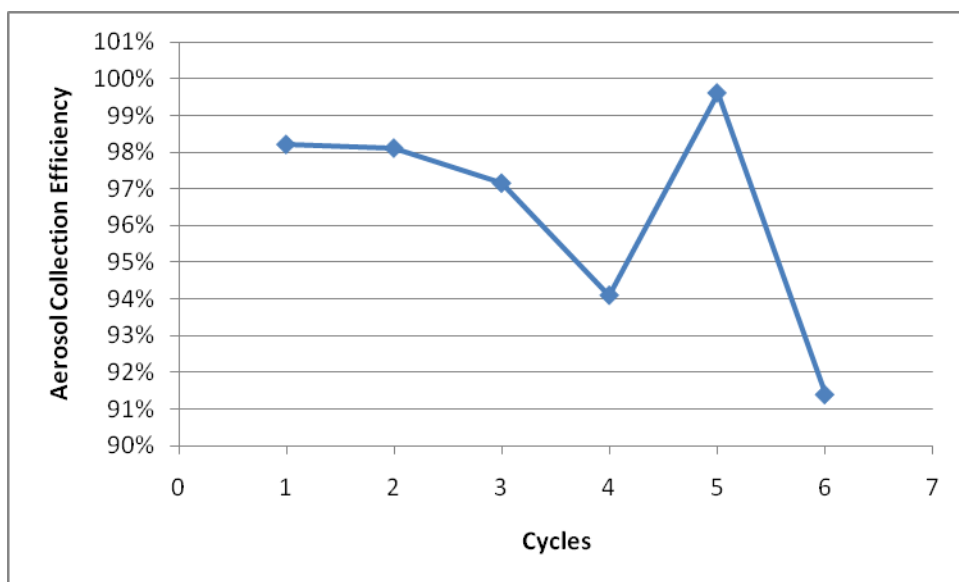


Figure 49: Saturation with DMMP of Lydair Filter on SiC Disk for 20 Minutes at 5.4-cm/s Face Velocity

Table 17: Regeneration of Lydair Filter SiC Disks for 20 Minutes

Microwave Power (W)	Flow Rate (m ³ /h)	Conditions	Regeneration Efficiency	Destruction Efficiency
300	1.7	N ₂ , 5 min Warm-up	100.6%	15.1%
600	1.7	Air, 5 min Warm-up	100.9%	27.1%
600	1.7	Air, No Warm-up	100.7%	15.6%
600	0.8	Air, 5 min Warm-up	100.0%	73.9%
600	0.8	Air, No Warm-up	100.9%	58.2%

3.4.3 Bench-Scale Pressure Drop Testing

Figure 50 shows the pressure drop across the SiC tube for several reactor and SiC tube configurations. The pressure drop across the tube was very low, well within the acceptable range to replace existing HEPA filters. The flow rate of $9.0\text{-m}^3/\text{h}$ (5.3-scfm) corresponded to a face velocity of 5.3-cm/s for the first reactor. The pressure drop at the target flow of $8.5\text{-m}^3/\text{h}$ (5-scfm) was close to 0.5 kPa (2 inches water) in the second reactor, which was comparable to HEPA filters. The pressure drop between the two tube setups for each reactor was insignificant.

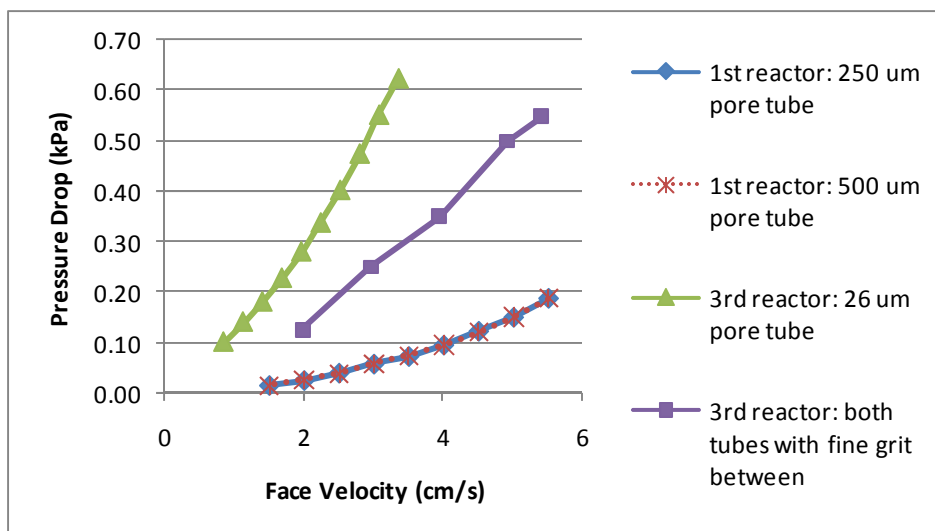


Figure 50: Pressure Drop as a Function of Face Velocity on Bench-Scale Reactors

3.4.4 Bench-Scale Saturation/Regeneration

3.4.4.1 First Bench-Scale Microwave Reactor

Initial testing was done with the 500 μm pore SiC tube. The first two saturation tests used additional process air besides that from the nebulizer at 3.4 and $10.2\text{-m}^3/\text{h}$ (2 and 6-scfm). The results showed only 0.1 g weight gain each, which is insignificant compared to the mass of the SiC tube. The remaining tests, on both available SiC tubes, were performed at different

nebulizer pressures to provide different air flows with no additional air added and were run for 50 minutes for each of the two SiC tubes. These tests did show measurable mass gain on the core. Results are shown in Figure 51. As the air flow rate increased, the aerosol collection efficiency decreased. The collection efficiency calculated based on weight gain of SiC tube and nebulizer weight loss was quite poor, but since this was simply the base that was to be used to support the nanofiber filter, its collection efficiency was less important than its heating efficiency. The mass collected showed very little dependence on the nebulizer pressure. The mass gain was between 8 and 11 g DMMP regardless of the amount nebulized, which varied from 13 to 27 g DMMP. It was hoped that the smaller pore size SiC tube would provide higher aerosol collection efficiency.

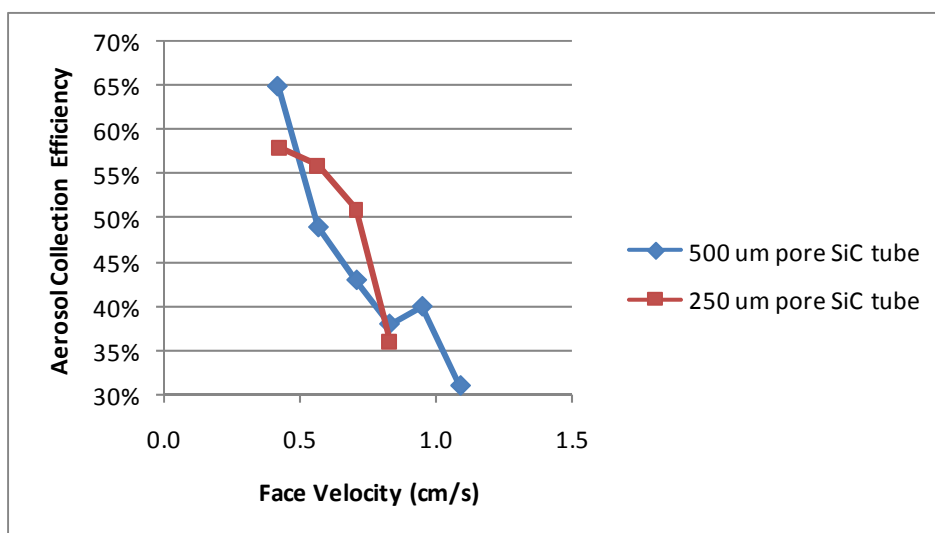


Figure 51: Saturation with DMMP of SiC Tube on First Reactor for 50 Minutes

Regeneration on 500 μm SiC tubes are shown in Table 18. The regeneration results are quite encouraging, indicating that the system heated rapidly and readily regained the initial core mass. The regeneration tests show that the SiC tube was essentially 100% regenerated. During the initial tests, the outlet was monitored by the THC analyzer as an endpoint determination.

Nonetheless, the THC's did not spike and fell back to zero as expected so the times for the first tests were erratic from trying to monitor the outlet. For later tests, the regeneration time was reduced to 20 minutes, then further to ten minutes, and still achieved complete regeneration.

Table 18: Regeneration on 500 μm Pore SiC Tube with 5 Minute Warm-up

Test	Microwave Power (kW)	Air Flow Rate (m^3/h)	Time (min)	Core Mass Loss (g)	Regeneration Efficiency (%)
3	2.00	10.2	40	8.8	101.1%
4	1.00	10.2	70	8.3	97.6%
5	1.00	3.4	48	8.7	101.2%
6	1.00	3.4	20	8.5	98.8%
7	2.00	3.4	20	11.2	101.8%
8	2.00	10.2	20	8.3	98.8%
9	1.00	3.4	10	10.6	101.9%
10	2.00	10.2	10	9.7	99.0%
11	2.00	3.4	10	9.2	100.0%
12	1.00	10.2	10	9.1	97.8%

For the regeneration tests on the 250 μm pore SiC tube, the microwave power was at 2.00 kW and the process air flow was at 10.2- m^3/h (6-scfm) for 20 minutes. These results are similar to the results obtained from the larger pore size SiC tube with the mean regeneration efficiency of 100.1%.

3.4.4.2 Second Bench-Scale Microwave Reactor

Saturation and regeneration testing was done on the second bench-scale reactor for one hour with the single 26 μm pore size SiC tube and with both SiC tubes with a Lydair filter on the

outside of the inner tube. Aerosol collection efficiencies are shown in Figure 52 as a function of face velocity. The presence of the filter gave improved collection efficiencies at both nebulizer pressures. At the given face velocity, the aerosol collection efficiencies were about the same for both, indicating that the rate of aerosol generation had no effect. Without the filter, the efficiency depends on the nebulizer pressure or rate, with the higher rate giving lower efficiencies. Plugging the end of the tube to avoid bypass did not increase efficiency.

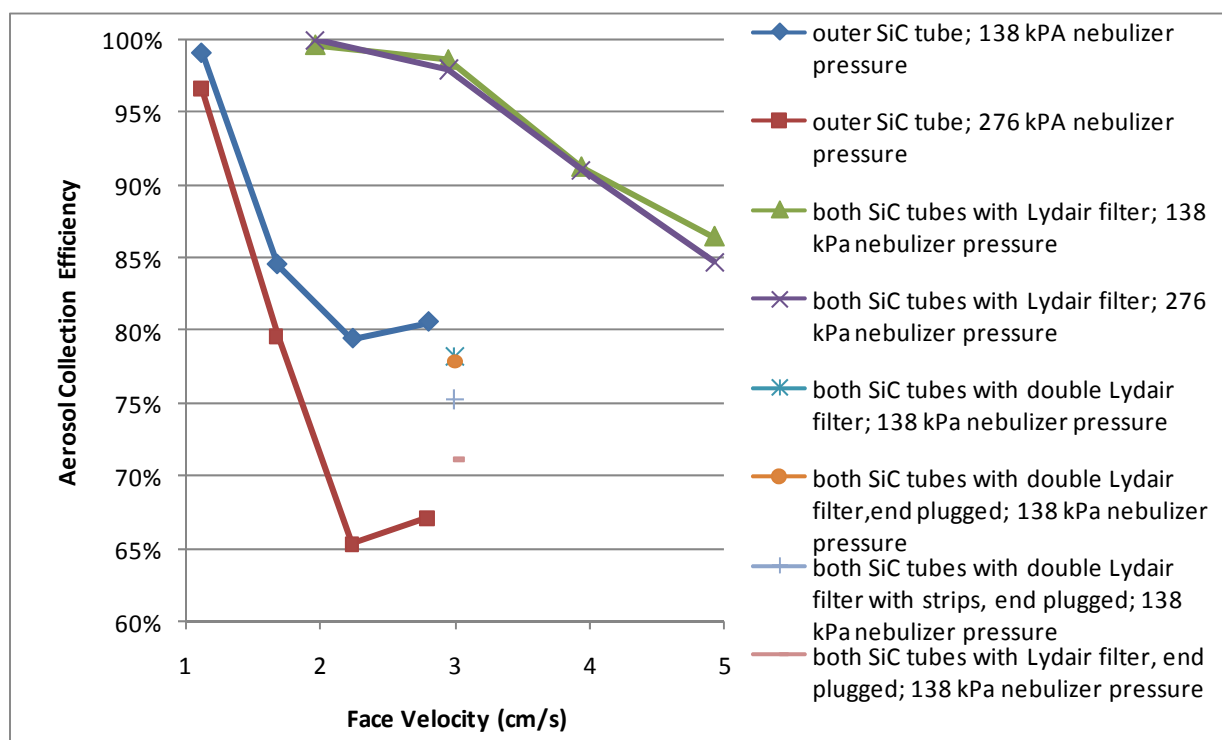


Figure 52: Saturation with DMMP on Second Reactor for One Hour

The regeneration was also done at a variety of microwave powers and air face velocities. Figure 53 shows the microwave regeneration results. The results are fairly erratic. The tests done on both tubes with a single layer of Lydair filter at 2.55-kW power gave fairly good results, but identical conditions on other configurations did not give good destruction efficiencies. The regeneration process should not be dependent on the presence or absence of the filter, since the

SiC should be catalyzing the reaction. Hence, it was unclear what was causing the variation. As seen with the lab-scale testing, the amount of recovered inorganic phosphate was negligible.

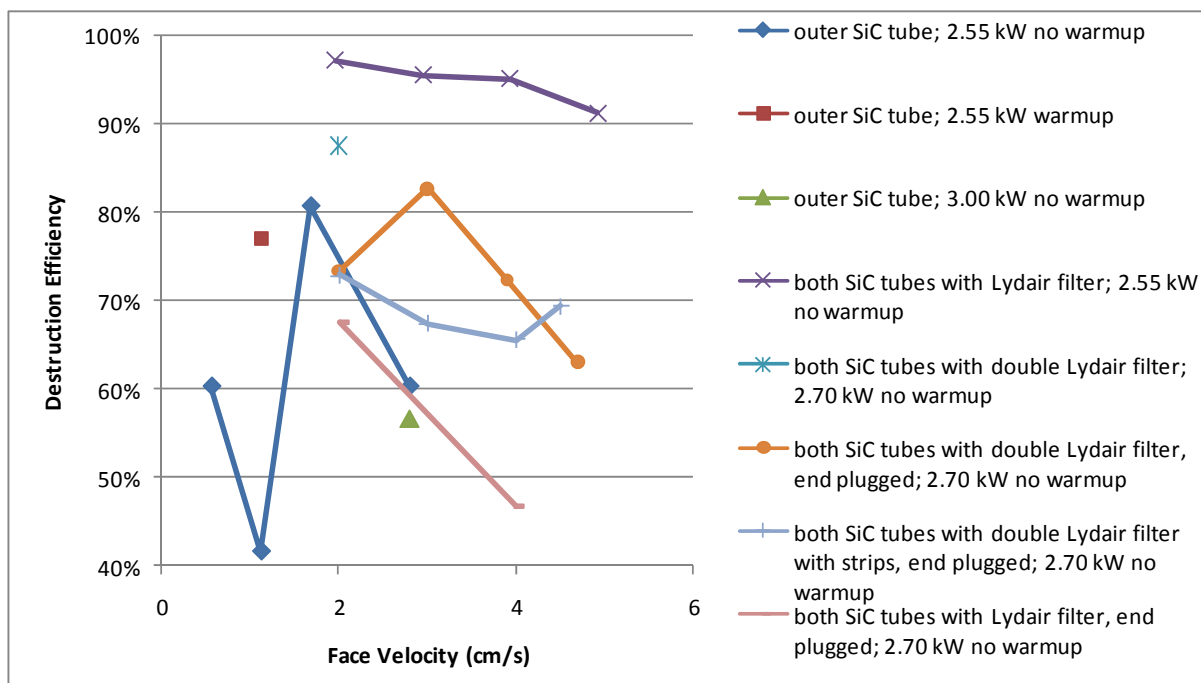


Figure 53: Regeneration on Second Reactor for 30 Minutes

The one-hour saturation tests gave us a limited picture of the saturation process. The filter was not likely to be completely saturated. As the filter got more saturated, the aerosol collection efficiency would be expected to increase since the already collected aerosol should block the filter openings and act to catch more of the aerosol over time. In addition, the pressure drop would be expected to increase as the filter openings became filled. Extended saturation tests were done on the two SiC tubes with a single layer of the Lydair filter for six hours to look at aerosol collection efficiency over longer time periods and to look at cumulative effects. Initial extended tests were done in duplicate at both nebulizer pressures that had been used for the shorter tests and at 8.5-m³/h (5.0-scfm) total air flow which corresponds to a face velocity of 9.3 cm/s. Since this air flow rate gave lower efficiencies and higher initial pressure drops, it should

be easier to see increases in both over time than if a lower flow rate were used. One test was done at a lower flow rate of $5.1\text{-m}^3/\text{h}$ (3.0-scfm) for comparison which corresponds to a face velocity of 5.6 cm/s which is approximately the target velocity. The water for collecting the outlet gas was sampled at 30-minute intervals so that cumulative aerosol collection efficiencies could be determined. For regeneration after these extended saturation tests, testing was performed at 2,550-W microwave power for 60 minutes at an air flow rate of $3.4\text{-m}^3/\text{h}$ (2.0-scfm).

Figure 54 shows the aerosol collection efficiency as a function of saturation time. The figure clearly shows that increasing the air flow rate resulted in a lower aerosol collection efficiency. There was a trend of slightly decreasing efficiency with time which was strongest at the 40-psig (276 kPa) nebulizer pressure and $5.1\text{-m}^3/\text{h}$ (3.0-scfm) total air flow rate, which was the most severe set of conditions. In addition, the pressure drop did not change with time after the first ten minutes and was also dependent only on the total air flow rate. The tests at 9.3-cm/s face velocity each had a pressure drop difference of 0.72 kPa (2.9 inches water) while the test at 5.6-cm/s face velocity had a pressure drop change of 0.47 kPa (1.9 inches water).

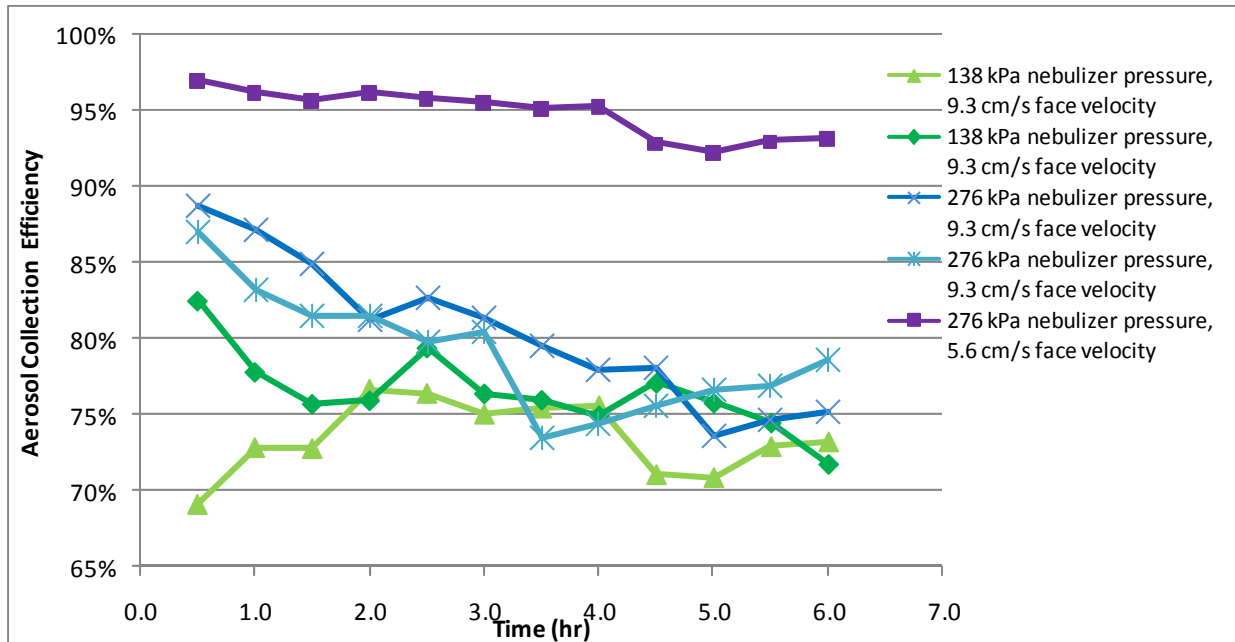


Figure 54: Aerosol Collection Efficiency as a Function of Saturation Time on Second Reactor with Both SiC Tubes and a Single Layer Lydair Filter

Figure 55 shows another way to look at the aerosol collection data. This figure shows much more clearly that the tests with identical flow rates gave essentially identical results. The filter collected a larger amount of the aerosols at a lower air flow rate.

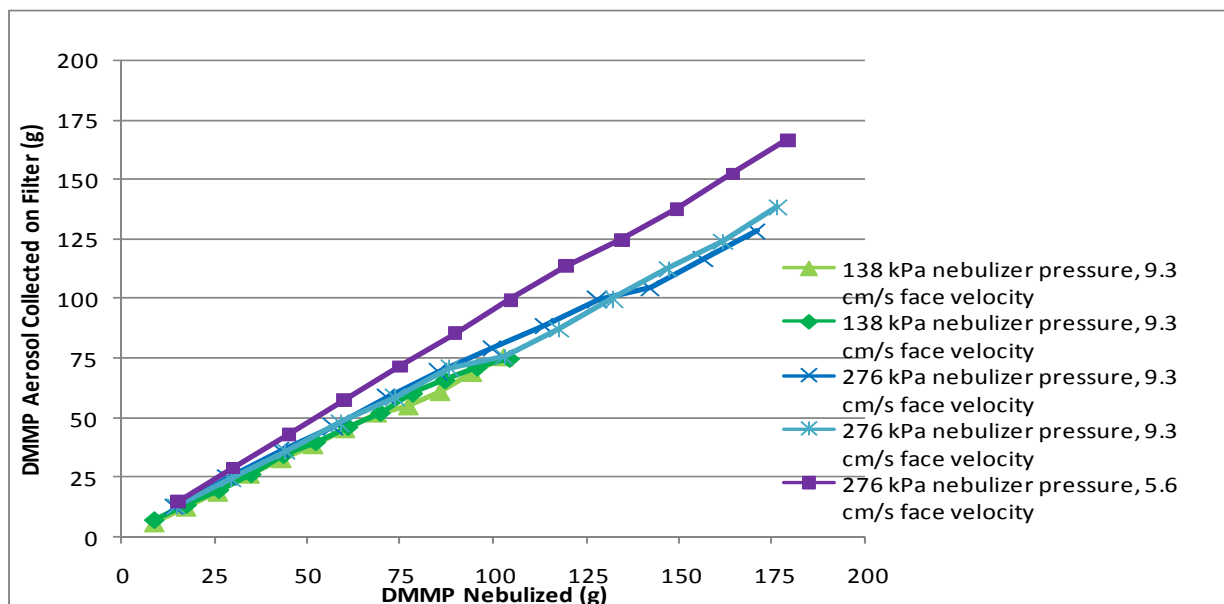


Figure 55: DMMP Aerosol Collected on Filter as a Function of DMMP Nebulized with Both SiC Tubes and a Single Layer Lydair Filter for Six Hour Saturation

Figure 56 presents the destruction efficiency as a function of the amount of DMMP aerosols collected in the filter. The results are fairly consistent with a bit of scatter. The mean destruction efficiency was 92.6% with a standard deviation of 1.6%, which is slightly lower than seen before with the shorter saturation/regeneration tests, although with some overlap. It is not clear whether the drop in DMMP destruction efficiency was significant and was due to the increased amount of DMMP. This shows that the DMMP destruction efficiency was not dependent on the total amount of DMMP that needs to be destroyed.

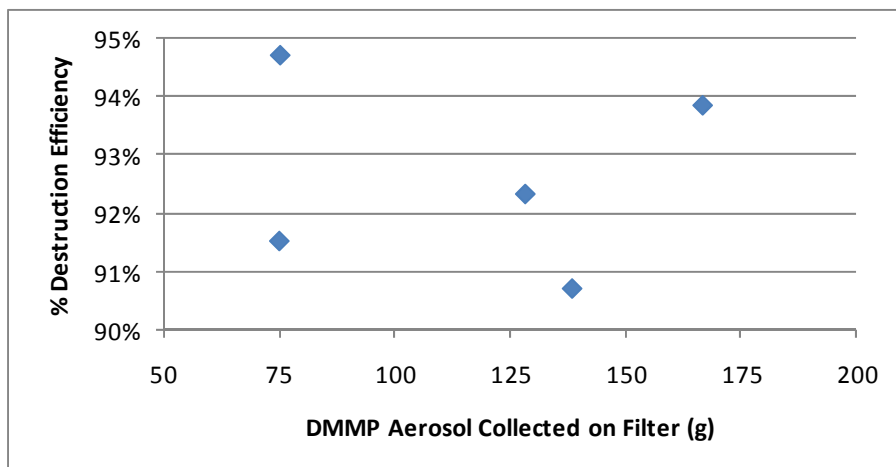


Figure 56: Percent Destruction Efficiency as a Function of DMMP Collected on Filter during Saturation Using 2.55 kW and 3.4-m³/h for One Hour

3.4.5 Bench-Scale Direct Oxidation

3.4.5.1 First Bench-Scale Microwave Reactor

Direct oxidation was investigated on the first reactor using each of the SiC tubes. A summary of the results is depicted in Figure 57. The individual data do show slight fluctuations over time, but the averages stay very steady. The average from after the first five minutes was essentially the same as for the last half hour. The results showed a tendency to have a spike, usually early, in the percent oxidized before completely settling down, but this spike was no more than 4% in all cases. The oxidation was most complete at the 20 psig nebulizer pressure (0.4 cm/s), even though that was the highest DMMP concentration being introduced and the lowest air flow to DMMP ratio. This is probably due to the longer residence time in the SiC chamber. There was sufficient air in all cases to allow for complete oxidation of the DMMP aerosols.

The 500 μm pore SiC tube was weighed before and after testing. Initial weight was 999.6 g and after all testing was 1022.6 g. Black soot was visible on the tube and in the chamber after testing. This black soot was not observed in tests with oxidation of aerosols collected during saturation. The chamber was cleaned and the SiC tube was regenerated for about two hours at 2.4-kW microwave power to see if some of it might be carbon soot that could be oxidized further, but no weight loss was observed. The phosphorus in the DMMP would end up as P_2O_5 at its most oxidized state, which is a white solid. P_2O_5 is water soluble to give phosphoric acid, and the soot cleaned from the chamber was not water soluble, indicating that the bulk of the soot was not a result of the presence of P_2O_5 although there might have been small amounts of it mixed in. P_2O_5 sublimates at 360°C (680°F). Although the air outlet did not reach that high temperature, it is not known how hot the SiC tube was getting and some P_2O_5 could be subliming.

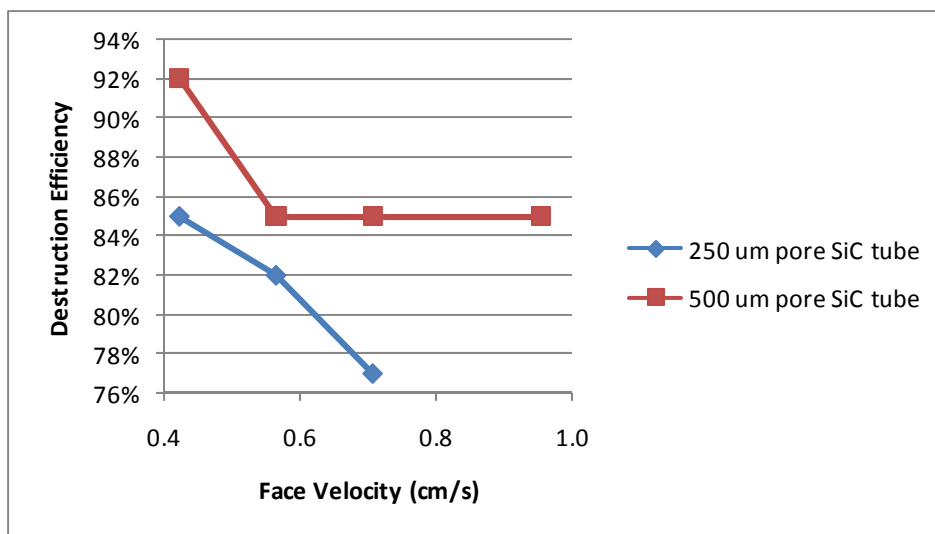


Figure 57: Direct Oxidation on First Reactor at 2.55 kW Microwave Power for One Hour

3.4.5.2 Second bench-scale microwave reactor

Direct oxidation test was conducted on the second bench-scale microwave reactor using several configurations of the SiC tubes. A summary of the results is depicted in Figure 58. The amounts of inorganic phosphate or carbon recovered in the diffuser water were insignificant. The lower nebulizer pressure gave concentrations that were 1-2 g/m³ lower than the higher nebulizer pressure at the same overall flow rate.

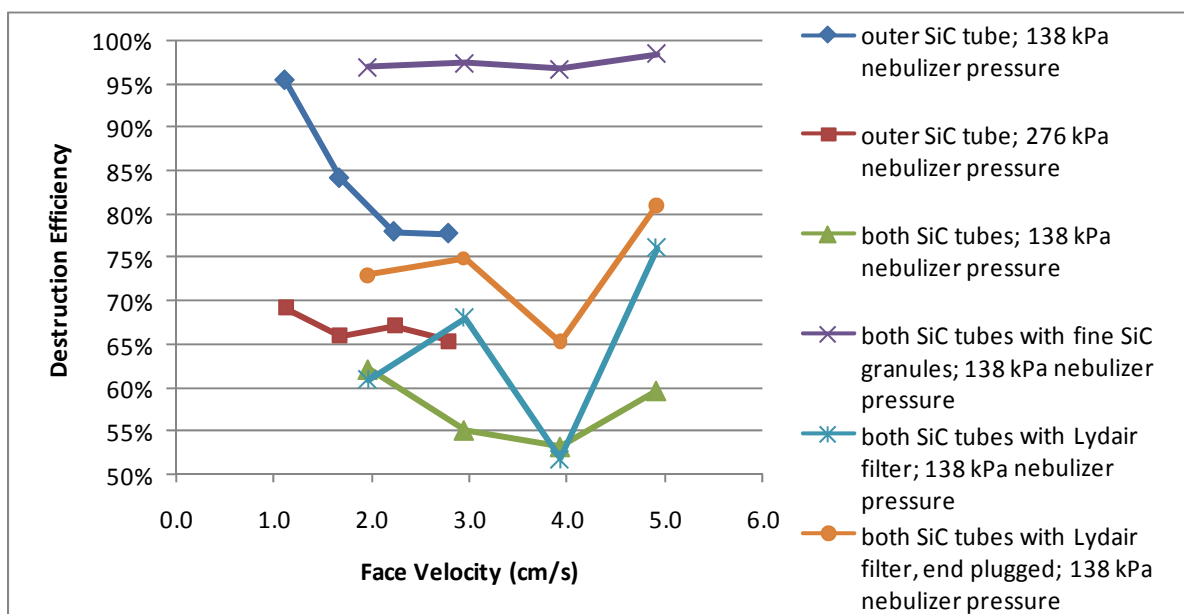


Figure 58: Direct Oxidation on Second Reactor at 2.55 kW Microwave Power for 1 Hour

After completion of the first tests with the single SiC tube, the cavity was opened and examined. There was no noticeable DMMP left in the cavity and no sign of soot as had been seen in previous oxidation studies on the first bench-scale reactor. The lack of soot was encouraging as it indicates that what was being oxidized was more completely oxidized than in the earlier unit.

Testing on the configuration with both SiC tubes and the fine granules was done by measuring THC concentration in the outlet air with the THC analyzer. When this was repeated

with the plugged end, two tests were done by the THC analyzer and the rest were done by phosphorus testing of the diffuser water. The change was due to issues with the instrument. The two tests by THC analyzer, which are not shown on Figure 58, gave 96.4% destruction at a face velocity of 2.0 cm/s and 96.0% at 3.0 cm/s. This is close to what was seen originally without the plug. These results indicate that using THC concentration of the outlet air is not accurately measuring the destruction. Most likely the THC analyzer system was collecting DMMP which never reached the detector and caused the problems with the instrument. The two sets of tests on the single SiC tube at different nebulizer pressures show that concentration of DMMP does affect the DMMP aerosol destruction efficiency with higher concentration leading to lower efficiency.

4. CONCLUSIONS

Because the project was terminated at the end of Year 2 that is earlier than planned, comprehensive testing of the RHELP system was not conducted. The conclusions and recommendations, therefore, are presented here based on knowledge learned from each individual research area.

4.1 Materials Research

Pure TiO_2 nanofibermats as the air filtration media were successfully fabricated via the electrospinning method. In order to enhance the mechanical stability of the thin ceramic fibermat, conditions of the heat treatment on the ceramic fibermat have to be controlled. Based on the results obtained up-to-date, samples that are heat-treated at 500°C for 3 hours are expected to achieve the most stable fibermats. Sandwich structure of microfiber-nanofiber-microfiber also enhances the mechanical stability of the ceramic fiber mat.

In the other approach, hybrid ceramic fibers of $\text{TiO}_2\text{-SiO}_2$ from novel aqueous sol system could build robust fibermats. The chemical reaction of the aqueous sol system was characterized and analyzed by NMR spectroscopy. The d_f was about 500 nm which is thinner than fibers of commercial HEPA filters. Since the thinner fibers lead to higher filtration efficiency as well as low pressure drop, it is believed that the filtration system of fibermats made of the aqueous sol would be not only better than HEPA filters, but also make them regenerable by microwaves with improved mechanical durability.

The fibermat made of $\text{TiO}_2\text{-SiO}_2$ hybrid composite material from aqueous sol system has shown promising characteristics. However, the diameter of electrospun fibers must be reduced in

order to be effectively used in the RHELP system. Therefore, further study should focus on decreasing the fiber diameter by controlling parameters in sol preparation and electrospinning.

4.2 Physical Collection Efficiency

Polyacrylonitrile (PAN) nanofiber filters were tested for collection efficiency, pressure drop, most penetrating particle size and other characteristics. Based on the filter quality factor, the optimal electrospinning deposition time for the filters was determined. In experiments, the fabricated nanofiber filters were found to outperform conventional HEPA filters in both collection efficiency and pressure drop. Furthermore, it was observed that layering nanofiber filters resulted in a greater quality factor than single layer nanofiber filters of the same deposition time.

4.3 Bioaerosol Testing

Microwave assisted filtration coupling nanofiber filters and microwave radiation was found to be a promising method in removing and inactivating bioaerosols. Based on encouraging static on-filter inactivation of the three test microorganisms, an in-flight filtration system using microwave technology was developed. The system proved successful in removing all bioaerosols at high power and periodic microwave application with both PAN 60 and X-linked PAN filters.

The extent of removal from the system or the filter depended on the microbe tested. *E. coli* (vegetative cell), with a greater heat sensitivity and larger size was relatively simple to inactivate requiring only low microwave power and short application time. In contrast, *B. subtilis* endospores required a SiC heating disk along with increased power for similar destruction.

Placing the SiC heating disk, which absorbed microwaves more readily, in contact with the nanofiber filter significantly improved the inactivation on the filter and subsequently aided in

bioaerosol removal from the airstream. Another finding that provided increased inactivation was flow rate or face velocity reduction during periodic microwave irradiation. While the microwave was on, a face velocity decrease resulted in a higher filter temperature. In bioaerosol experiments with decreased flow conditions, a significant increase in inactivation was achieved. This indicates that the system can be further optimized to provide high efficiency at a lower cost.

As temperature is the critical factor in microbe inactivation, in future studies the use of an infrared thermal imaging camera to determine temperature of the filter during irradiation should be considered. This would provide quantitative information whether the filter was achieving a high enough temperature for inactivation of a particular microbe. Additionally, it is recommended to install a mode stirrer inside the microwave cavity. If the thermal imaging camera detects hot and cold spots on the filter, a stirrer would provide more uniform heating and increased microbe inactivation.

4.4 Chemical Aerosol Testing

SiC discs loaded with cross-linked PAN nanofibers gave greater than 90% aerosol collection efficiency even after eight cycles of regeneration, and discs loaded with TiO₂ mats gave greater than 95% aerosol collection efficiencies even after six cycles of regeneration. Regeneration of the nanofiber was complete although the destruction efficiency of the DMMP was low. They have been demonstrated for their ability to endure microwave irradiation. Meanwhile, their mechanical stability for handling needs to be improved, as they were brittle or tended to tear easily. For comparison, the baseline SiC discs had lower than 50% aerosol collection efficiency but regenerated completely. As an alternative, SiC discs loaded with commercially available Lydair HEPA grade 4405 HS filter gave >90% aerosol collection

efficiency even after 6 cycles of regeneration. Regeneration was completed and DMMP destruction efficiency was over 50% with low air flow rates.

DMMP aerosol collection on the bench-scale SiC tube without any filter was greater than 95%. Destruction efficiency reached over 90% on SiC tubes with Lydair filter. Both collection and destruction efficiencies decreased as flow rate increased. Direct oxidation of the aerosol as an alternative to collection of aerosol followed by destruction of the aerosol shows some promise, however, optimum conditions have yet to be determined. Direct oxidation with two SiC tubes packed with fine grit SiC gave the most promising results with greater than 95% destruction efficiency at all face velocities tested. With Lydair filter, direct oxidation by two SiC tubes varied between 50% and 75%. Alternatively, a two stage system with direct oxidation on the first stage and a collection system that could be regenerated on the second stage with periodic application of microwave energy for destruction of aerosol collected on the filter could be used.

5. ABBREVIATIONS AND SYMBOLS

HEPA: high efficiency particulate air

F_D : dragging force

μ : air viscosity

V : air velocity

d_f : mean fiber diameter

C_c : gas slip correction factor

l : mean free path of air, 66nm at standard temperature and pressure

ACF: activated carbon fiber

ϵ : complex permittivity

ϵ' : real part of the permittivity

ϵ'' : imaginary part of the permittivity

TB: titanium (IV) n-butoxide

AA: acetic acid

EtOH: ethyl alcohol

PVP: polyvinylpyrrolidone

SEM: scanning electron microscope

C_v : coefficient of variation, standard deviation/mean

XRD: X-ray diffraction

TEM: transmission electron microscope

t : size of crystals

λ : wavelength of the X-ray

B : full-width-at-half-maximum of the peak

θ_B : average of lower and upper limits of the peak in radian.

TGA: thermogravimetric analysis

F108: BASF Pluronic[®] F108 Prill

NMR: nuclear magnetic resonance

GPTMS: 3-glycidoxypropyltrimethoxysilane

6. REFERENCES

1. http://www.johnzink.com/products/thermal_ox/pdfs/tp_catalyst.pdf
2. Cooper, C. D. and F. C. Alley, "Air Pollution Control, 2nd Edition," Waveland Press, 1994, Chapter 15 and 16.
3. Johnson, R. W., "Catalytic Oxidation Technology: Application to Collective Protection," Presented at Advanced Air Purification Technologies for CBRN Protection Unit Process and Systems Conference, Marriott's Bay Point Resort Village, Panama City, Florida 17-20 November 2003.
4. Chapman, T. E., D. C. Rennie and W. B. Wang, "A Comparison of Innovative Air Treatment Technology Demonstration at McClellan Air Force Base," Presented at the 1999 AIChE Spring National Meeting, Houston, Texas, 15-18 March 1999.
5. Advani, N. and A. Chainani, "An Integration Approach to Air Purification," Presented at Advanced Air Purification Technologies for CBRN Protection Unit Process and Systems Conference, Marriott's Bay Point Resort Village, Panama City, Florida 17-20 November 2003.
6. Kakit, Y., N. Kashige, K. Murata, A. Kuroiwa, M. Funatsu and K. Watanabe, "Inactivation of Lactobacillus bacteriophage PL-1 by Microwave Irradiation," *Microbial Immunology*, 1995, 39, 571-576.
7. Rosaspina, S., D. Anzanel and G. Salvatorelli, "Microwave Sterilization of Enterobacteria," *Microbios*, 1993, 76, 263-270.
8. Hinds, W. C., *Aerosol technology : properties, behavior, and measurement of airborne particles*, 2nd ed. (Wiley, New York, 1999).

9. Allen, M. D. and Raabe, O. G., "Slip correction measurements of spherical solid aerosol-particles in a improved millikan apparatus," *Aerosol Science and Technology*, 1985, 4 (3), 269.
10. Allen, M. D. and Raabe, O. G., "Re-evaluation of millikan's oil drop data for the motion of small particles in air," *Journal of Aerosol Science*, 1982, 13 (6), 537.
11. Jianxin, M., Fang, M., Li, P., Zhu, B., Lu, X., and Lau, N.T., "Microwave-assisted catalytic combustion of diesel soot," *Applied Catalysis a-General*, 1997, 159, 211.
12. Meyers, M. C. and Chawla, K. K., *Mechanical Behavior of Materials*. (Prentice-Hall International, London, UK, 1999).
13. Kalapathy, U., Proctor, A., and Shultz, "A simple method for production of pure silica from rice hull ash," J., *Bioresource Technology*, 2000, 73 (3), 257.
14. Williams, D. B. and Carter, C. B., *Transmission Electron Microscopy II Diffraction*. (Springer Science+Business Media, Inc., New York, 1996).
15. Nuansing, W. Ninmuang, S., Jarernboon, W., Maensiri, S., and Seraphin, S., "Structural characterization and morphology of electrospun TiO₂ nanofibers," *Materials Science and Engineering B-Solid State Materials for Advanced Technology*, 2006, 131 (1-3), 147.